UNIVERSITÀ POLITECNICA DELLE MARCHE

Doctoral school in Science

Civil and Environmental Protection – XVI cycle

AA. 2016-2017

ANALYSIS OF EXTREME EVENTS OVER MEDITERRANEAN SEA WITH COUPLED NUMERICAL MODELS

Dissertation by:

Antonio Ricchi

Tutor:

Prof. Aniello Russo

Co-tutor:

Dott. Sandro Carniel

Dottorando:

Antonio Ricchi

Abstract

This thesis is the result of the work carried out in the three years of course, dealing with the issue of the application of numerical simulations related to extreme events, both atmospheric and oceanic, that appear over the Mediterranean basin and that are strongly influenced by the air-sea interaction. In the first phase of this work the physical characterization of the studied events is proposed. The phenomena studied are i) a case of Cold Air Outbreak (CAO) formed in the winter of 2012 on the central Mediterranean area, and in particular in the north of Italy; ii) a Dense Waters Formation (DWF) produced by this CAO event; and iii) one event of "Tropical-Like Cyclone" (TLC) (called "ROLF") that developed on the Balearic Islands between the 6th and the 9th of November 2011. Moreover, preliminary results about a Flash Flood formed over the Venice Lagoon are showed in the end of this manuscript. We will discuss the physical characteristics that govern these phenomena, in particular the interaction between sea and atmosphere. After describing and studying the above mentioned phenomena, we propose some considerations regarding the numerical applications that are needed in order to obtain better results. The modeling techniques used for this thesis are mainly three. The first approach used is a classical "Uncoupled", which consists in the use of atmospheric models uncoupled to ocean models and wave models that exploit SST satellite data. The second approach used refers to the use of "Coupled" ocean-atmosphere models, and the third presents the ocean-wave atmosphere coupling. The purpose of these modeling techniques is to try to describe accurately the momentum and heat fluxes that appear at the air-sea interface, and that characterize, very often, some atmospheric and oceanic phenomena. Results show that the use of coupled models provide improved results, having this approach a direct impact mostly on some heat and momentum fluxes and the SST evolution, fundamental in some applications. Moreover, other indirect implications brought along by the use of coupled models, that are often important at the basin scale and regarding also the case of deep marine ventilation, are presented and discussed (Benetazzo et al., 2013, Carniel et al., 2016, Ricchi et al., 2016, Ricchi et al., 2017, Bonaldo et al., 2017).

Contents

Introduction

Overview

Climate change and its consequences are increasingly being regarded as one of the most significant challenges of the new millennium, and our vulnerability to atmospheric and oceanic events is evident on a daily basis. Extreme events play a great role in terms of strong impact on economics and society, and the need to understand better the dynamics that drive the climatic system is nowadays of paramount importance. Until a few decades ago there was no great certainty about the anthropogenic impact on climate change, and for a long time its effect was mostly studied on the atmosphere, from the synoptic scale to the local scale. However, in the last decades it has been observed that a fundamental role in the regulation of the climate system, at each scale, is played by the ocean. The ocean has been identified as one of the key factors for knowledge of climate change, since it is estimated that 90% of the heat produced as the result of the increased greenhouse gases concentration from 1970 has been stored in the ocean (Levitus et al 2005, Rhein et al., 2013) and in particular in the first 700 meters of depth (Gleckler et al 2016). While the atmosphere seems to have been heated by about 0.74 °C, particularly in the northern hemisphere and at medium-high latitudes, with more warming on the ground if you compared with the sea areas. Without going into climatological detail we can affirm that the climate change is reflected in a visible manner on the atmosphere and in a less manner over the oceans, which have greater thermal inertia, compared to air; for this reason they change their temperature much more slowly, but they have a greater ability to keep heat too. Moreover, observations at sea are subject to great "observation gaps", being much more difficult to acquire measurements at sea with respect to the atmosphere. In addition, you can have data with a decent synoptic coverage only for the surface of the sea, but not for the depth. Because there are very few fixed stations at sea, the knowledge of the complex feedback that exists between the atmosphere and the ocean, and how the heat is shared between the two environments, is therefore not sufficient. Many works (Warner et al 2010, Olabarrieta et al 2012, Davolio et al 2014, Miglietta et al 2017, Cioni et al 2016) have identified the importance of the ocean even on shorter time scales, such as for some extreme phenomena that appears in the coastal area (Cassola et al 2015). In addition, strong anthropization has stimulated the vulnerability of coastal areas. One of the main methods of studying both climate change and its consequences in terms of extreme events, is the use of numerical models. Numerical models are one of the most advanced technique of reproducing, studying and trying to predict the weather, oceanic and climatic dynamics of the environmental system. The development

of many atmospheric and oceanic dynamics, is very complex, even if we have a great physical knowledge and many IT resource. One of the main objectives of numerical modeling is to reproduce as much realistic as possible the phenomenon studied and to do so in the environmental field, it is necessary to implement in the numerical model a wide range of initial and boundary conditions. It is easy to see how the role of the soil, the ocean and the initial state of the simulation, it is essential to obtain correct results, but also for an exact interpretation of numerical data. These considerations encourage the scientific community to consider the environment as a unique coupled system, in which interact the atmosphere, ocean and waves. This work goes into this complex scientific context and it can be articulated in several steps. Initially, we identify some particularly significant extreme events, characterizing the Mediterranean basin, analyzing them from a physical aspects. In a second step are simulated by means of different numerical techniques, adapted to implement step-by-step the various possible numerical configurations, which lead to a complete coupling ocean-atmosphere interface. In this way you can compare the response of the phenomena to the different environmental "partitions" and the responses of the individual models with various levels of coupling. So you try to make it clear which is the effect of each single model, and each implementation used. The extreme phenomena chosen for this thesis work are considered to be of great interest both for their physical complexity, that for the strong social and economic impacts. That's why we are trying to investigate this phenomena with complex numeric models, which may also prove helpful in the forecasting system and in the building of more sophisticated and reliable alert systems. The selected events are a case of "Cold Air Outbreak" (CAO), and the resulting "Dense Water Formation", a case of Tropical-like Cyclones (TLC or Medicanes, from the English MEDIterranean hurriCANEs). Finally, some preliminary and unpublished results are reported, dealing with an intense case of Flash Flood on the Venice Lagoon and on the urban areas of the mainland such as Venice Mestre and Venice Marghera, with great damage to structures and agriculture. The results show a strong sensitivity to SST and to coupling of the models for all events we studied especially for the CAO, DWF and Flash-Floods. This improvement is due to a better description of the SST fields and the fluxes at air-sea interface. Regarding the TLC "ROLF" sensitivity study, the data will show how this type of phenomenon is only partially driven by SST (and within a certain range of SST variability) in terms of trajectory and intensity, instead of the tropical cyclones. But the use of coupled models shows how the slightest differences can be attributed to the different evolution of SST at the passage of the cyclone.

Extreme events over the Mediterranean Sea

The Mediterranean Sea basin is located in the temperate climate zone and extends approximately from latitude 30 ° N to 46 ° N and from longitude -5.5 ° W to 36 ° E, measuring about 3860 km in the west-east direction and about 1600 km in the north-south one. It consists of several sub-basins, but in total it has an extension of about 2.511.000 km2 or about 0.8% of the total marine surface. It has a maximum depth of 5270 meters and an average depth of 1500 meters, for a total volume of 3.700.000 km3 of marine water. The Mediterranean Sea is a densification basin, therefore Is a basin where evaporation of seawater tends to increase the ratio of salinity. Because of the strong cooling of some areas caused by Cold Air Outbreak events (CAO), surface water increases its density and sinks; strong evaporation is only partially compensated by the fluvial inputs. The Mediterranean Sea is an excellent example of interaction among atmosphere-ocean-waves, being a mild basin characterized by high daily and seasonal thermal gradients, and intense surface stress. In addition, the Mediterranean Sea is surrounded on three continents, with many complex and high mountain ranges, vast plains, deserts and continental areas (Figure 1).

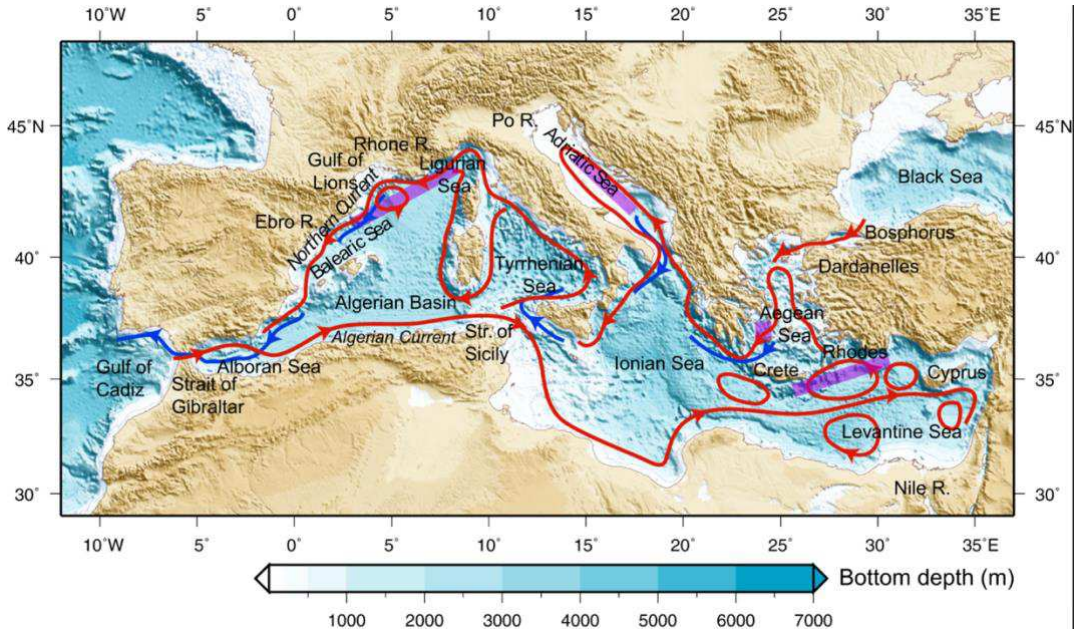

Figure 1. Bathymetry, topography and main features of the ocean circulation in the Mediterranean basin.

The Mediterranean Basin is characterized by hot and dry summers and relatively humid and wet winters. In winter, the Atlantic climate, mild and humid, is very frequent. The most frequent dynamics with Atlantic perturbations in the first phase cause hot and dry air suction from North Africa, and in a second phase cause precipitation, wet air, and intense winds from the northern quadrants (Figure 2 panel A) that often generate (in some areas) intense boulders (it is not uncommon to reach significant heights of over 8 meters). The Mediterranean is also characterized by another type of atmospheric circulation. These are cold and dry air spits that break in from the northern quadrants (Figure 2 panel A) or from the Russian-Siberian continent (Figure 2 panel B). These advection (especially the most intense and long cases) are caused by the formation of dynamic anti-cyclones that are located in the center of Europe (Figure 2 panel A) or thermal anticyclones that are located over the Russian place. Often, these can combine, forming a Voejkov-bridge (Aleksandr Ivanovič) (Figure 2 panel B). This configuration closes the way for the Atlantic flow, and attracts cold and dry air from Siberia. The Siberian air comes over the Mediterranean basin from the Adriatic Sea and the Aegean Sea. During the summer, the Mediterranean basin is predominantly affected by the Aztec Anti-cyclone. Instead, when an anti-cyclone is formed on North African, it sparks very hot air (15-25 ° C to 850 hpa) on the sea. This mass of hot and dry air, through evaporation, greatly influences both the atmosphere and the characteristics of the mixed layer.

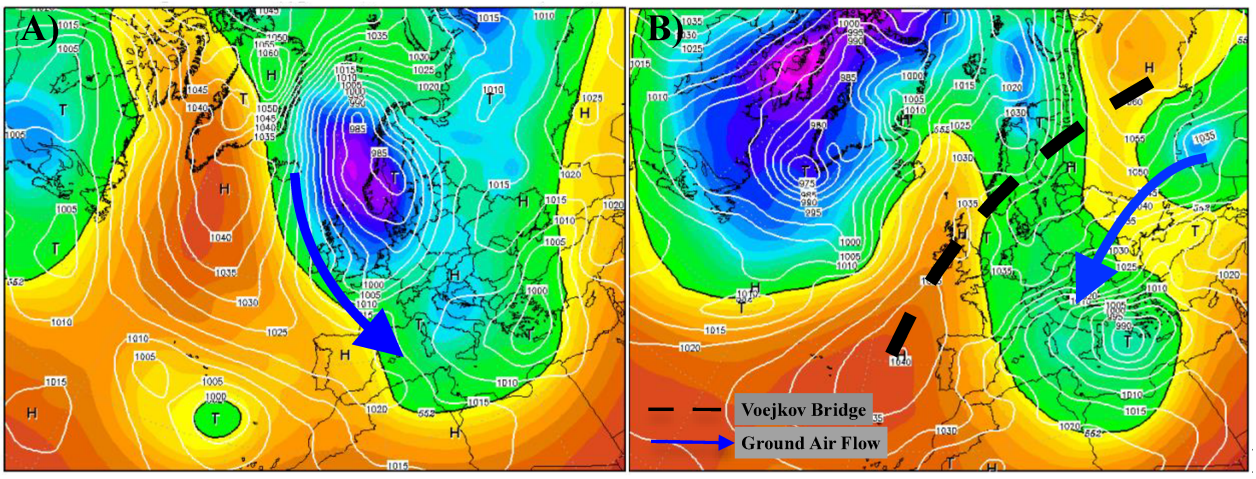

Figure 2. CAO events, in the left panel are showed the Atlantic CAO, in the right panel are showed the continental CAO and the Voejkov anticyclonic bridge.

The water masses present in the various sub-basins of the Mediterranean are quite different from each other. The western basin is characterized by strong annual thermal gradients with peak summer (on the surface) that can reach 28 -30 °C, and minima close to 5-10 °C in areas of dense water formation such as the Gulf of León, the North Adriatic and the Aegean Sea, but on average its winter temperature is close to 13 °C on the surface. The eastern basin is milder and its densification is mainly due to evaporation, which increases the salinity of the basin (salinity has a higher densification capacity if compared to the temperature). Dense water formation areas are essential for the circulation of the Mediterranean Sea. Especially for deep circulation, with strong repercussions on the biological environment (Luna et al 2015). From this brief description it is easy to understand how the western Mediterranean is characterized for several months (especially in autumn and winter) by having strong gradients between SST and Atlantic or continental air. The strong evaporation, which is activated by these thermal gradients, influences the formation of new air masses and transports large volumes of water vapor into the atmosphere. This water vapor fluxes is the fuel of many extreme atmospheric phenomena. From this description it is understood that, for the western Mediterranean basin, energy exchanges between the atmosphere and the sea can give rise, more frequently, to atmospheric and oceanic phenomena of considerable intensity. Some examples may be CAO events, possibly dense water formation in some areas, tropical-like cyclones and flash floods. In the description of the climatology and meteorology of the Mediterranean basin, and the extreme events that characterize it, the morphological and hydrological characteristics of the Mediterranean basin are not very important. Rivers, for example, are a very important hydrological feature for the Mediterranean, and their importance and influence on the marine environment is governed by both precipitation and melting of winter snow on mountain ranges. An example of direct influence of river hydrology on the marine environment is found in pre-conditioning the sea surface by river fresh water. During CAO events, there is a possibility that DWF occurs, but a condition that limits its formation is the preconditioning produced by freshwater masses. These freshwater masses invade the densification basin, and create a less dense water layer, which isolates deep water from the atmosphere. This does not allow heat exchangers, which activate the DWF. With regard to the influence of morphology on the formation of extreme events in the Mediterranean basin, we can see the example of the "hydraulic jumps" that mountain ranges cause when they are impacted by large-scale flow (for example baroclinic waves). When a mass of air crosses a mountain range from the Atlantic to the Mediterranean Sea, it undergoes a "thin" and then "elongation" and this can lead to significant variations in relative vorticity (Figure 3) which in turn induces formation of cyclonic circulations located in certain areas such as the Gulf of Genoa, the Balearic Islands, the Ionian Sea. These cyclogenesis, when interacting with SST, and the pre-existent wet state on the basin, can give rise to very important cyclogenesis namely "TLC",

or tropicalized cyclogenesis at Mediterranean latitudes. Another very intense phenomenon caused by the air-sea interaction and with the complicity of topography, is called “Flash Flood”. This strong thunderstorms that are mainly formed on coastal areas. Flash floods are the result of the formation of convergence lines at the ground, between dry and fresh air masses, coming from the plains, or from mountain area, and the mild and humid air masses that are generated from prefrontal flux (Davolio et al 2009). These phenomena can cause precipitation with total accumulated rainfall often between 300 and 500 mm very small areas.

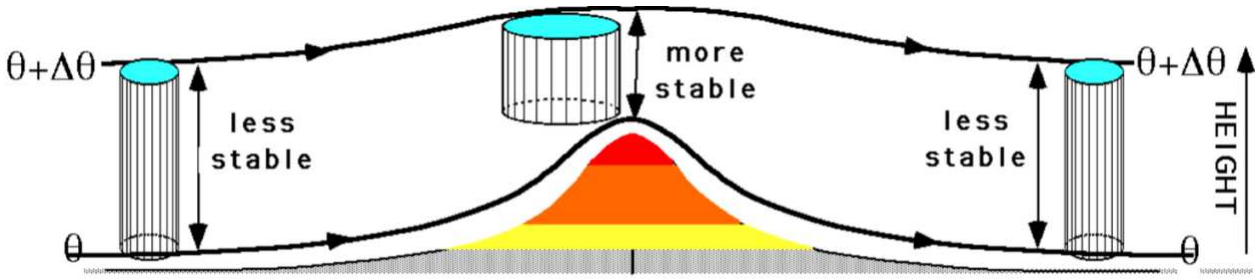

Figure 3. Variation of vorticity during the overcoming an orographic barrier by an air mass.

Cold Air Outbreak (CAO)

Cold Air Outbreaks (CAOs) are frequent atmospheric events that appear as cold air advection, from high latitudes to middle latitudes (Figure 2 panel A, B). Causes of an CAO event can be various. In general we can say that a CAO event is caused by intense meridian undulation of the polar front. CAO events are fairly common and any depression that is formed close to the polar front, with its own frontogenesis, is potentially capable of generating a CAO at medium latitudes. However, the most intense and long-lasting CAOs develop within long-term atmospheric waves or anticyclonic block configurations. CAOs, therefore, have to evaluate four main factors: duration, intensity, the origin of air mass, secondary phenomena that are generated by CAO and which can amplify or limit evolution. The duration of a CAO event depends mainly on the pressure fields configuration. Indeed, two main types of CAO can be formed on the Mediterranean basin. The CAO caused by depressions located on Central Europe and with north-south axis, (Figure 2 panel A), which convey on the Mediterranean, cold sea air, humid and mitigated by the passage on the North Sea. This air mass is colder at the ground if compared with the upper atmosphere and before arriving on the Mediterranean basin must the European continent and also the mountain, such as the Alps or the Pyrenees. Frequently these CAO events are less intense and less durable. Another category of CAOs on the Mediterranean basin are those generated by the closure of the Atlantic circulation caused by an anti-cyclonic bridge (Voejkov's bridge) that is formed between the dynamic anticyclone of the Azores present on Western Europe and the thermal anticyclone that form over the Russian-Siberian area. The axis of this anticyclonic bridge, which is usually southwest to the northeast, prevents the arrival of Atlantic perturbations over the Mediterranean Sea, and causes a very cold and dry air advection that flow along the southern edge of the high pressure field (Figure 2 panel 2B). The dry and cold air which pours out into the Mediterranean sea quickly extract a latent and sensitive heat from the sea (with net heat flows often reaching 800-1000 w/m^2 over the Adriatic basin and the Aegean Sea). This strong thermal gradient can generate depressions on the central Mediterranean, usually centered on the Tyrrhenian Sea. These depressions, increase the horizontal pressure gradient that intensifies the advection of cold air from the continent. This blocking situation may last for several days or weeks. For example, this happened between January and February 2012, and is one of the most favorable conditions for intense and persistent CAOs on the Mediterranean Sea basin.

Dense Water Formation (DWF)

Dense Water Formation is one of the fundamental processes underlying the global ocean circulation both physically and biologically and climatologically. This convective circulation, which features about 61 spots (Ivanov et al 2004), is one of the causes of the surface dynamics of large ocean masses such as the Gulf Stream (CdG). Although the CdG is activated and maintained by the Earth's rotation, the DWF area in North Atlantic regulates the intensity and extension towards North, and once activated densification processes, becomes an active part of the Conveyor Belt. DWF processes can be of different types, depending on the characteristics of water masses and climate. In addition there are preconditioning phenomenon of water masses that limit or prevent the DWF. DWF can be obtained by heat extracting from the atmospheric phenomena, for presence of already cold water masses (for example Polar Waters Masses) or for the presence of warmer waters, but with a higher salinity. Salinity has a capacity to increase the density greater than the decrease in temperature. The second dynamic of DWF prevails at polar latitudes. In the Mediterranean basin we can observe the DWF mainly due to high heat fluxes from sea to the atmosphere caused by CAO phenomena. In the Mediterranean, DWF areas are in the Gulf of León, under the action of Mistral wind; in Aegean Sea, caused by CAO continental events, and in the Adriatic Sea during continental CAO events that occur through the Bora (Figure 4). Due to the complexity of the "jets of snow", the DWF in Adriatic occurs in three sub-basins: the North Adriatic, the northern coast of Croatia, the Adriatic south. In the North Adriatic the largest volume of dense waters is formed. This is due to the bathymetry of the basin and the intensity of the Bora, which reaches the sea through the Gulf of Trieste, which causes heat fluxes of more than 1000 W/m2 (Benetazzo et al 2014, Supić and Orlić, 1999) . River flows are very important for dynamics of the North Adriatic. DWF is possible only in absence of large river outflow (Falcieri et al 2014) (mainly caused by the Po river) that isolates the atmosphere from the rest of the water column, and restricts the mixing and DWF. The mean density of DW in North Adriatic is around 1029 kg/m^2. CAO events such as those in 2012 and subject to the study of this thesis, under the aesthetic aspect, are investigated and studied by means of modeling techniques (Benetazzo et al. 2013, Benetazzo et al 2014, Carniel et al 2016).

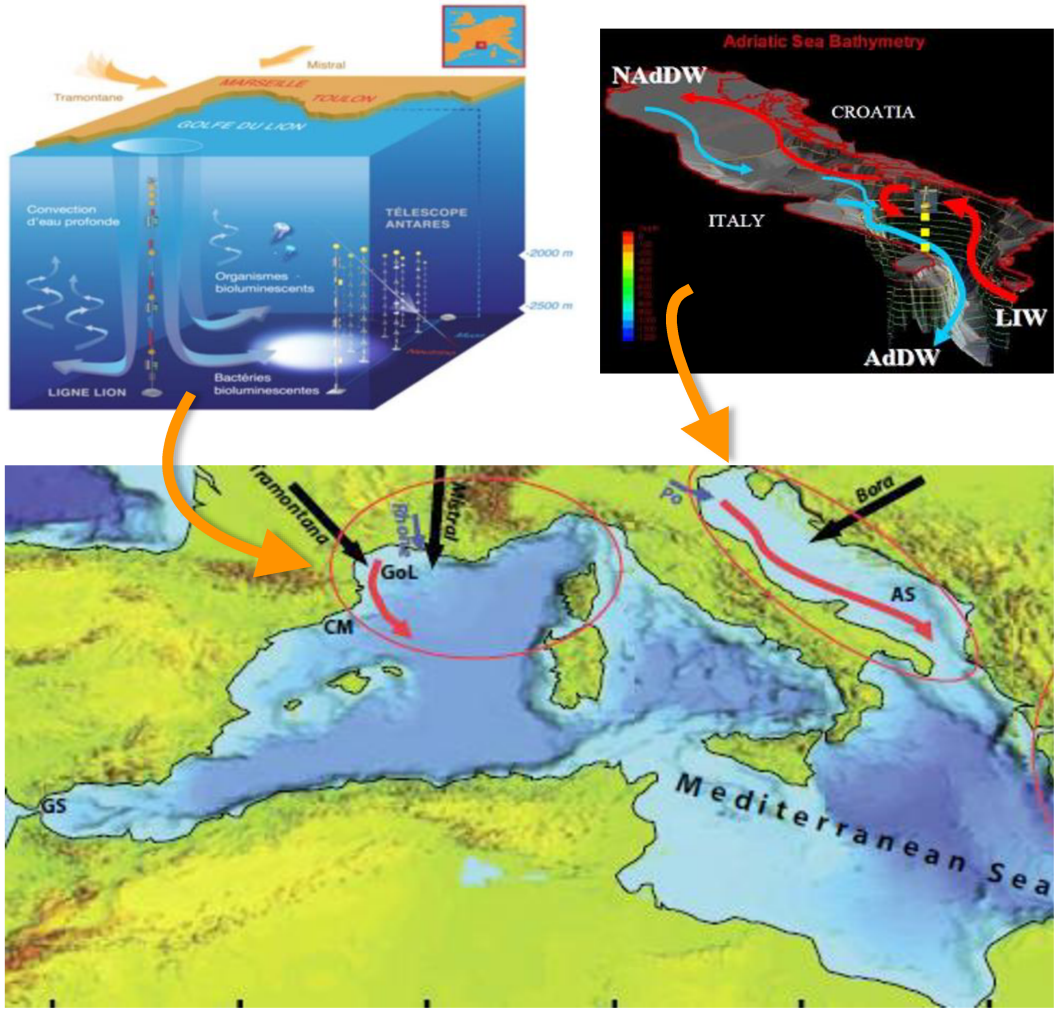

Figure 4. Dense water formation (DWF) sites in the Mediterranean sea.

Tropical-Like Cyclones (TLC)

As previously discussed, the Mediterranean Sea is characterized by a strong seasonal climatic variability, strongly amplified by the orography. The SST of the basin, fairly mild, is a very important factor in terms of variability of the climate and extreme events. There are wide differences in SST between the Western Mediterranean sea, with a higher annual thermal excursion, and the Eastern Mediterranean with less thermal excursion. As a result we can say that the Mediterranean interacts strongly with atmospheric dynamics on a synoptic scale, and that through the heat reserve provided by the sea and the effect of the orography it is able to modify the baroclinic waves that pass through the surrounding basins. It is subject to a wide variety of baric structures and atmospheric phenomena. The distribution of cyclonic areas is driven by orography and the formation areas are quite well known. Mediterranean cyclones have extratropical characteristics, and unlike tropical cyclones that capture their energy both from SST and from the latent condensation heat release during convection (barotropic structure), they are characterized by a strong baroclinic structure with well defined frontogenesis and therefore taking their energy from the horizontal gradients of temperature (Cioni et al 2016). At medium and high latitudes (except for rare cases such as Polar Low), the cyclones have baroclinic caracteristics, but nothing prohibits that baroclinic phenomena develop a deep convection around the minimum pressure, and assisted by the release of latent condensation heat in the atmosphere, can generate a "Warm core" in the air column, and thus changing from an extra-tropical system to a hybrid system, or a system that has assumed tropical characteristics in the surrounding area of the cyclone eye, whose maintenance depends, at least in part, on this tropicalization of the minimum of pressure. In the early 1980s with the improvement of satellite technologies, depressions were identified with very similar characteristics to small hurricanes and were called Medicanes ("Mediterranean hurricanes") (Emanuel 2005), but which can in fact be defined as extratropical systems, tropicalized, so called "Tropical-Like cyclones" (TLC). These extra-tropical cyclones evolve into a new phase, where intensification is guaranteed by deep convection, which releases latent heat. This phenomenon generates additional useful energy for convection. This cyclogenesis may be intensified by intense air-sea heat fluxes caused by an SST threshold of at least 15 ° C (Tous et al., 2013). Despite this, it is observed that a decisive factor is not SST, but the air-sea thermal gradient (Miglietta et al 2013, Davolio et al. 2012, Cioni et al 2016, Ricchi et al 2017). The characteristics of the TLC are a "warm core" present around the eye of the cyclone extending to at least 500 hpa, a developed vertical symmetry, cloud cover and precipitations organized in spirally bands around the minimum pressure, and distinct and visible eye. The size of these phenomena is short if compared to Tropical Cyclones (TC) and are close to 100-300 km of diameter, against more than 500-800 km in TC. Modeling TLC is always very complex, especially

for operational models, which often fail to identify the formation of convection around the minimum pressure. The main reason could be that the operational models do not implement a high-resolution SST and therefore do not generate the vertical gradients and heat fluxes necessary for the formation of TLC. Usually, the SST used by operational models is low resolution, does not evolve in time (during simulation), therefore it does not vary in according to the atmospheric dynamics. An important aspect of the satellite SST is that it is generated by an average of the measurements made during the previous seven days (this technique is often used to eliminate the “observational holes” caused by cloudiness). This can cause significant bias in the data, especially during winter and in coastal areas and over semi-closed basins (Ricchi et al 2016, Carniel et al 2016). It is therefore very important to use a “realistic” SST (Cioni et al 2016), so for this thesis we have used numerical techniques to understand how different implementation techniques can be useful for TLC modeling (Ricchi et al 2017).

Numerical approach – COAWST Model

Numerical environmental modeling is a branch of Earth sciences that has became more and more important in recent years. Through complex numerical methods, the climate system in its completeness and as detailed as possible is then translated into appropriate equations solved numerically, in order to investigate (and simulate) phenomena that otherwise would not be possible to represent. Numerical modeling requires a significant scientific effort, since models must be validated and tested against observations. In practice, relying on the "scientific method" the scientist must be able to discern the use of the numerical model as "means" to achieve a certain result, such as simulating an environmental event; or as "end", that is, the scientific application to improve and test the qualities and characteristics of the model in use on certain environmental phenomena (often this second method is defined as a "numerical sensitivity study"). In this thesis, we have chosen to use both methods by focusing attention on a first part on the sensitivity study in order to calibrate the numerical model with the best parametrizations for the study of the extreme events analyzed. In a second phase, we studied air-sea interactions by adopting the coupled models technique. As mentioned above, the purpose of this dissertation is to analyze extreme, atmospheric and oceanic events on the Mediterranean basin. For this reason we have chosen to use "coupled” numerical models. This category of numerical models is still rather experimental, complex, and costly in terms of computing resources, but has the potential advantage of describing the "ocean-atmosphere-wave" system in a consistent and more realistic way. Although numerous atmospheric, oceanic, and wave

models exist the main problem is therefore represented by coupling them together in order to described the complex energy feedbacks among the different compartments (Figure 5).

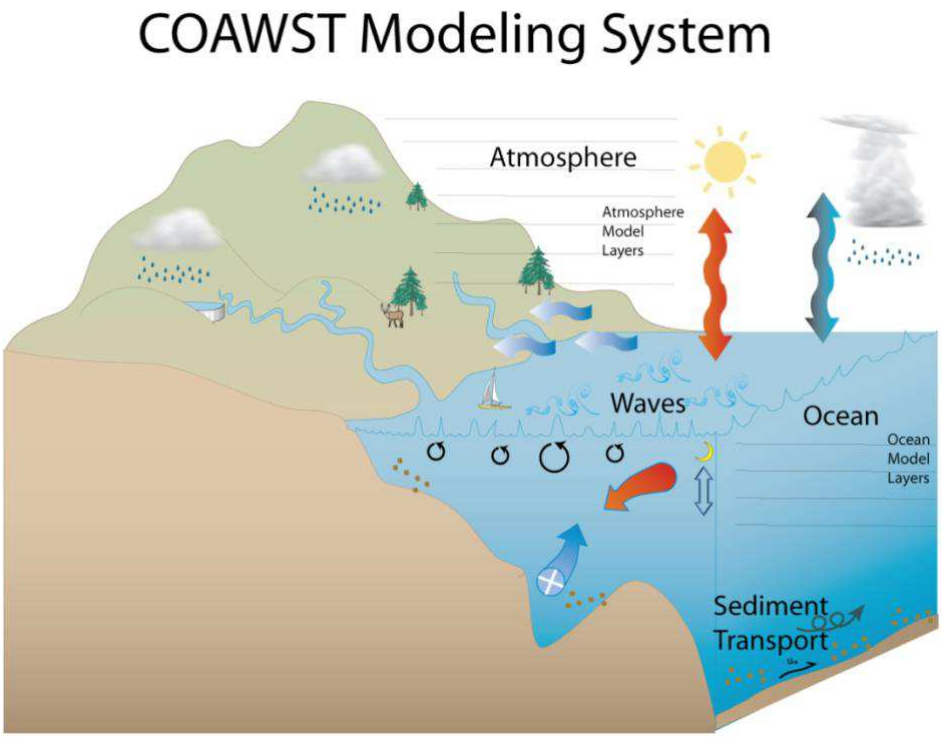

Figure 5. Cartoon representation of feedback between atmosphere and ocean

The most common use of environmental numeric models is to use a single model for the specific compartment (air, wave, ocean) by receiving the necessary input form other models. This means that, for example, when we use an ocean numerical model, we do receive the wind field data from another numerical model that was run detached from the one we are actually running. This uncoupled approach is the most common way of using environmental numeric models, and although it can provide realistic results, it can nevertheless be responsible of producing very different result when compared with reality, as shown in Chapter 1. Obviously, even using coupled models mistakes relative to the divergence of each model can appear. In fact, each model simulates a different environment, which has different physical characteristics, so it may have a different divergence speed than other models. By using coupled models, however, we can simulate the three environments consistently, and evaluate the behavior of each model when interacting with others. The thesis presented here fits in this context by simulating "uncoupled" and "coupled" techniques to various atmospheric and oceanic phenomena. The numerical modeling system used in this work is called COAWST (Coupled Ocean Atmosphere Wave Sediment System, Warner et al 2008, Warner et al

2010) (Figure 6). COAWST is a complex numerical frame-work that combines different prediction models in order to solve the dynamics of atmospheric-ocean--wave interaction in a consistent model

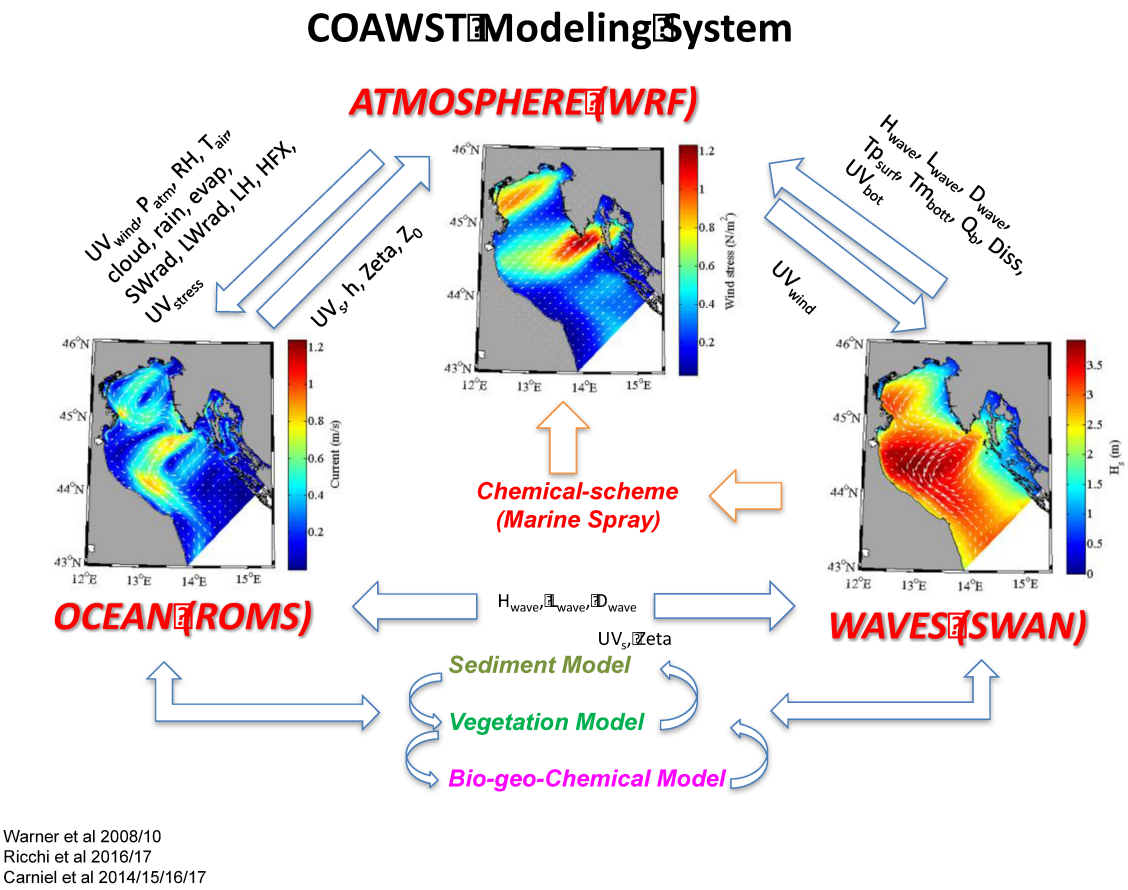

Figure 6. Structure of COAWST modeling system.

COAWST was developed by the USGS (Warner et al 2010), and uses a "community model" approach defining a state-of-art modeling system. The atmospheric model used by COAWST is WRF-ARW (Weather Research and Forecasting System). WRF (Smagorinsky et al., 2007), is developed by NCEP (National Center for Environmental Prediction). WRF is a numerical weather prediction (NWP) developed for both research and forecast uses; is a model at “finite differences” that uses vertical “terrain-following” coordinates, and horizontal Arakawa-C grid (Arakawa et al 1977). WRF implements a large number of numeric schemes that make it applicable from scales of tens of kilometers to scale a few meters (LES, Large Eddyes Simulation scale). For the oceanic compartment COAWST uses a Reginal Ocean Modeling System (ROMS, Haidvogel et al 2000, Marchesiello et al 2003, Warner et al 2005, Di Lorenzo et al 2003), is a free surface model that solves RANS (Reynold

Averaged Navier -Stokes), in a three-dimensional domain in curvilinear coordinates, using the technique of the finite differences, on vertical coordinates "Sigma", terrain-following. Timing integration occurs with the decomposition of 3D fields in barotropic part (depth-mediated) and baroclinic part, in order to limit the effect of short-term surface gravity waves (and higher phase velocities). Again it is a "community model" full parallel. For the generation and evolution of wave motion, COAWST uses the SWAN spectral model (Simulating Wave in Nearshore; Booij et al., 1999) which is a "wave action model" or a third generation model that describes the evolution of the spectrum of energy density in arbitrary wind conditions, currents and bathymetry. The coupling between the different models is done through the Model Coupling Toolkit (MCT) libraries, which deal with model management when exchanging variables and distributing data across the different grids, decomposed during computational parallelization. The interpolation between the grids of different models (which can use different computing domains) is through the SCRIP software (Jones et al 1988), which creates arrays on which interpolation of data exchanged through MCT occurs. COAWST is a very flexible numerical system that allows you to use every single model either in "uncoupled" mode or forced externally, but without coupling, either in "Coupled" mode. In this thesis work we have the objective of studying the importance of SST and exchanges at the air-sea interface in extreme events. To do this, in each chapter and work presented, we apply the same technique of analysis. It starts with uncoupled runs where SST comes from satellite data (Figure 7 panel A). In this case, SST is used in two ways. The simplest case uses satellite SST that does not change over time. The second case evolves SST during simulation every 6 hours. In this way we will evaluate both the "Forecast" application, where only the first SST field is available, and the "Hindcast" application where SST daily data is always interpolated every six hours for consistency with the Boundary Condition of the Atmospheric Model. The second type of configuration used is the coupling between the atmospheric model and the ocean model (Figure 7 panel B). In this case the two models communicate with each other and exchange momentum and heat fluxes. In this case, WRF receives SST from ROMS every timestep selected by users, and ROMS receives superficial stress variables, 2 mt temperature, solar radiation, atmospheric pressure, precipitation, cloudiness, and humidity to compute the fluxes with the same algorithm used by WRF (COARE, Fairfall et al 2003). In this configuration, therefore, the atmosphere influences bi-directionally the ocean and vice versa. In the third technique used, the wave model is added to the previous case (Figure 7 panel C). Therefore, the wave model computes the geometric parameters of the wave motion and exchanges them with ROMs and WRF using the same schematic diagram for surface roughness, PBL and MDL (Figure 8c). In return, SWAN receives the surface circulation components by using them in the next wave field calculation. COAWST proposes several calculation schemes for surface roughness in the atmosphere

and ocean. In the case of uncoupled runs and in the case of coupled ocean atmosphere, the Charnock scheme (Charnock et al. 1956) is automatically used. In the case of fully coupled with the wave model, the roughness algorithm with Taylor-Yelland (Taylor and Yelland 2001), Drennan (Drennan et al 2003), Oost (Oost et al 2002) are used. These schemes utilize wave geometry parameters with different physical approaches, taking count of wave age or wave stiffness, to cover a wide range of applications under different wave conditions and on different basins. A shortage of this application is to not use the Charnock scheme (Charnock 1956) that takes account of wave geometry (Janssen et al 1992). In the following chapters three cases of applications are proposed in which three extreme events on the Mediterranean basin are studied, with the various techniques described above.

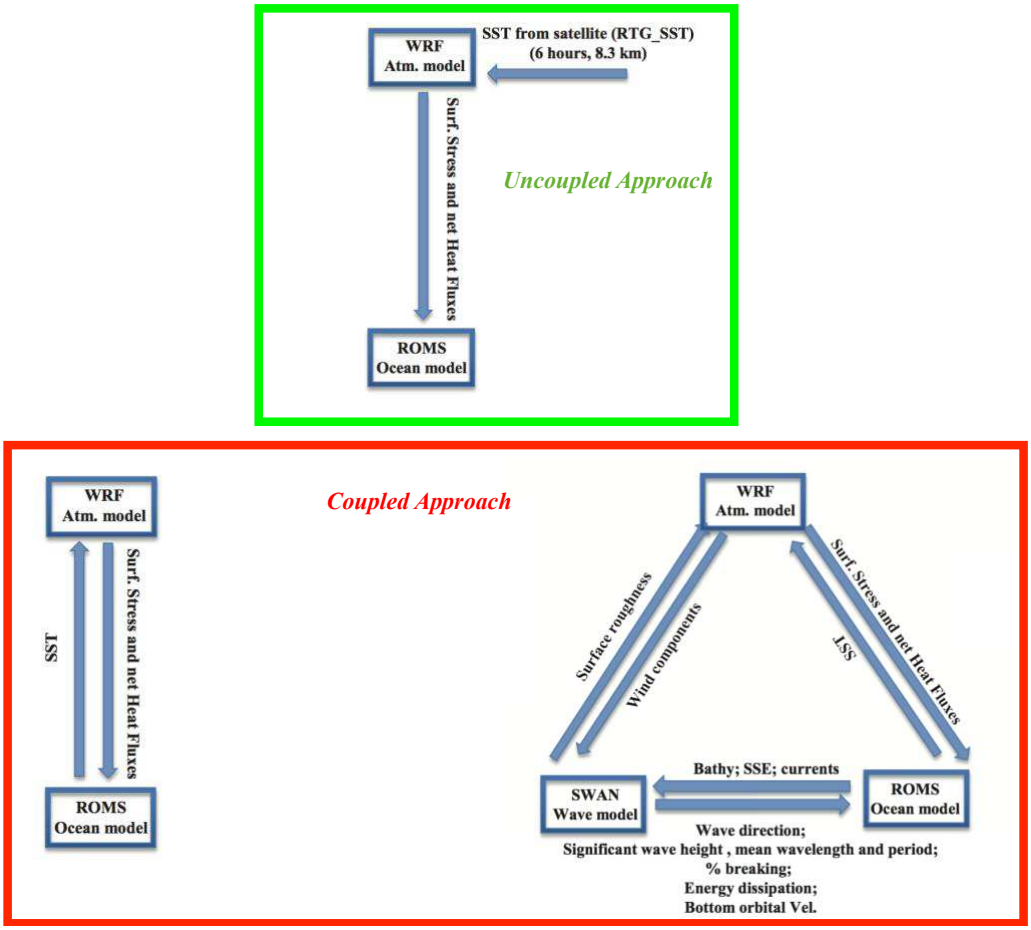

Figure 7. Coupled and Uncoupled numerical approach usable in COAWST and used in this thesis work.

1. On the use of coupled ocean-atmosphere-wave model during an extreme cold-air-outbreak over the Adriatic Sea

1.1. Overview

An intense cold air outbreak affected the northern Adriatic Sea during winter 2012, determining an exceptional persistence of northeasterly Bora wind over the basin, which lasted for about 3 weeks. The cold air coming from the Balkans produced icing in the Venice lagoon and very intense snowfall in the Apennines Mountains and even near the coasts. In order to understand the importance and role of air–sea interactions for the evolution of the atmospheric fields, simulations with the Weather Research and Forecasting (WRF) model encompassing the whole period have been performed using sea surface temperature (SST) fields with an increasing level of complexity. Starting from a large-scale static sea temperature, the SST in the initial and boundary conditions has been progressively made more realistic. First, a more refined field, retrieved from a satellite radiometer was used; then, the same field was updated every 6 h. Next, the effect of including a simplified 1D ocean model reproducing the Oceanic Mixed Layer (OML) evolution has been tested. Finally, the potential improvements coming from a coupled description of atmosphere–ocean and atmosphere–ocean–waves interactions have been explored within the Coupled Ocean–Atmosphere–Wave Sediment Transport (COAWST) modeling system. Results highlight that the energy exchange between air and sea does not significantly impact the atmospheric fields, in particular 10 m wind and 2 m temperature, also because of the geography of the basin and the predominance of synoptic-scale flow in intense events of Bora, in the northern Adriatic. However, when sensible and latent heat fluxes, which are dependent on atmospheric and oceanic variables, are analyzed, the more realistic representation of SST drastically improves the model performances.

1.2. Introduction

The 2012 winter has been a mild and dry season, characterized by positive NAO and strong activity of the Azores anticyclone, on the western basin of the Mediterranean Sea. The season exhibited peculiar meteo-oceanic processes involving the Mediterranean Basin, since it was characterized with a cold air outbreak (CAO, namely an intrusion of polar air down to mid-latitudes regions) of outstanding intensity. One of the areas most exposed to such extreme cooling was the northern Adriatic Sea, where the Venice lagoon partially iced (an exceptional occurrence, as discussed in Camuffo, 1987). The effects of such intense weather event were remarkable also inland, where large snow accumulation, even in the proximity of coastal regions, led to remarkable damages to transportation systems and agricultural activities. Similar events were already documented in the northern Adriatic basin, but rarely with such a severity and long persistence (Mihanović et al., 2013; Davolio et al., 2015). The most critical period lasted from January 29 to February 15, when repeated cold air spits originating in eastern Europe brought temperatures down to −23 °C in northern Italy (western Po valley). The effects of such a strong cooling affected not only the atmospheric fields (Davolio et al., 2015) but also the sea, with unusually cold and dense water production (Raicich et al., 2013; Janeković et al., 2014; Benetazzo et al., 2014). On the one hand, some intense wind episodes in the Adriatic Sea were analyzed in the past using in situ data (Dorman et al., 2006). Such studies had the merit to highlight the role and to increase the knowledge of thermal and momentum exchanges at the air–sea interface. In particular, the heat fluxes and the wind stresses emerged as the main forcings, through which the atmosphere drives the ocean dynamics during CAO events. However, even when accessing to a relatively large amount of in situ data, many aspects still need to be understood.

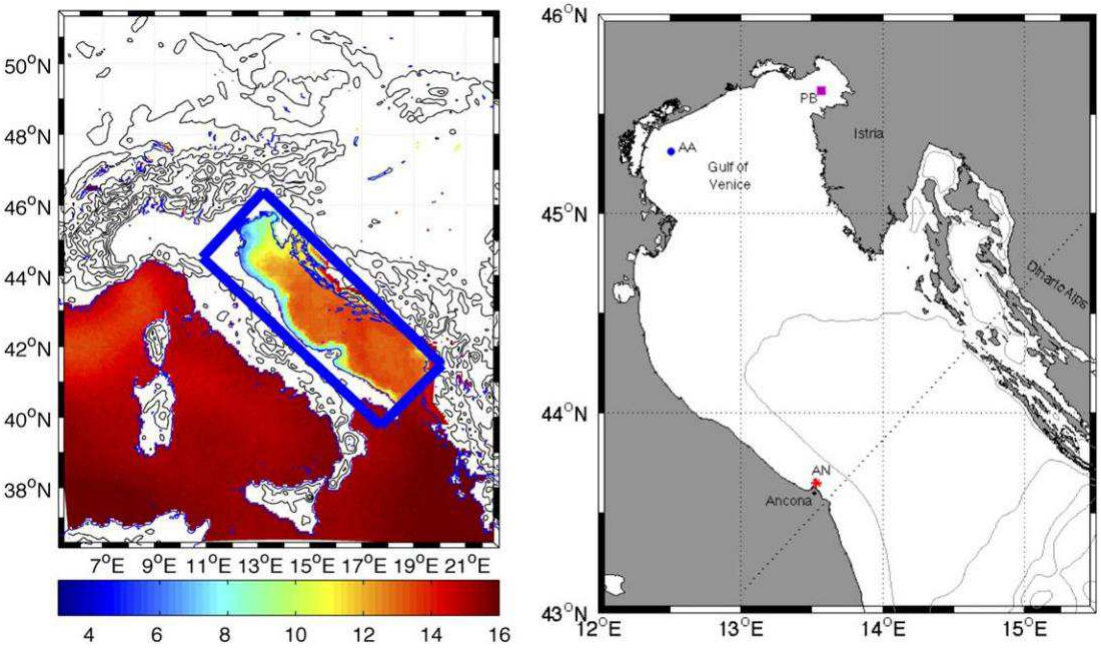

Fig. 1. Left: Domains for WRF model (external box) and ROMS-SWAN models (blue box); right: location of stations considered in northern Adriatic.

The availability of long time series in coastal observatories, such as the CNR tower "Acqua Alta" (position shown in Fig. 1 with AA), can be very helpful in shedding further light on this topic. On the other hand, numerical studies (Davolio et al., 2015) framed these CAO events from a different perspective, focusing on the existing limits within numerical models, such as the inaccurate description of the atmospheric boundary layer (ABL) physics, or the coarse horizontal resolution (Fita et al., 2010). Fortunately, in the last years several aspects contributed to increase the quality of meteorological fields, such as low-level wind, simulated by numerical weather prediction (NWP) models. Above all, the increased availability of computational resources allowed for a finer horizontal resolution in numerical models; such an advancement is particularly relevant in a region with complex orography such as the northern Adriatic basin, characterized by very steep mountain ridges especially on its eastern part (e.g. Signell et al., 2005). Nevertheless, operational NWP systems were not able to adequately forecast the precipitation amount during the 2012 CAO event, with a significant underestimation of the snow accumulation on the Italian side. The interaction of the atmospheric flow with the Adriatic Sea appears as an important forcing in such episodes, being responsible for the "Lake-Effect Snow" (Liu and Moore, 2004). Therefore, a deeper analysis of the interaction between the atmosphere and the ocean appears necessary to understand the nature of the 2012 event and

addresses the reasons of the failure in the atmospheric model simulations. Different levels of complexity exist when processes and interactions focused at the air–sea interface are considered within numerical models. Generally speaking, the real-time meteorological forecasts available nowadays are generated by atmospheric models, which use the sea surface temperature resulting from a largescale analysis or from radiometer measurements as a constant field during the whole integration period. This "stand-alone" methodology includes only the evolution of the atmospheric variables and keeps the ocean variables fixed at the initial time. Such an approach has several drawbacks, since the real SST may significantly evolve during the time of the simulation and, due to the coarse resolution of the datum, may be locally affected by significant biases (Gemmill et al., 2007). This is true especially in coastal regions or in sub-areas where complex thermal patterns appear at the sub-mesoscale. In order to better represent the heat and moisture exchanges at the air–sea interface, atmospheric and oceanic models have been first implemented in a one-way coupled configuration. From the oceanic perspective, wind fields and air temperature produced by atmospheric model simulations are adopted to force (one-way coupling) ocean models. Several studies have considered this kind of application in the Adriatic Sea (Boldrin et al., 2009; Bignami et al., 2007; Carniel et al., 2009; Benetazzo et al., 2013). Although such a routine approach generally produces satisfactory results for sea surface temperature (SST) estimates, it does not take into account the feedback of the oceanographic fields into the atmospheric dynamics, which implies that the dynamically consistent SST provided by an oceanic model is used as a boundary condition for the atmospheric counterpart. Also, especially during intense meteorological events, the different formulations adopted for the calculation of heat fluxes respectively in the oceanic and atmospheric models, may lead to significant inconsistencies between the two modeling systems (Olabarrieta et al., 2012a). To surmount this limitation, in the recent past the use of two-way coupled atmosphere–ocean models has been proposed, with the aim of properly representing the air–sea interactions, providing a more realistic and consistent evolution of atmospheric and oceanic fields. In such an implementation, the atmospheric and the oceanic models exchange information at the air–sea interface in a consistent way. A pioneering work for the Adriatic region was presented in Pullen et al. (2006), where the atmospheric model was supplied with 6-hourly SST fields produced by an ocean model. The authors were able to demonstrate that such a two-way coupled approach increased the skill in wind speed forecasts (which were generally overestimated in the uncoupled case) at selected sites in the northern Adriatic. Turbulent fluxes were examined in Pullen et al. (2007), extending the previous study to a February 2003 hindcast. Although focusing mostly on the comparison between two Bora wind cases, that work showed that two-way coupled simulations improved the heat fluxes estimation (diminishing them) with respect to the one-way coupled run. A further improvement in

the coupling system is the inclusion of a third kind of models, explicitly describing wind-wave dynamics. Wave models provide relevant information about the wave patterns, which are necessary for the proper representation of the sea surface roughness in the atmospheric models, and to modulate momentum exchanges at the air–sea interface and throughout the water column (Carniel et al., 2009; Benetazzo et al., 2013; Benetazzo et al., 2014). The purpose of the present work is to understand the effect of the air–sea interaction on different atmospheric variables during the 2012 CAO event that affected the northern Adriatic Sea. To accomplish this task, atmospheric model simulations are performed using an SST with an increasing level of complexity and then validated against in situ measurements. First, the Weather Research and Forecasting model (WRF) is implemented in a stand-alone approach, using different SST fields, which range from constant in time and coarsely resolved in space, to variable over time and with a high spatial resolution. As a second approach, the WRF model is two-way coupled in the framework of the COAWST (Coupled Ocean–Atmosphere–Wave and Sediment Transport; Warner et al., 2010a) modeling system, including ROMS (Regional Ocean Modeling System; Haidvogel et al., 2008) as ocean circulation model and SWAN (Simulating Waves Nearshore; Booij et al., 1996) as wave model. A first test is performed coupling only the atmospheric and oceanic modules. In the third implementation, the wave module is also included, reaching a fully coupled atmosphere–ocean–wave configuration. To our knowledge, this is the first time a fully coupled modeling system is implemented in the Adriatic basin (previous studies in the region considered only the coupling between atmosphere and ocean components without waves; see also Loglisci et al., 2004; Dubois et al., 2012). The present paper will mostly deal with atmospheric or air–sea interface aspects; focus on the oceanic side will be treated with more details in a companion paper (Carniel et al., 2015b). Table 1 summarizes the main features of the simulations considered in this study. The paper is organized as follows. The synoptic conditions reported during the event are briefly analyzed in Section 2. The observations available in the northern Adriatic Sea, and the modules in COAWST modeling system are described in Section 3. The different numerical experiments are introduced in Section 4. Results are presented in Section 5, while discussion and conclusions cover respectively Section 6 and 7.

1.3. The 2012 CAO event

In mid-January 2012, the synoptic situation over Europe is characterized by a blocking configuration, associated with the Azores high extending over the Atlantic and the Siberian high pressure over Eastern Europe (the detailed evolution of the synoptic conditions can be reconstructed in Fig. 2, source http://www.wetterzentrale.de/topkarten/ fsreaeur.html based on GFS-FNL dataset). Around January 24, a low pressure system develops over northern Italy and then moves towards the Balkans while the two high-pressure systems join, isolating the Mediterranean circulation from the Atlantic flow during the following days. As a consequence of this configuration, an intense flow of cold air blows from the east on the southern edge of the high-pressure band in the lower layers. Meanwhile, an intense upper level Arctic flow affects the western Mediterranean. In the following days the situation remains nearly stationary, with new minima generated in the Gulf of Genoa on January 29 (Fig. 2a,b) and on February 1, persisting for several days in the Ionian Sea, and the widening of the high pressure band intensifying above 1060 hPa over northern Europe. As a consequence of the persistent advection of very cold air, on February 3 the 850 hPa temperature falls down to −18 °C on Northeastern Italy, while intense snowfalls start affecting the Po Valley reaching even the Adriatic coasts. From 3 to 6 February 2012 the northeasterly air currents remain intense, pushing the 850 hPa temperature down to −20 °C in northeastern Italy (Fig. 2c,d). February 6 is the coldest day at the ground during the entire event, with high temperatures below 0 °C almost everywhere in northern Italy and with minimum values of about −15 °C spread across northern Italy, down to −23 °C in the western Po valley (Fig. 2e,f). Intense snowfalls persist, especially upwind (eastward) of the Apennines where snow accumulations at the ground are diffusely larger than 1 m but extending also downwind up to the Tyrrhenian coast, with 30 cm of ground accumulation measured in Rome. Fig. 3 shows the 500 hPa geopotential height and the mean sea level pressure map at 00 UTC, February 6, which is representative for the synoptic conditions during the whole event. The high-pressure band from the Atlantic to Northern Europe can be easily identified, together with the intense pressure gradient across the Italian peninsula, associated also with a low pressure far south in the Mediterranean. An intense upper level northerly flow affects the western Mediterranean down to northern Africa. After a temporary weakening on February 9, a new boost of very cold air affects Italy between 10 and 12 February, associated with a new low-pressure center originated on the Tyrrhenian Sea and moving across the Ionian sea in the following days (Fig. 2g,h). Albeit with less extreme values, the 850 hPa temperature is still below −10 °C in northern Italy and snowfall still affects northern and central Italy on February 13. Afterward, the synoptic circulation changes, and the cold Arctic air remains localized mostly to the north of the Alps, so that the temperature progressively increases over Italy, although the snowpack persists to the ground for several days.

From the above analysis, it is clear that the 2012 CAO event was exceptional not only for the relevant snowfall accumulation, but also for the intensity and the duration of the Bora wind, unceasingly persisting over the northern Adriatic Sea for more than 2 weeks (Fig. 4). Bora is a very strong northeasterly wind blowing on the Adriatic and originates when a cold and dry air mass over the Dinaric Alps becomes thick enough to cross the mountain gaps. Then, it creates characteristic propagation lobes (Horvath et al., 2011) as it flows into the Adriatic basin, from which it draws heat and moisture. The distribution of Bora is rather complex and variable among different episodes, while generally its duration is limited to a few days (Bignami et al., 2007). Fig. 4 shows the 10-m wind speed between January 23 and February 16 recorded at the Acqua Alta Platform (AA), located about 15 km offshore Venice. The beginning of the CAO event can be identified around January 28 (Raicich et al., 2013), when the strong pressure gradient determined by the blocking configuration across Central Europe combined with an intense depression over Central Italy generated intense wind speeds, exceeding 15 m/s in the two observing stations of AA platform and Paloma buoy (BP, see Fig. 1) in the northern Adriatic sea (Raicich et al., 2013).

RUN	SST Type	SST Update	SST Resolution	Coupling
GFS	Global Model	None	1°	NO
STA	RTG_SST	None	8.3 km	NO
OML	RTG SST + Model 1D	1 h	8.3 km + WRF Res.	NO
DYN	RTG_SST	6 h	8.3 km	NO
AO	ROMS	30 min	1 km	Yes (2-way) WRF + ROMS
AOW	ROMS	30 min	1 km	Yes (2-way) WRF + ROMS + SWAN

Table 1. List of model runs: the SST field used in different runs and the way it has been updated are also shown. In all "stand-alone" simulations no data is exchanged between the various models. In the AO case, the WRF model passes wind components, air pressure, humidity, temperature, cloud cover, rain, evaporation, heat fluxes, solar radiation to ROMS, while ROMS provides SST to WRF. In the AOW case, the WRF exchanges the same variable as in the AO case to ROMS, and passes the 10 m wind field to SWAN, while SWAN exchanges peak wavelength, peak significative wave height and peak wave period with WRF and ROMS.

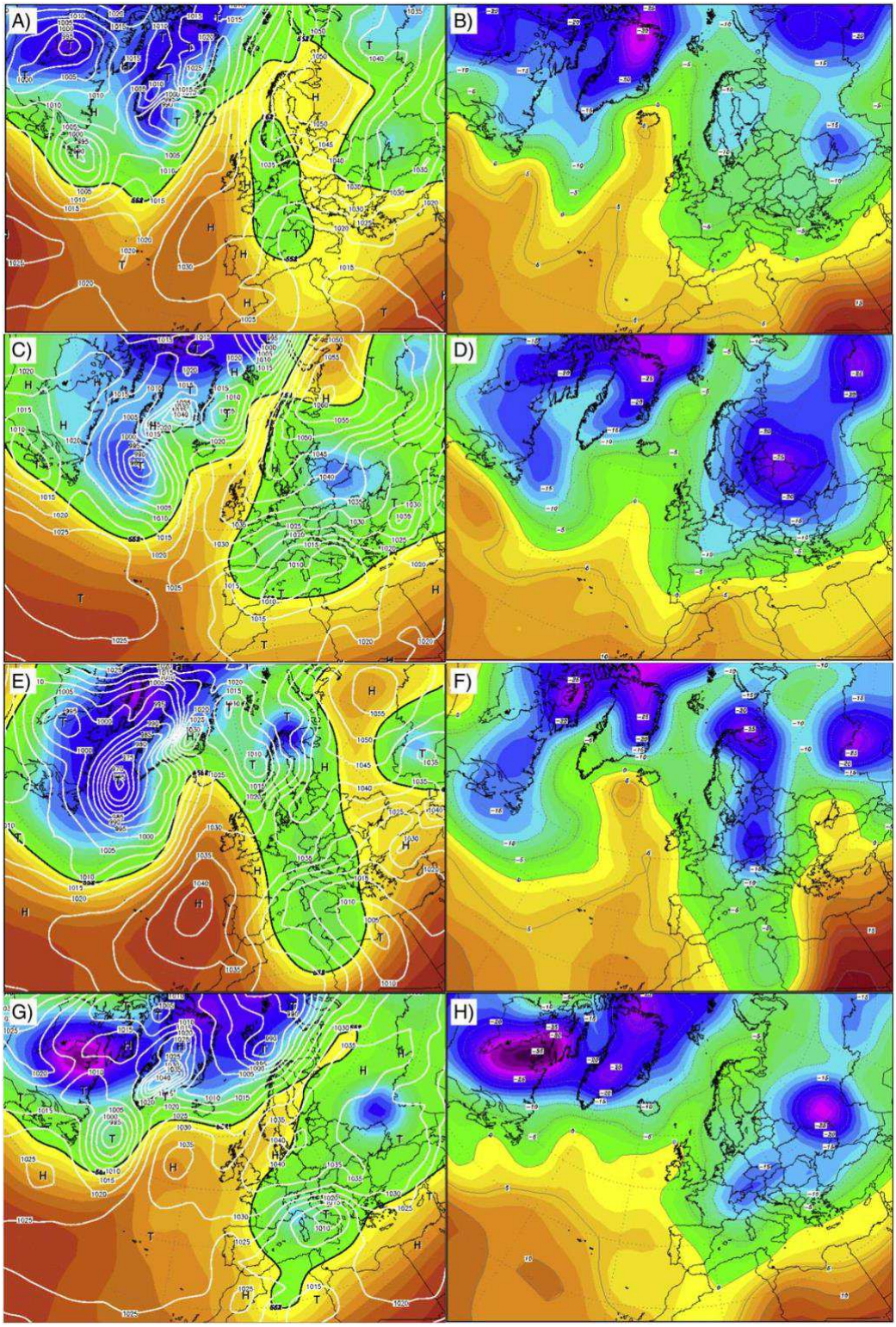

Fig. 2. Fields of sea level pressure and geopotential height at 500 hPa (left) and the temperature at 850 hPa (right). A) and B): initial phase of the event, January 29, 00:00. C) and D): intensification of the high pressure and arrival of the cold air on the central Mediterranean region, February 02, 00:00. E) and F): CAO at its maximum intensity over the Adriatic basin, February 06, 2012. G) and H): new intensification of CAO over Italy and weakening of the anticyclone over Europe. February 11, 00:00 (source: www.wetterzentrale.de GFS-FNL dataset).

In the period from 1 to 5 February the intensity of the 10 min-average wind remained around 15–20 m/s, but with gusts up to 35 m/s (Fig. 4). After a temporary weakening, a new intensification was recorded around February 8, followed by a rapid decrease until 10 February, when another intense depression deepened over southern Italy determining strong northeasterly winds until February 15. Finally, the zonal flow extended again over the central Mediterranean determining the end of the Bora episode. As well, the measured total heat fluxes reached exceptional values throughout the Northern Adriatic. In particular, peak values close to −800 W/m2 were estimated at AA, and of about −1000 W/m2 at BP (Raicich et al., 2013). The former value is particularly relevant considering that the platform AA is located in an area where heat fluxes are generally 3–4 times smaller (in absolute value) than those reported offshore in the North Adriatic (Pullen et al., 2007).

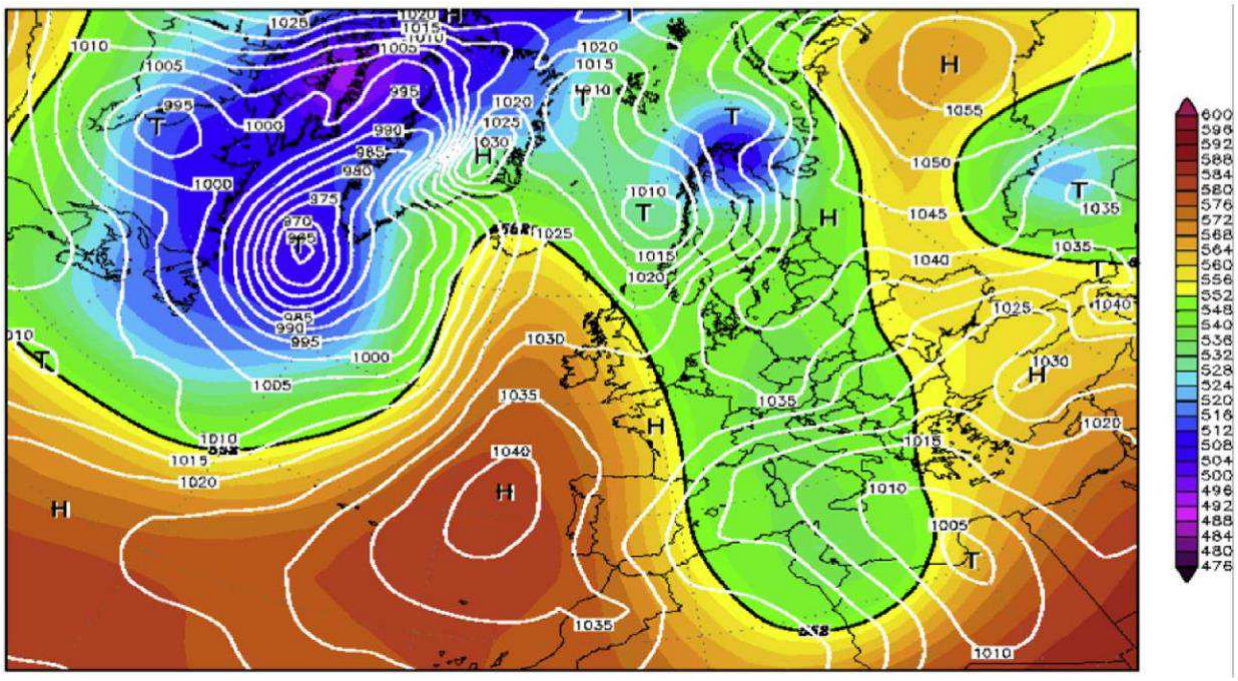

Fig. 3. 500 hPa geopotential height (gpm/10) and mean sea level pressure at 00:00 UTC, 12 February 2012 based on GFS-FNL Reanalysis 0.5×0.5 degrees (source:www.wetterzentrale.de).

1.4. Materials and methods

1.4.1. Available datasets of atmospheric and oceanic data

Three observational stations have been selected in the northern Adriatic for the analysis of the Bora episode and for evaluating the performances of the numerical simulations. We have already mentioned the data sampled at the Paloma buoy, in the middle of the Gulf of Trieste on a bathymetry of 25 m, and at the Acqua Alta Platform offshore of the Venice lagoon, on a bathymetry of 17 m. SST is measured by sensors located 1.9 m below sea surface at both sampling points. Meteorological observations are also performed at AA and BP. In addition, we used meteorological data from the station at the port of Ancona (AN), belonging to the National tide-gauge network, which is representative of the central Adriatic basin (western coast). From raw data, latent and sensible heat fluxes, specific humidity both at sea level and 2 m height are calculated with the aid of the Coupled Ocean–Atmosphere Response Experiment (COARE) model (Fairall et al., 1996). The Paloma buoy is located westward of the orography of the eastern Adriatic basin (Fig. 1), just 7 km off from the coast, where the sea wave state is generally not fully developed. Since the grid spacing in the WRF model is 7 km, in the numerical grid the buoy is located very close to the first sea grid point west of Trieste. Thus, it is potentially strongly affected by the interaction of the flow with the orography, while the air–sea interaction along the Adriatic Sea has only a marginal role. By contrast, since AA is located further downwind of Paloma, it is more affected by the interaction of the flow with waves and ocean conditions, thus the effect of air–sea interaction on the atmospheric variables can be relevant.

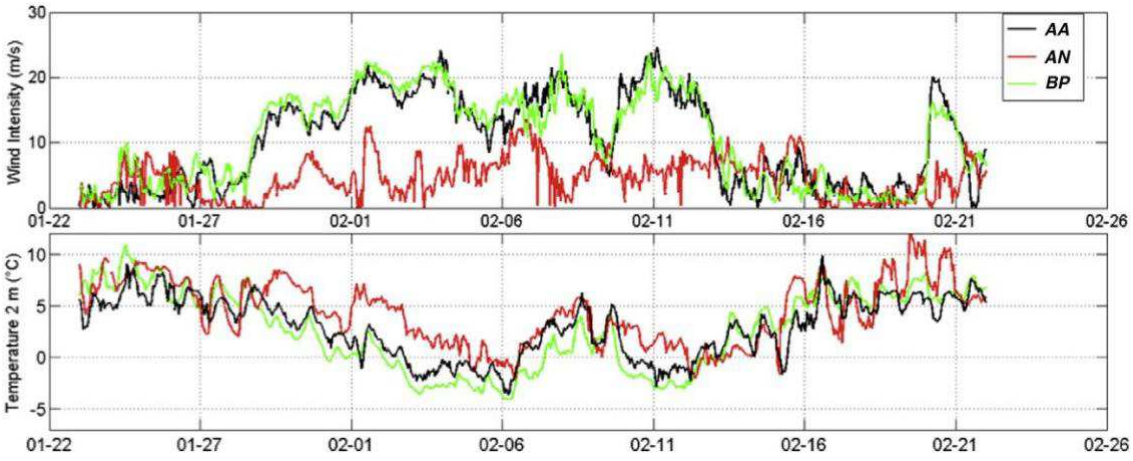

Fig. 4. 10 m wind speed (m s−1) and 2 m temperature (°C) recorded at BP, AA and Ancona stations.

Due to its position, the AA platform undergoes processes related to the coastal front, open sea circulation and mesoscale dynamics (Sclavo et al., 2013). Therefore, the variability and inhomogeneity of the circulation next to AA can be depicted with difficulties by satellite data, also because of the presence of sediment-rich waters, phytoplankton and suspended material that often induce relevant errors in the radiometric measurement (Bignami et al., 2007). Finally, the AN station, located farther south, allows a comprehensive representation of the fluxes that are more typical of the central Adriatic, reflecting the interaction of the flow coming from the Croatian side and the sea surface in the area.

1.4.2. The COAWST modeling system

The coupled modeling system COAWST (Warner et al., 2010a) consists mainly of four modules, namely the atmospheric model WRF, the ocean model ROMS and the wave model SWAN, together with the Community Sediment Transport Modeling System (CSTMS, not discussed in this manuscript). In its simplest configuration, the COAWST system allows the use of each model (with the exception of CSTMS) in pure stand-alone mode, i.e. running independently of any other. In more complex setups, COAWST permits to implement the different models in one or two-way coupling configurations. Communication among the different models is performed through the Model Coupling Toolkit (MCT) and through the SCRIP software, which allows the interpolation of model output fields among numerical grids of different resolution. In the fully coupled runs, the way the surface fluxes are calculated in the atmospheric and the ocean models are consistent (Zambon et al., 2014a). Therefore, COAWST allows simulating in a realistic way the complex processes that regulate the atmospheric and marine dynamics and their mutual feedbacks. This coupling capability turns out to be particularly useful for climate simulations, but also for specific applications in the medium or even short time range, especially in cases where the air–sea interactions are important (e.g., tropical cyclones – see Olabarrieta et al., 2012a; Jullien at al., 2014 or tropical-like cyclones in the Mediterranean Sea; Moscatello et al., 2008, Miglietta et al., 2011, 2013; Akhtar et al., 2014). Significant improvements in reproducing the intensity of Hurricane Ivan (1996) were found by Zambon et al. (2014a) when adopting COAWST in its coupled configuration. On the other hand, the extent to which interface processes can influence strong meteo-oceanic processes is still to be completely understood. For instance, Zambon et al. (2014b) documented that the dynamics of superstorm Sandy, that hit the eastern coast of the United States in 2012, were mainly controlled by large-scale synoptic atmospheric circulation, with only a minor effect from smaller scale processes described by model coupling. The atmospheric model employed in COAWST is the Advanced

Research WRF version 3.4.1 (Skamarock et al., 2005). It is a state-of-the-art numerical model, which simulates a wide range of meteorological processes by means of a variety of dedicated numerical schemes, developed and consolidated within a broad community of users. The physics parameterization schemes can be selected among several possibilities. Here WRF is employed using a horizontal grid having 215 × 240 points and grid spacing of 7 km (see Fig. 1), with 60 sigma (terrain-following) vertical levels, more closely spaced in the atmospheric boundary layer. A comprehensive sensitivity study to different physics parameterization schemes for a case of intense sea surface fluxes in the Mediterranean Sea is provided in Miglietta et al. (2015), showing that the choice of parameterization schemes may slightly modify the simulation results, but that such changes are minor compared to those due to different initial conditions. Here, the convection scheme adopted is the modified Kain-Fritsch (Kain, 2004), the Lin et al. (1983) is used as microphysics, while the surface model is Noah (Chen et al., 1996; Koren et al., 1999). Finally, the Rapid Radiative Transfer Model (RRTM), based on Mlawer et al. (1997), is used for longwave radiation, the Dudhia (1989) scheme for shortwave radiation. About boundary layer, COAWST allows currently only two options, which implement the wave geometry in the calculation of the sea surface roughness. These are based on Mellor–Yamada–Janjic (Janjić, 1990, 1994), a 1.5-order closure scheme, and on Mellor–Yamada–Nakanishi–Niino (MYNN; Nakanishi and Niino, 2009, Nakanishi and Niino, 2006), a 2.5-order scheme applicable to a variety of different static stability regimes (Cohen et al., 2015). Preliminary stand-alone simulations show that MYNN produces results more consistent with observations; thus, the latter scheme has been selected. The hydrodynamic model employed in COAWST is the Regional Ocean Modeling System (ROMS; Haidvogel and Beckmann, 1999; Shchepetkin and McWilliams, 2005), version 4.5.5. ROMS is a freesurface model that solves the Reynolds Averaged Navier–Stokes equations in curvilinear coordinates. In our implementation, the turbulence closure scheme is the Generic Length Scale (Umlauf and Burchard, 2003; Warner et al., 2005). Wave effects are included in the circulation model using the Vortex Forces formulation (McWilliams et al., 2004; Uchiyama et al., 2010) introduced in COAWST by Kumar et al. (2012a). The atmosphere–ocean interaction through heat and momentum flux exchanges can be formulated in COAWST choosing among three different closure models. In this work, the formulation of surface roughness due to wave motion is that provided in Oost et al. (2002), which is appropriate to represent a fully developed sea characterized by short period and high steepness (Olabarrieta et al., 2012a). Here ROMS is implemented using a numerical grid having horizontal spacing of 1 × 1 km (see Fig. 1), and 30 sigma vertical levels. In COAWST, sea waves are reproduced using the Simulating Waves Nearshore model (SWAN; Booij et al., 1996, version 40.91 A). SWAN is a phase-averaged spectral wave model that represents the evolution of the energy spectrum in arbitrary conditions of wind, currents and

bathymetry, and it was specifically designed to overcome the difficulties in the application of wave models (WAMDI Group, 1988; Komen et al., 1994) to shallow coastal areas. SWAN solves the wave action equations taking into account for different mechanisms of energy injection, transport and dissipation, such as wind-driven generation, dissipation due to white-capping, wave breaking, bottom friction, and redistribution of the energy spectrum due to nonlinear three and four-wave interactions. When activated in our experiments, SWAN is implemented over the same grid as ROMS (Fig. 1), with the wave spectrum discretized in 36 equally spaced directions and 40 geometrically distributed intrinsic frequencies. Quantities exchanged when model coupling is enabled are summarized in Section 4 and in Table 1.

1.5. Numerical experiments

The numerical simulations encompass the entire event, extending from January 23, 2012 to February 23, 2012. The starting date anticipates the cold air outbreak by a few days, when the water circulation, the atmospheric circulation, and the wave action are not forced yet by the intensification of Bora wind in the Adriatic. All atmospheric simulations are initialized using here the Global Forecasting System-Final Reanalysis (GFS-FNL) dataset, with a grid spacing of 1.0° × 1.0°. The same data also provide the boundary conditions every 6 h. As briefly discussed above, a series of WRF stand-alone runs and of coupled simulations are performed, where the SST is provided in different ways. The full list of experiments is provided in Table 1 and described hereafter. The former four experiments use the atmospheric model alone, while the latter two simulations rely on the other modules available within COAWST, respectively for the simulation of the oceanic circulation (ROMS) and of the wave dynamics (SWAN). In these coupled runs, ROMS is initialized at 00:00 UTC on January 23 using the SST field resulting from previous runs used for an oceanographic analysis of the 2012 winter–spring conditions (Benetazzo et al., 2014). Due to the identical grid structure, the latter simulations can be used at any time step as initial conditions for the run discussed in the present paper without requiring any spin-up procedure, which has recently been shown to be an important issue for ocean simulations (Winterbottom et al., 2012). The boundary conditions for ROMS at the southern boundary (namely Otranto Strait) are prescribed as re-interpolated daily values of sea surface elevation, 2D and 3D momentum, potential temperature and salinity, originally provided as 1/16° × 1/16° horizontal resolution by the Mediterranean Forecasting System (MFS, see Pinardi et al., 2003). As in previous SWAN implementations carried out in the Adriatic Sea (e.g. Benetazzo et al., 2012; Benetazzo et al., 2014), no incident waves are imposed at Otranto Strait for SWAN, whereas the sea state generated within the basin is allowed to radiate off the domain.

The full list of the experiments performed in the present study is shown hereafter.

a) Run GFS

The WRF model uses the large-scale SST derived from the GFS-FNL reanalysis. The SST has a resolution of about 100 km and is kept constant throughout the duration of the simulation. This run therefore allows understanding how the WRF model behaves without receiving a realistic sea surface temperature, and represents a sort of initial benchmark

b) Run STA

As in the previous run, the SST remains static, but in this case it is obtained from satellite data, the RTG_SST (Real Time Global SST Analysis) High Resolution dataset (Gemmill et al., 2007), provided by the National Center for Environmental Prediction (NCEP). The dataset consists of daily data with horizontal resolution of about 8.3 km. With this simulation, the benefit of using a higher-resolution initial SST is explored compared to the very coarse data adopted in GFS run. However, the SST is not updated during the simulation.

c) Run DYN

The initial SST is the same provided in Run STA (RTG_SST), but now the SST update is carried out every 6 h. The original data, which are available with daily frequency, are thus interpolated every 6 h during a pre-processing phase. As a consequence, the SST includes the long-term variations but does not contain any diurnal variation.

d) Run OML

In this run a simplified ocean model, available in WRF, is used to simulate the atmosphere–ocean interaction. A schematic 1D ocean model reproduces the Oceanic Mixed Layer evolution (Pollard et al., 1972) and requires as input the initial SST and two parameters that are kept uniform in the whole basin, namely the mixed layer depth and the thermal gradient within the thermocline. In our simulations, the thermocline depth was set to 50 m and the thermal gradient to 0.14 °C/m. Depending on the thickness of the mixed layer, WRF calculates how much heat the ocean can exchange with the atmosphere and updates the value of SST according to the heat fluxes at the interface. The initial sea surface temperature is given by RTG_SST.

e) Run AO

The AO (Atmosphere–Ocean) configuration adopts both WRF and ROMS, two-way coupled within the COAWST system. The hydrodynamic model feeds back the SST to the atmospheric model every 1800 s, while WRF provides 2-m air temperature, 10-m wind speed and direction, mean sea level pressure, humidity, short-wave radiation, cloud cover, and rain to ROMS (Table 1). These fields are necessary for ROMS to compute the heat and momentum fluxes via bulk formulae. The surface roughness is computed using the Charnock formula (Charnock, 1955), which is also adopted in the stand-alone cases. No wave information is accounted for in this configuration.

f) Run AOW

The last simulation uses all the models available within COAWST, except for the sediment transport module, with WRF, ROMS and SWAN running in a fully two-way coupled configuration, again exchanging information every 1800 s. Different values of the exchange interval have been tested in the Adriatic basin in Benetazzo et al. (2013, 2014), 1800 s representing a suitable compromise between computational costs and capabilities of resolving the basin associated dynamics (see also Olabarrieta et al., 2012a). Compared to the AO run, an additional model interaction is provided by the inclusion of SWAN model (Table 1). WRF uses the results from the wave model to update the surface roughness, while SWAN is forced with the wind field components from the atmospheric model. In turn, ROMS modifies the circulation according to the energy and momentum inputs received by SWAN, and the latter exploits the circulation fields to modify the wave conditions according to wave–current interactions as described by Benetazzo et al. (2013).

1.6. Results

In the present section, the results of the simulations are discussed, considering oceanic fields (SST), atmospheric variables (2 m air temperature and 10 m wind), and the turbulent fluxes determined by the air– sea interaction. Fig. 5 shows the SST fields in the different runs at 00:00 UTC, 6 February 2012, during the most intense phase of the CAO, while Table 2 includes some statistics on SST for the six experiments. This field represents the boundary condition for the stand-alone runs, while it is a result of the COAWST (and in particular of ROMS) simulations in the coupled implementations. A first sight reveals that the differences among the simulations are relevant, showing in particular that mesoscale structures emerging in the coupled simulations are completely absent in the stand-alone runs. As anticipated earlier, the GFS run (panel a) is an initial benchmark, where a very coarse (1° × 1°) sea surface temperature field is kept constant during the simulation, thus it is not able to represent the SST field evolution and is particularly poor nearby coastal regions. Compared to other panels in Fig. 5, the SST appears warmer by several degrees, especially in the northern side of the Adriatic (Fig. 5a). Since the STA run keeps as well the SST constant throughout the simulation, though at a finer resolution, even this implementation does not include the SST evolution (i.e. cooling) emerging in the northern Adriatic (cf. Fig. 5b with Fig. 5d). As a consequence, in the coastal stations AA and BP, a significant overestimation of SST is evident (by 3.7 °C and 1.3 °C, respectively; Table 2). In the OML run, the SST evolution is determined by a simple 1D ocean model. The resulting SST field on February 6 (Fig. 5c) is pretty close to the radiometric field on January 23 (Fig. 5b), which is its initial condition, although it is slightly warmer in the southwestern part of the Adriatic and cooler near Croatia, where the evolution is more similar to that simulated in the coupled runs (compare Fig. 5c with Fig. 5e). By including the field evolution as retrieved by the satellite, the DYN run is, among the uncoupled implementations, the closest to the SST measurements in the northern Adriatic. It includes, therefore, the cooling from the initial condition (see Fig. 5d,b), and its overestimation of SST is limited to only 0.8 °C in AA and 1.1 °C in BP (Table 2).

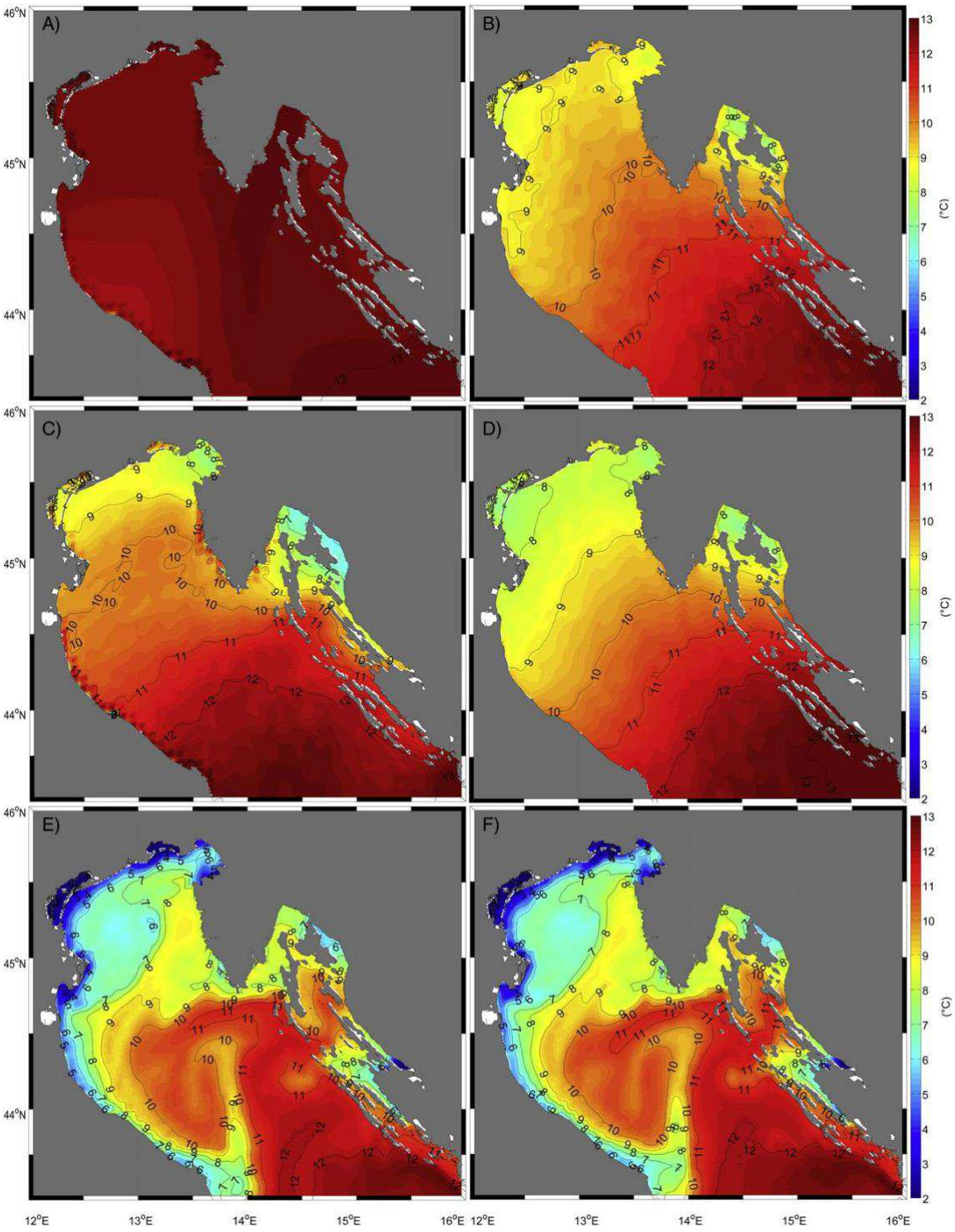

Fig. 5. Sea surface temperature (°C) at the peak of CAO, at 00:00 UTC, February 6. Panels represent, respectively, runs GFS (A), STA (B), OML (C), DYN (D), AO (E) and AOW (F) (see Table 1).

However, the relatively coarse resolution of the field prevents from an accurate representation of SST features near the coasts of the central Adriatic, where the smaller scale patterns characterizing the ocean circulation in that area (O'Neill et al., 2005) cannot be properly resolved by satellite. As a consequence, the SST is still strongly overestimated near Ancona (cf. Fig. 5d with Fig. 4e,f and Table 2). Finally, AO and AOW runs show similar results and appear to be the closest to the point measurements over the basin, being characterized by a bias of −1 °C at AA, 0.6 °C at BP and 0.2 °C in Ancona (Table 2). In particular, the improvement compared to all the "stand-alone" runs is very high especially in the central Adriatic area. Moreover, the spatial distribution and temporal evolution of SST seem to be more accurate and consistent with the oceanic structures observed in the Adriatic basin during such events (O'Neill et al., 2005). These mesoscale features are known to be responsible for a substantial change in heat and moisture fluxes in the proximity of the coast, leading to the formation of a significant amount of dense waters in the northern basin (Benetazzo et al., 2014). Fig. 6 shows the 10 m wind vectors in the northern Adriatic at the same time as Fig. 5 (00:00 UTC, 6 February 2012) for the six simulations. Modeled wind fields are very similar among the different runs, showing substantially the same patterns in terms of speed and direction.

Run	AA Bias			BP Bias			AN Bias		
	Initial time	Peak (06 February, 00 UTC)	Average	Initial time	Peak (06 February, 00 UTC)	Average	Initial time	Peak (06 February, 00 UTC)	Average
GFS	5.9	3.5	5.9	3.6	6.3	3.6	3.6	4.6	3.9
STA	3.7	2.6	3.7	1.3	3.3	1.3	5.8	8.0	5.2
OML	3.7	0.6	3.1	1.3	0.6	3.1	5.8	6.4	7.8
DYN	3.7	0.9	0.8	1.3	0.5	1.1	5.8	6.1	6.0
AO	0.4	1.9	−0.9	−0.5	−1.4	−0.6	−0.2	0.1	0.2
AOW	0.4	2.0	−0.9	−0.5	−1.4	−0.6	−0.2	0.1	0.2

Table 2. Statistical results for SST in all experiments. The bias in SST (simulated minus observed values) at the starting time (left column), at the peak of the cold air outbreak (6 Feb., 00 UTC) (mid-dle column), and the average bias over the whole simulation duration right column) in the various runs are shown for the measurement stations (AA, BP, AN).

Thus, the presence of different SST fields apparently affects the low-level flow only to a lesser extent. Standing the very intense wind speed characterizing the CAO, it is somewhat expected that the synoptic-scale forcing prevails over the possible influence of SST on the air–sea interactions. The largest (albeit not very large) differences in the wind fields among the simulations are registered slightly out of the major Bora jets, as in the vicinity of the Po Delta-Istria section, where the wind speed is smaller and the air–sea interaction processes are able to exert their influence for a longer time. The comparison between the simulated and the observed time series in the stations considered here is shown in Fig. 7 for the AA and BP stations. From Fig. 7 (upper panels) it is possible to conclude that at BP the wind is generally overestimated in all runs, on average by more than 2 m/s

during the most intense CAO phase, between February 2 and 13. Being BP located very close to the northeastern coast, on the lee side of the steep orography of the Karst region, the station is indeed marginally influenced by the air–sea interaction processes. We argue that the overestimation may be due to a well-acknowledged modeling problem, namely the underestimation of the surface sub-grid roughness in WRF, which is known to occur in mountainous areas (Jiménez and Dudhia, 2012). On the contrary, AA is located on the West Coast, after the airflow has crossed the Adriatic, and a more relevant influence of the air–sea exchange is expected. Thus, the model underestimation of the wind field observed in the latter station for most of the simulation period, as shown in Fig. 7 (bottom panels), can be ascribed to the Charnock formula adopted in WRF, which is known to overestimate the sea surface roughness for large wind speeds (see Davis et al., 2008; Kim and Hong, 2010). Differences in the 10 m wind fields between the coupled runs AO and AOW appear negligible (Fig. 6e,f). The main effect of the inclusion of the waves is a slight rotation of wind direction and a slight change in Bora jet magnitude in run AOW,2 which can however hardly be detected from Fig. 6. Figs. 8 and 9 show respectively the snapshot of 2 m air temperature in the different runs at 00:00 UTC, February 6, and the 2 m temperature observations in the different "in situ" stations in comparison with the model data. The simulated temperature fields are very similar in the northern Adriatic, whereas in the central region they show larger differences (of about 2 °C on average). The different response in the different sub-regions of the basin is a consequence of the dominant processes in the two areas. The very intense Bora wind affects mainly the northern region, and synoptic-scale processes are dominant over air–sea interaction. Advection is represented in a similar way by the different runs, as it depends mainly on the large-scale forcing, thus all simulations provide very similar 2 m temperatures in BP for all their duration (Fig. 9). At AA, the situation is slightly different with respect to BP since, before reaching the western Adriatic coast where AA is located, the airflow from the Balkans interacts for a longer period with the sea surface. The effect of the air–sea interaction is thus more relevant in AA, and the spread among the simulations is more evident, showing more clearly the benefit of adopting a more realistic SST field compared to the BP station. Finally, the fetch in the central Adriatic is much longer compared to the northern basin, thus the air–sea interactions have more time to develop and their effect becomes evident in AN station. The air–sea exchange depends on SST, which differs significantly among the simulations; thus, in AN, the spread is larger (Fig. 9), and coupled runs can generally discriminate better the temperature evolution. This improvement is a consequence of the mesoscale sea patterns and in particular of the cold coastal features near the western Adriatic coast, which are better discriminated in the coupled runs while they are absent in the other simulations forced with radiometer or static data (Fig. 5). The sum of the sensible and latent heat fluxes (namely, total turbulent heat fluxes, hereafter THF) at 00:00 UTC,

February 6, is shown in Fig. 10 for all the considered runs. From the definition (bulk formulae), THF depend among others on the difference in temperature and humidity between the sea surface and 2 m height, and on the wind speed. The net fluxes on the northern Adriatic basin are thus strongly affected by the SST field used in the various runs, and, as a consequence, relatively small differences in temperature and humidity can be strongly amplified when combined in THF. The differences among the simulations emerging in Fig. 10 are significant in terms of intensity, while the spatial distribution is rather similar. The GFS case (panel a) is characterized by very intense THF especially in the Gulf of Trieste and in between the Croatian islands, with modeled peak intensity of about 1400 W/m2. THF (absolute) values are higher than in the other runs, on average by about 15–20% over the whole domain, with the Bora jets appearing more intense and wider. The other "stand-alone" simulations (Fig. 10, panels b to d) are also characterized by very intense heat fluxes, with peaks of about 1000–1200 W/m2. On the opposite, the coupled runs (panel e–f) show much lower THF, in particular along the Bora jets, reaching peaks of about 1000 W/m2 only in a few grid points near the Croatian islands, and of about 600–700 W/m2 in the gulf of Trieste. The difference in heat fluxes among the runs is mainly due to SST, which has been shown to exhibit a larger variability compared to the atmospheric variables. In the GFS run, SST is significantly overestimated especially in the coastal strip of the northern Adriatic, where differences of about 6 °C arise at the peak of the event (February 6) in comparison with the observed values. These results are consistent with those reported by Davolio et al. (2015), where different limited area atmospheric model simulations were performed for the same case study analyzed here, starting from different SST provided either by global models or satellite analyses.

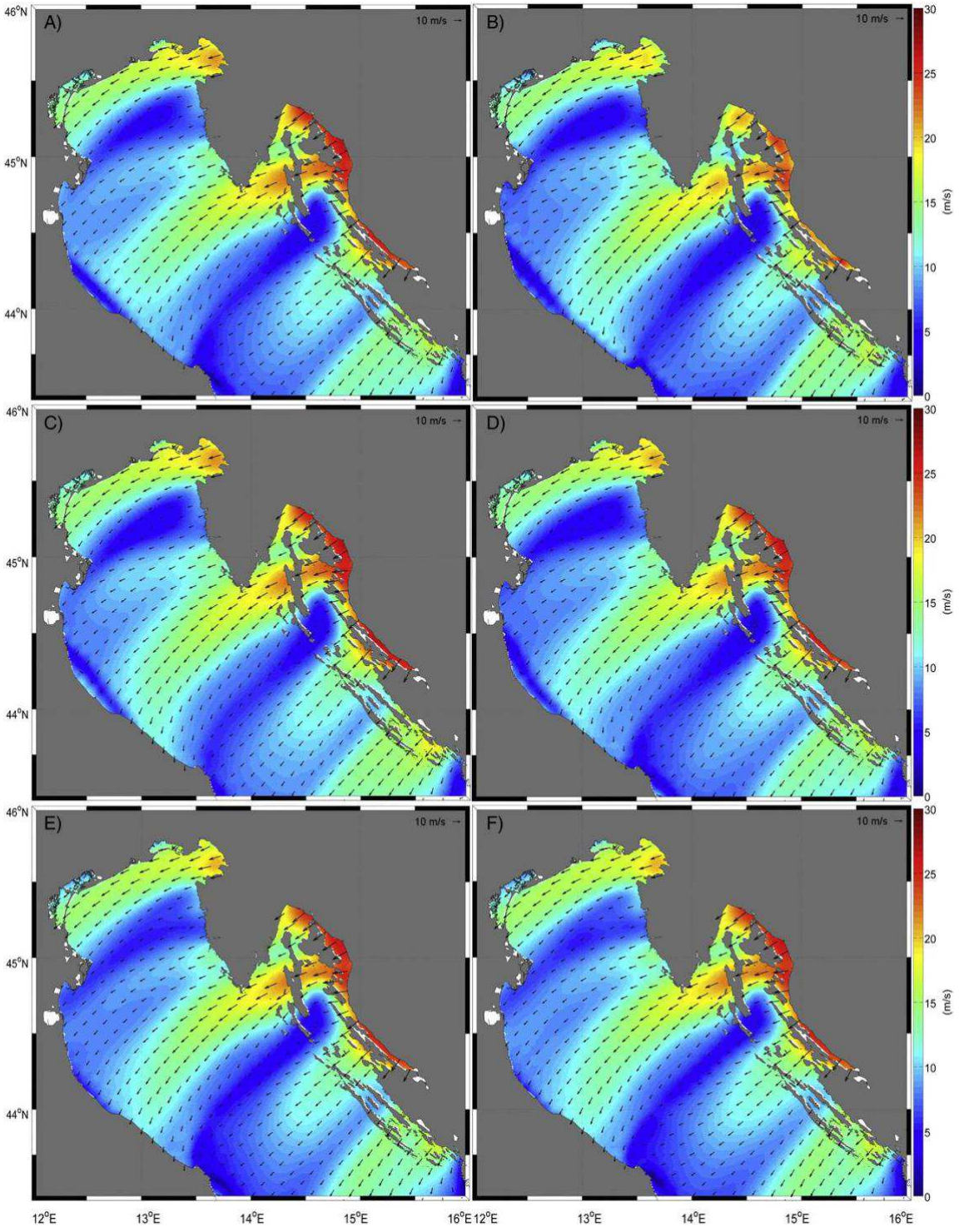

Fig. 6. 10 m wind speed (m s−1) and direction at the peak of CAO, at 00:00 UTC, February 6. Panels represent, respectively, runs GFS (A), STA (B), OML (C), DYN (D), AO (E) and AOW (F) (see Table 1).

Large differences were found in the simulated sensible and latent heat fluxes, showing that the specific SST fields used as initial conditions represent a critical issue for an accurate description of the sea surface fluxes at least for this exceptionally severe event. The warm bias in the SST field provided by GFS is thus in detriment of the model performance. On the other hand the coupled runs shown here, representing more accurately the SST values and its spatial patterns, provide values of THF much closer to the observations.

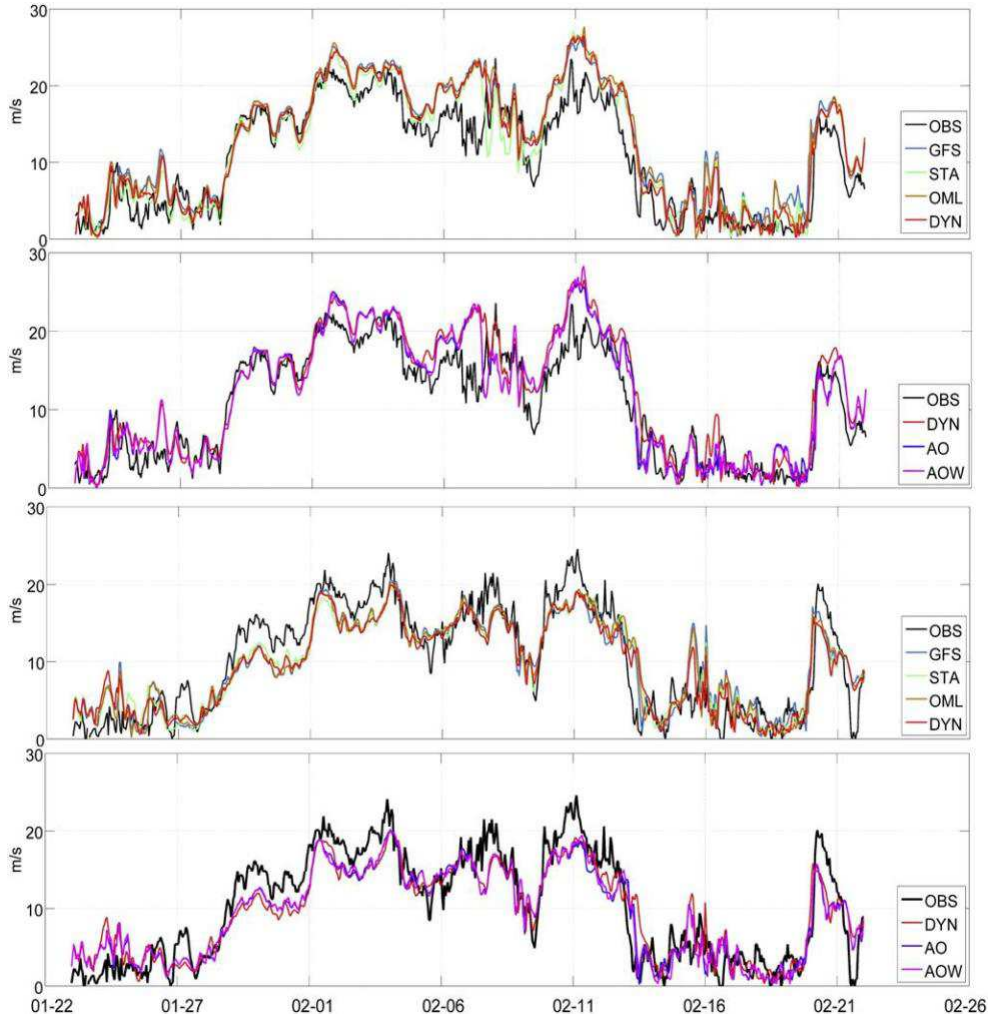

Fig. 7. 10 m wind speed time series at BP (two upper panels) and AA (two lower panels). Run labels are shown in Table 1.

Time series of the simulated heat fluxes compared to observations in the three considered stations (Fig. 11) give a better quantification of the differences among the runs and their modulation time. Although in the northern Adriatic basin the fetch and the effect of the air–sea processes are limited, the spread in SST among the "stand-alone" simulations is remarkable and affects significantly the THF, which are largely overestimated both in BP (two upper panels) and in AA (two central panels). The more detailed SST field in the coupled runs provides a further improvement compared to DYN, showing THF values very close to the observations. On the opposite, in Ancona (Fig. 11, lower panels) the observed net heat fluxes reach 300 W/m2 only during the most intense phase of the event, remaining generally around 100 W/m2. All "stand-alone" simulations generate results similar to each other but all rather distant from the observations, with values of about 700 W/m2 during the peak. Also the DYN experiment strongly overestimates the intensity of the fluxes, confirming that the satellite is not able to reproduce the fine SST pattern observed near the coast. These structures are reproduced only by the coupled simulations (see again Fig. 5), which thus emerge as the only runs capable to simulate THF values that are very close to the measurements. Only minor differences can be depicted when comparing AO and AOW results in all stations (Fig. 11). The inclusion of the wave model in the coupled system does not seem to add relevant information for the THF simulation, at least for this specific case. The Taylor diagram (Fig. 12) summarizes the previous analyses. With the increased realism of the SST provided to the atmospheric model, the 2 m temperature (not shown) standard deviation gets closer to the observations, while the changes are negligible for 10 m wind speed (not shown). By contrast, heat fluxes show a relevant improvement, especially in terms of standard deviation. Particularly at AN, the improvement of THF due to the coupled simulations is indeed very significant. The overall performance of the coupled simulations compared to the "stand-alone" runs suggests that the presence of a realistic SST is crucial for a correct simulation of THF—especially in a basin such as the Adriatic Sea, characterized by a very cold coastal circulation on the Italian side. Such an oceanic current greatly influences the heat fluxes along the Italian Adriatic coastal area, particularly in the central part of the basin, where the onshore SST gradients are very strong and sharper than the spatial resolution of the satellite data. The difficulty in reproducing exactly this circulation, even by means of coupled models, may be responsible for the smaller THF correlation coefficient between simulations and measurements emerging in AN from all runs (see again Fig. 12). In addition, an outstanding element confirming the importance of computing SST within a coupled modeling system lies in the consistent frame of ocean and atmosphere in which energy fluxes are computed, leading to realistic thermodynamic evaluations.

1.7. Discussion

The increasing availability of computational resources allows a wider use of coupled modeling systems to describe atmospheric and marine dynamics. However, several aspects need to be considered when proceeding along this direction. The need for additional data is an obstacle that can be mitigated by the new-generation of operational oceanographic models (Russo et al., 2013) and the standardization of interoperable "large model outputs" (Bergamasco, 2012). It is expected that using such coupled numerical systems should not only improve the description of processes directly linked to the air-water interaction, but also lead to a more realistic prediction of some atmospheric variables depending on it. In our example, the heat fluxes and the vapor fluxes over the sea surface associated with the CAO event, poorly simulated by the operational NWP in 2012, might benefit the proper representation of the coupled air–sea interactions across the Adriatic. The results of the present study could possibly be further improved with the use of grid spacing in the atmospheric model finer than the 7 km actually employed. The finer resolution allows solving with better detail the orographic obstacles delimiting the Adriatic Sea on its eastern side and thus the impact of the orography on the distribution of Bora jets. The limitations in computational time did not allow us to fully explore this aspect, particularly important also when convective processes, which require a grid spacing of few km for being treated explicitly, play an important role. A number of issues of extreme importance for the marine environment would benefit from the availability of a coupled atmosphere– ocean–wave model. Consider for example the processes of preconditioning, generation, formation and dispersion of dense waters in the Adriatic Sea (one of the very few formation basins of dense waters), which are so important for both ecological (deep water ventilation, nutrient transport, and habitat shaping) and hydrological (water transport from the Levantine basin, climatic teleconnections, etc.) aspects. These processes (Benetazzo et al., 2014) have still many aspects to be determined, many of which are linked to the correct estimation of the flows and volumes of water generated during the winter months, which in turn are strongly controlled by thermal and kinetic energy fluxes at the air–sea interface and throughout the water column (Carniel et al., 2015b). Therefore, it appears necessary that they will be properly investigated by means of coupled numerical tools and supported by adequate in situ measurements. Also, the possibility of accurate estimates of wave characteristics provides applications of immediate use, including the determination of safe ship routes, the identification of sea states possibly hampering engineering activities, or useful information for coastal vulnerability assessment, and the definition of shore protection strategies.

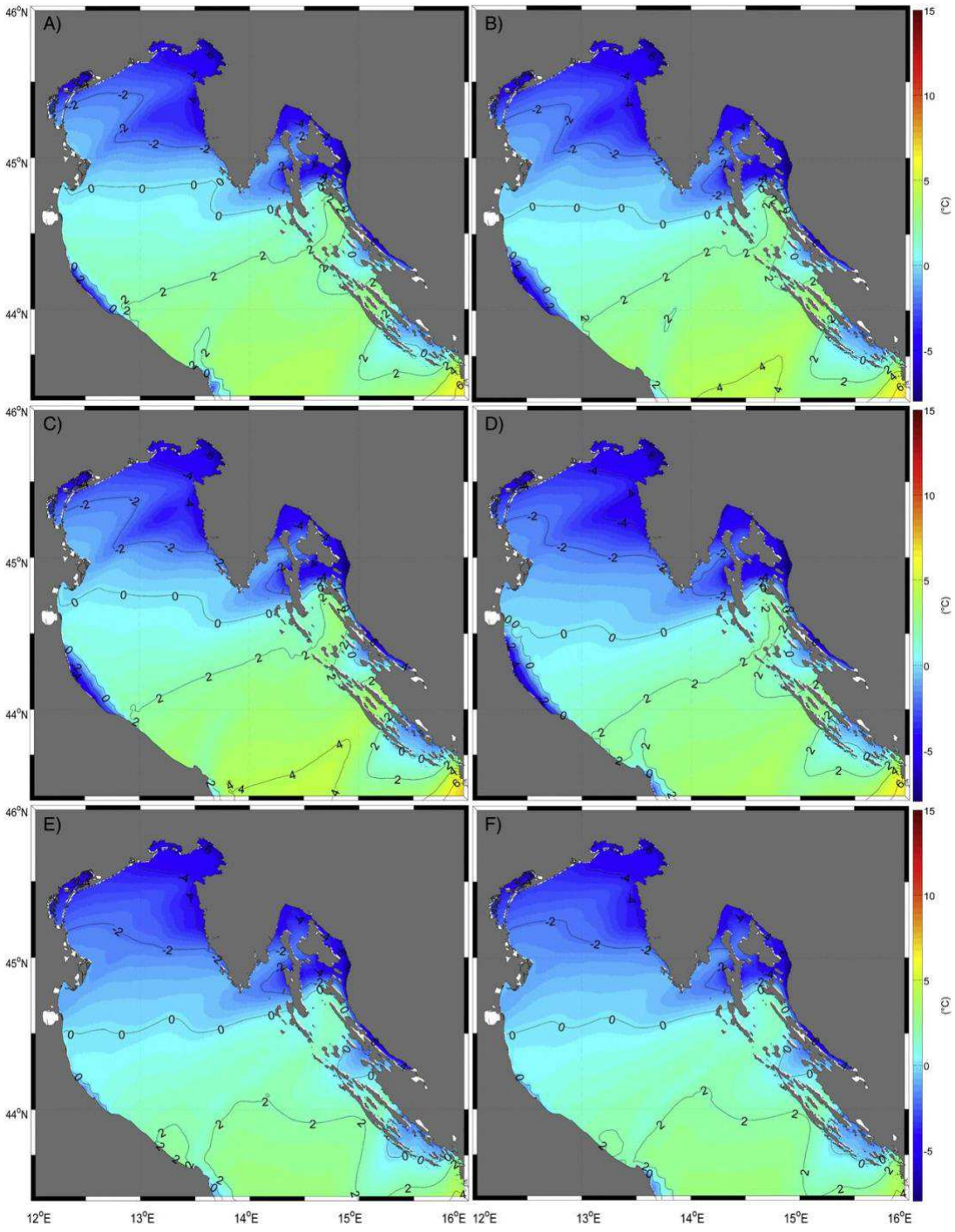

Fig. 8. Two-meter air temperature (°C) at the peak of CAO, at 00:00 UTC, February 6. Panels represent, respectively, runs GFS (A), STA (B), OML (C), DYN (D), AO (E) and AOW (F) (see Table 1).

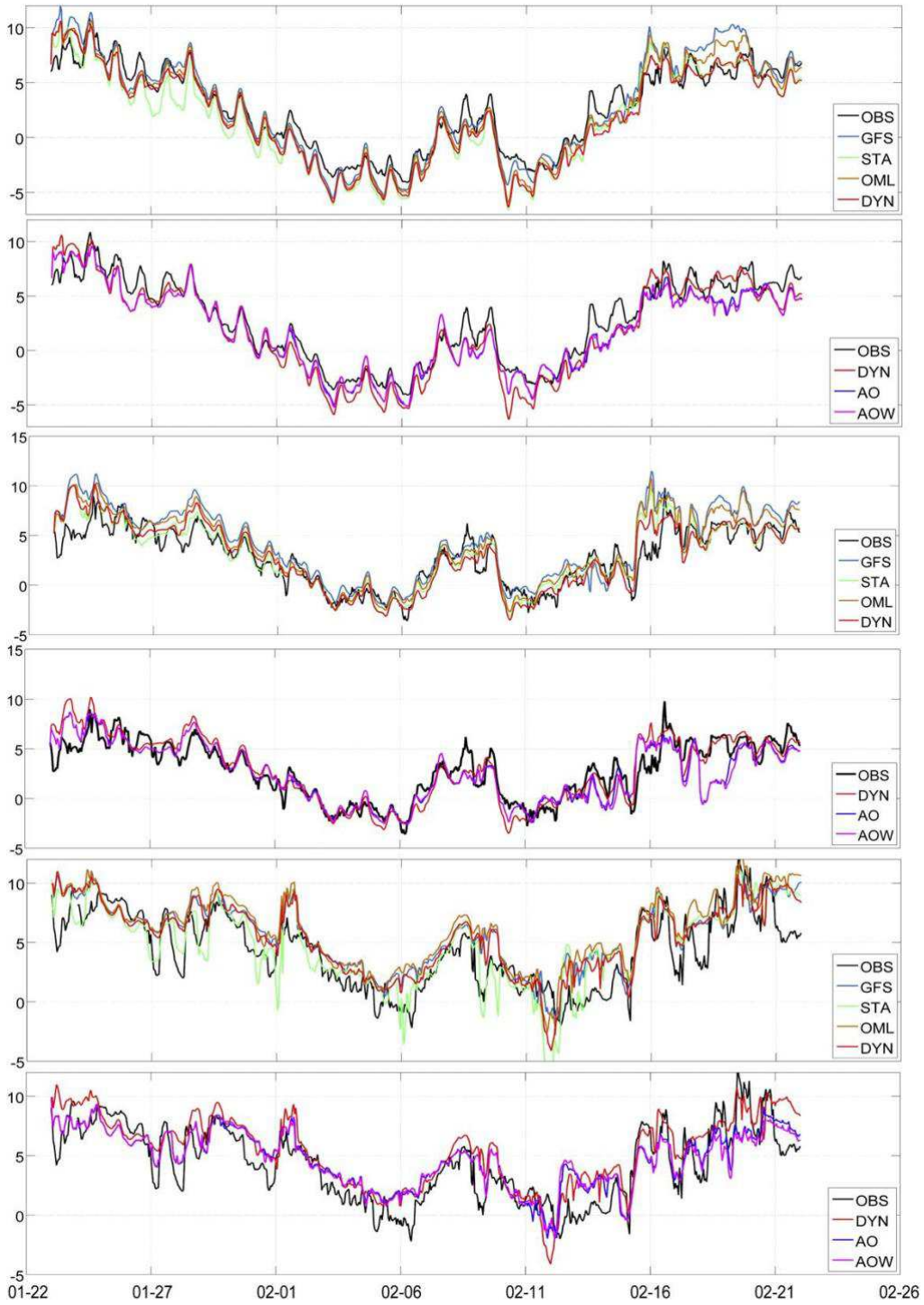

Fig. 9. 2 m air temperature time series at BP (upper two panels), AA (central two panels) and Ancona (lower two panels) stations. Run labels are shown in Table 1.

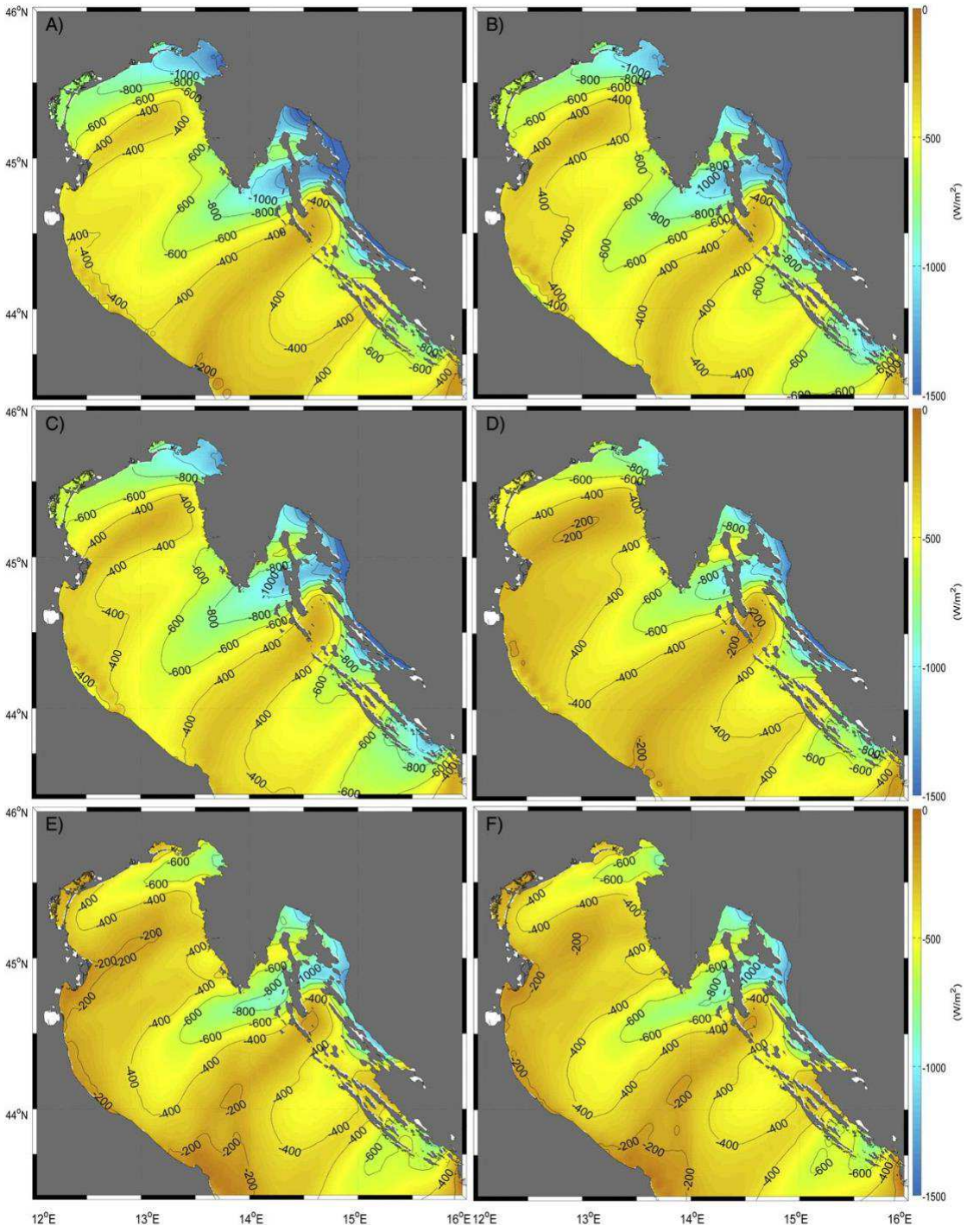

Fig. 10. Turbulent heat fluxes (W/m2) at the peak of CAO, at 00:00 UTC, February 6. Panels represent, respectively, runs GFS (A), STA (B), OML (C), DYN (D), AO (E) and AOW (F) (see Table 1).

1.8. Conclusions

The present paper investigates a case study of persistent cold air outbreak that affected the northern Adriatic basin (northern Mediterranean) for 2 weeks between January and February 2012. Since this case represents one of the most intense CAO events in the last 50 years, it has been analyzed in different studies (e.g., see Mihanović et al., 2013; Janeković et al., 2014; Benetazzo et al., 2014; Davolio et al., 2015), providing a solid background of the general features of the process. In order to understand the effects of air–sea interactions in such an exceptional meteorological phenomenon, here the event is analyzed using the COAWST modeling system for the first time also with a wave–ocean–atmosphere coupled configuration. This system was previously successfully adopted to simulate intense meteo-oceanic phenomena in the Atlantic Ocean (Warner et al., 2010a; Olabarrieta et al., 2012a; Zambon et al., 2014a) and in the Mediterranean Sea (Renault et al., 2012), while recent applications in the Adriatic Sea mainly focused on the effect of wave–current interactions (Benetazzo et al., 2013) on tracers and sediment transport processes (Sclavo et al., 2013), and on the formation and fate of dense waters (Benetazzo et al., 2014; Carniel et al., 2015a). In particular, the work first explores the effect related to the use of different SST fields as initial and boundary conditions, in some purely atmospheric (WRF model) simulations, carried out without coupling (stand-alone runs). The simulation results are compared with data from coastal platforms and buoys located in the northern and central Adriatic, allowing some insight on the spatial scale and the along-axis variability of the effects of the SST forcing. The use of a satellite retrieved high-resolution SST field, regularly updated in time (run DYN), significantly improves the simulation of turbulent heat fluxes compared to runs performed with constant and/or low resolution SST. In fact, a static prescription of the initial SST field throughout the whole simulation period (runs GFS and STA) is shown to induce an incorrect representation of the air–sea exchanges, especially during intense events. A simplified ocean model is also tested to continuously update the SST (run OML), however the oversimplification of the model formulation improves only marginally the results compared to the ones obtained by using a constant SST. The improvement induced by the ingestion of a fine scale, 6-hourly updated SST (run DYN) represents an important indication of the necessity of using realistic and dynamic SST fields in numerical simulations, as already noted for intense events in the Mediterranean. Unfortunately, the resolution of the SST retrieved from satellite (8.3 km from satellite interpolated at 7 km over WRF grid) in run DYN is still too coarse to properly reproduce mesoscale and smaller scale coastal features in central Adriatic.

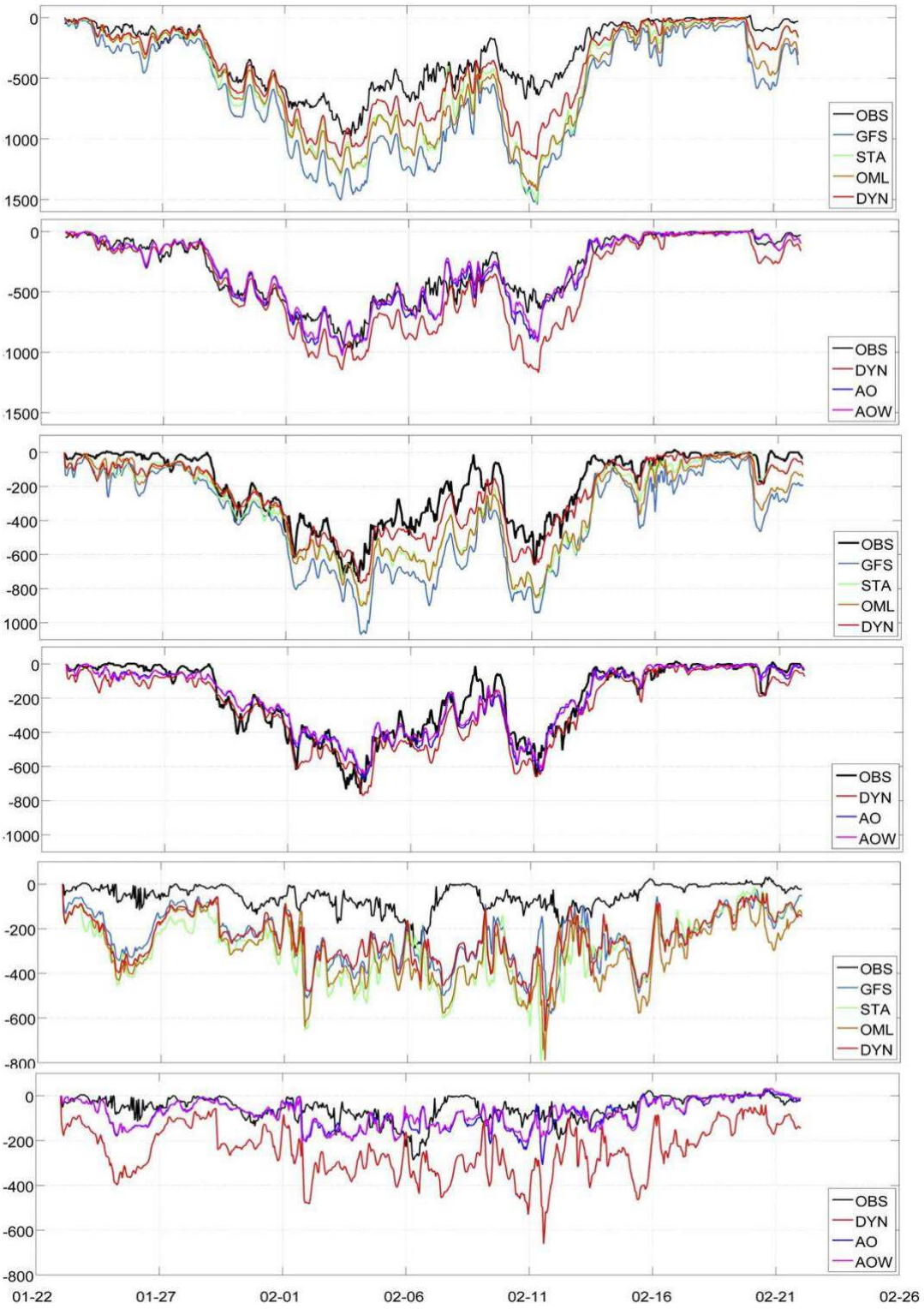

Fig. 11. Turbulent heat fluxes time series at BP (upper two panels), AA (central two panels) and Ancona (lower two panels) stations. Run labels are shown in Table 1.

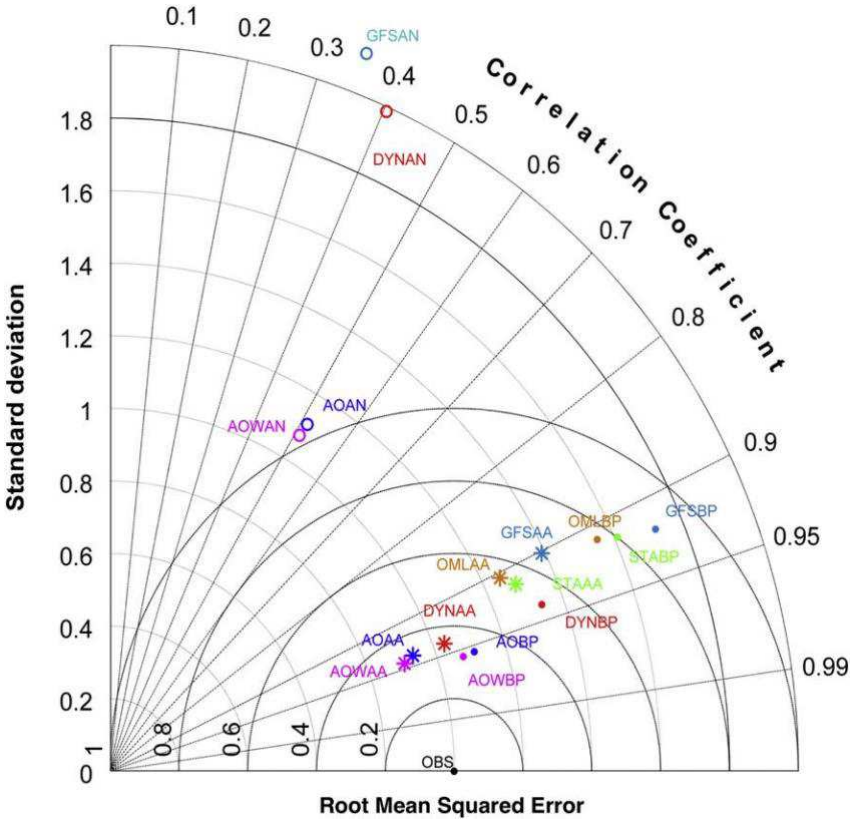

Fig. 12. Taylor diagram relative to THF. The colors and initial letter refer to the different model simulations (see Table 1). The last two letters refer to the station (AA = Acqua Alta Platform; BP = Paloma buoy; AN = Ancona).

The coupled runs clearly show how the effect of a high-resolution SST, updated consistently with ocean circulation and wave dynamics, is relevant in particular for the determination of the heat fluxes, while it is less important for other atmospheric variables, such as 2 m temperature and 10 m wind. This happens because in a semi-enclosed basin of relatively small dimensions, such as the northern Adriatic, and during a very intense and prolonged event characterized by strong directional persistence, 10 m wind and 2 m temperatures are mostly influenced by the synoptic-scale atmospheric circulation rather than by factors at a local scale (Zambon et al., 2014b). By contrast, specific and latent heat fluxes are driven by SST, exhibiting a strong horizontal gradient throughout the basin, and therefore are strongly sensitive to the way and the space–time resolution by which SST is described and sampled in the model. Among other advantages, a coupled system carries out the calculation of heat fluxes in the ocean and in the atmosphere consistently. In addition, the use of the wave model allows properly considering the wave steepness into the calculation of the sea surface roughness (although this effect appears, at least for this case study, relatively minor). In conclusion, despite the difficulties still inherent in the implementation of a coupled approach, the availability of a validated ocean– atmosphere–wave numerical system appears to be as an important achievement for the

scientific and operational communities. In this study, we do not analyze the results in terms of precipitation because during this atmospheric event the rainfall was almost completely snowy. Unfortunately it is extremely difficult to find snow depths data (recorded and reliable), so the comparisons would have been extremely distorted and unreliable.

References

Akhtar, N., Brauch, J., Dobler, A., Béranger, K., Ahrens, B., 2014. Medicanes in an ocean–atmosphere coupled regional climate model. Nat. Hazards Earth Syst. Sci. Discuss. 2, 2117–2149. http://dx.doi.org/10.5194/nhessd-2-2117-2014.

Benetazzo, A., Fedele, F., Carniel, S., Ricchi, A., Bucchignani, E., Sclavo, M., 2012. Wave climate of the Adriatic Sea: a future scenario simulation. Nat. Hazards Earth Syst. Sci. 12, 2065–2076.

Benetazzo, A., Carniel, S., Sclavo, M., Bergamasco, A., 2013. Wave–current interaction: effect on the wave field in a semi-enclosed basin. Ocean Model. 70, 152–165. http://dx. doi.org/10.1016/j.ocemod.2012.12.009.

Benetazzo, A., Bergamasco, A., Bonaldo, D., Falcieri, F.M., Sclavo, M., Langone, L., Carniel, S., 2014. Response of the Adriatic Sea to an intense cold air outbreak: dense water dynamics and wave-induced transport. Prog. Oceanogr. 128, 115–138. http://dx.doi. org/10.1016/j.pocean.2014.08.015.

Bergamasco, M., 2012. Continuous time model identification with applications to rotorcraft dynamics PhD Thesis, Politecnico di Milano.

Bignami, F., Sciarra, R., Carniel, S., Santoleri, R., 2007. Variability of Adriatic Sea coastal turbid waters from SeaWiFS imagery. J. Geophys. Res. 112, C03S10. http://dx.doi.org/10. 1029/2006JC003518.

Boldrin, A., Carniel, S., Giani, M., Marini, M., Bernardi Aubry, F., Campanelli, A., Grilli, F., Russo, A., 2009. Effects of Bora wind on physical and biogeochemical properties of stratified waters in the northern Adriatic. J. Geophys. Res. 114, C08S92. http://dx. doi.org/10.1029/2008JC004837.

Booij, N., Holthuijsen, L.H., Ris, R.C., 1996. The "SWAN" wave model for shallow water. Coast. Eng. Proc. http://dx.doi.org/10.9753/icce.v25.%p.

Camuffo, D., 1987. Freezing of the venetian lagoon since the 9th century AD in comparison to the climate of western Europe and England. Clim. Chang. 10, 43–66.

Carniel, S., Warner, J., Chiggiato, J., Sclavo, M., 2009. Investigating the impact of surface wave breaking on modelling the trajectories of drifters in the northern Adriatic sea during a wind-storm event. Ocean Model. 30, 225–239. http://dx.doi.org/10.1016/j. ocemod.2009.07.001.

Carniel, S., Benetazzo, A., Bergamasco, A., Boldrin, A., Bonaldo, D., Falcieri, F., Langone, L., Sclavo, M., 2015a. Off-shelf fluxes across the southern Adriatic margin: forcing factors controlling densewater-driven transport phenomena. Mar. Geol. http://dx.doi.org/10. 1016/j.margeo.2015.08.016.

Carniel, S., Benetazzo, A., Bonaldo, D., Falcieri, F.M., Miglietta, M.M., Ricchi, A., Sclavo, M., 2015b. Analysis of a Dense Water Formation Event Using a Coupled Modeling System, Ocean Modelling (in press).

Charnock, H., 1955. Wind stress on a water surface. Quart. J. Roy. Meteorol. Soc. 81, 639–640.

Chen, F., Mitchell, K., Schaake, J., Xue, Y., Pan, H., Koren, V., Duan, Y., Ek, M., Betts, A., 1996. Modeling of land-surface evaporation by four schemes and comparison with FIFE observations. J. Geophys. Res. 101, 7251–7268. Cohen, A.E., Cavallo, S.M., Coniglio, M.C., Brooks, H.E., 2015. A review of planetary boundary layer parameterization schemes and their sensitivity in simulating a southeast U.S. cold season severe weather environment. Weather Forecast. http://dx.doi.org/ 10.1175/WAF-D-14-00105.1 (150224120634008).

Davis, C., Wang, W., Chen, S.S., Chen, Y., Corbosiero, K., DeMaria, M., Dudhia, J., Holland, G., Klemp, J., Michalakes, J., Reeves, H., Rotunno, R., Snyder, C., Xiao, Q., 2008. Prediction of landfalling hurricanes with the advanced hurricane WRF model. Mon. Weather Rev. 136, 1990–2005. http://dx.doi.org/10.1175/ 2007MWR2085.1.

Davolio, S., Stocchi, P., Benetazzo, A., Bohm, E., Riminucci, F., Ravaioli, M., Li, X.-M., Carniel, S., 2015. Exceptional Bora outbreak in winter 2012: validation and analysis of high-resolution atmospheric model simulations in the northern Adriatic area. Dyn. Atmos. Oceans 71, 1–20. http://dx.doi.org/10.1016/j.dynatmoce. 2015.05.002.

Dorman, C.E., et al., 2006. February 2003 marine atmospheric conditions and the bora over the northern Adriatic. J. Geophys. Res. 111, C03S03. http://dx.doi.org/10.1029/ 2005JC003134.

Dubois, C., Somot, S., Calmanti, S., Carillo, a., Déqué, M., Dell'Aquilla, a., Elizalde, a., Gualdi, S., Jacob, D., L'Hévéder, B., Li, L., Oddo, P., Sannino, G., Scoccimarro, E., Sevault, F., 2012. Future projections of the surface heat and water budgets of the Mediterranean Sea in an ensemble of coupled atmosphere–ocean regional climate models. Clim. Dyn. 39, 1859–1884. http://dx.doi.org/10.1007/s00382-011-1261-4.

Dudhia, J., 1989. Numerical study of convection observed during theWinter Monsoon Experiment using a mesoscale two-dimensional model. J. Atmos. Sci. 46, 3077–3107. Fairall, C.W., Bradley, E.F., Rogers, D.P., Edson, J.P., Young, G.S., 1996. Bulk parameterization of air–sea fluxes in TOGA COARE. J. Geophys. Res. 101, 3747–3767.

Fita, L., Fernández, J., García-Díez, M., 2010. CLWRF: WRF modifications for regional climate simulation under future scenarios. Proc 11th WRF Users' Workshop, 21−25 June 2010. Boulder, CO.

Gemmill, W., Katz, B., Li, X., 2007. Daily Real-Time Global Sea Surface Temperature, A High-Resolution Analysis. RTG_SST_RH, NOAA/NWS/NCEP/MMAB Technical Note. 260 39 pp. Haidvogel, D.B., Beckmann, A., 1999. Numerical Ocean Circulation Modelling. Imperial College Press, p. 318.

Haidvogel, D.B., Arango, H., Budgell, W.P., Cornuelle, B.D., Curchitser, E., Di Lorenzo, E., Fennel, K., Geyer, W.R., Hermann, A.J., Lanerolle, L., Levin, J., McWilliams, J.C., Miller, A.J., Moore, A.M., Powell, T.M., Shchepetkin, A.F., Sherwood, C.R., Signell, R.P., Warner, J.C., Wilkin, J., 2008. Ocean forecasting in terrain-following coordinates: formulation and skill assessment of the regional ocean modeling system. J. Comput. Phys. 227, 3595–3624. http://dx.doi.org/10.1016/j.jcp.2007.06.016.

Horvath, K., Bajić, A., Ivatek-Šahdan, S., 2011. Dynamical downscaling of wind speed in complex terrain prone to Bora-type flows. J. Appl. Meteorol. Climatol. 50, 1676–1691. http://dx.doi.org/10.1175/2011JAMC2638.1.

Janeković, I., Mihanović, H., Vilibić, I., Tudor, M., 2014. Extreme cooling and dense water formation estimates in open and coastal regions of the Adriatic sea during the winter of 2012. J. Geophys. Res. Oceans 119, 3200–3218. http://dx.doi.org/ 10.1002/2014JC009865.

Janjić, Z.I., 1990. The step-mountain coordinate: physical package. Mon. Weather Rev. 118, 1429–1443. http://dx.doi.org/10.1175/1520-0493 ((1990)118b1429:TSMCPP2.0.CO;2).

Janjić, Z.I., 1994. The step-mountain eta coordinate model: further developments of the convection, viscous sublayer, and turbulence closure schemes. Mon. Weather Rev. http://dx.doi.org/10.1175/1520-0493(1994)122b0927:TSMECMN2.0.CO;2.

Jiménez, P.A., Dudhia, J., 2012. Improving the representation of resolved and unresolved topographic effects on surface wind in the WRF model. J. Appl. Meteorol. Climatol. 51, 300–316. http://dx.doi.org/10.1175/JAMC-D-11-084.1.

Jullien, S., Marchesiello, P., Menkes, C.E., Lefèvre, J., Jourdain, N.C., Samson, G., Lengaigne, M., 2014. Ocean feedback to tropical cyclones: climatology and processes. Clim. Dyn. 43, 2831–2854.

Kain, J.S., 2004. The Kain–Fritsch convective parameterization: an update. J. Appl. Meteorol. 43, 170–181.

Kim, E.-J., Hong, S.-Y., 2010. Impact of air–sea interaction on east Asian summer monsoon climate in WRF. J. Geophys. Res. 115, D19118. http://dx.doi.org/10.1029/2009JD013253.

Komen, G.J., Cavaleri, L., Donelan, M., Hasselmann, K., Hasselmann, S., Janssen, P.A.E.M., 1994. Dynamics and Modelling of Ocean Waves.

Koren, V., Schaake, J., Mitchell, K., Duan, Q.-Y., Chen, F., 1999. A parameterization of snowpack and frozen ground intended for NCEP weather and climate models. J. Geophys. Res. 104, 19569–19585.

Kumar, N., Voulgaris, G., Warner, J.C., Olabarrieta, M., 2012a. Implementation of the vortex force formalism in the coupled ocean–atmosphere–wave–sediment transport (COAWST) modeling system for inner shelf and surf zone applications. Ocean Model. 47, 65–95. http://dx.doi.org/10.1016/j.ocemod.2012.01.003.

Lin, Y.-L., Farley, R.D., Orville, H.D., 1983. Bulk parameterization of the snow field in a cloud model. J. Clim. Appl. Meteorol. 22, 1065–1092. http://dx.doi.org/10.1175/ 1520-0450(1983)022b1065:BPOTSFN2.0.CO;2.

Liu, A.Q., Moore, G.W.K., 2004. Lake-Effect Snowstorms over Southern Ontario, Canada, and Their Associated Synoptic-Scale Environment. Mon. Weather Rev. 132, 2595–2609.

Loglisci, N., Qian, M.W., Rachev, N., Cassardo, C., Longhetto, A., Purini, R., Trivero, P., Ferrarese, S., Giraud, C., 2004. Development of an atmosphere–ocean coupled model and its application over the Adriatic sea during a severe weather event of Bora wind. J. Geophys. Res. 109, D01102. http://dx.doi.org/10.1029/2003JD003956.

McWilliams, J.C., Restrepo, J.M., Lane, E.M., 2004. An asymptotic theory for the interaction of waves and currents in coastal waters. J. Fluid Mech. 511, 135–178. http://dx.doi. org/10.1017/S0022112004009358.

Miglietta, M.M., Moscatello, A., Conte, D., Mannarini, G., Lacorata, G., Rotunno, R., 2011. Numerical analysis of a Mediterranean 'hurricane' over south-eastern Italy: sensitivity experiments to sea surface temperature. Atmos. Res. 101, 412–426.

Miglietta, M.M., Laviola, S., Malvaldi, A., Conte, D., Levizzani, V., Price, C., 2013. Analysis of tropical-like cyclones over the Mediterranean Seathrough a combined modeling and satellite approach. Geophys. Res. Lett. 40, 2400–2405. http://dx.doi.org/10.1002/grl.50432.

Miglietta, M.M., Mastrangelo, D., Conte, D., 2015. Influence of physics parameterization schemes on the simulation of a tropical-like cyclone in the Mediterranean Sea. Atmos. Res. 153, 360–375. http://dx.doi.org/10.1016/j.atmosres.2014.09.008.

Mihanović, H., Vilibić, I., Carniel, S., Tudor, M., Russo, A., Bergamasco, A., Bubić, N., Ljubešić, Z., Viličić, D., Boldrin, A., Malačič, V., Celio, M., Comici, C., Raicich, F., 2013. Exceptional dense water formation on the Adriatic shelf in the winter of 2012. Ocean Sci. 9, 561–572. http://dx.doi.org/10.5194/os-9-561-2013.

Mlawer, E.J., Taubman, S.J., Brown, P.D., Iacono, M.J., Clough, S.A., 1997. Radiative transfer for inhomogeneous atmosphere: RRTM, a validated correlated-k model for the longwave. J. Geophys. Res. 102, 16663–16682. Moscatello,

A., Miglietta, M.M., Rotunno, R., 2008. Numerical analysis of a Mediterranean "hurricane" over south-eastern Italy. Mon. Weather Rev. 136, 4373–4397.

Nakanishi, M., Niino, H., 2009. Development of an improved turbulence closure model for the atmospheric boundary layer. J. Meteorol. Soc. Jpn. 87, 895–912. http://dx.doi.org/10.2151/jmsj.87.895.

Nakanishi, M., Niino, H., 2006. An improved Mellor-Yamada level-3 model: its numerical stability and application to a regional prediction of advection fog. Bound.-Layer Meteorol. 119, 397–407. http://dx.doi.org/10.1007/s10546-005-9030-8.

Olabarrieta, M., Warner, J.C., Armstrong, B., Zambon, J.B., He, R., 2012a. Ocean–atmosphere dynamics during hurricane Ida and nor'Ida: an application of the coupled ocean– atmosphere–wave–sediment transport (COAWST) modeling system. Ocean Model. 43-44, 112–137. http://dx.doi.org/10.1016/j.ocemod.2011.12.008.

O'Neill, L.W., Chelton, D.B., Esbensen, S.K., Wentz, F.J., 2005. High-resolution satellite measurements of the atmospheric boundary layer response to SST variations along the Agulhas return current. J. Clim. 18, 2706–2723. http://dx.doi.org/10.1175/JCLI3415.1.

Oost, W.A., Komen, G.J., Jacobs, C.M.J., Van Oort, C., 2002. New evidence for a relation between wind stress and wave age from measurements during ASGAMAGE. Bound Layer Meteorol. 103, 409–438. Pinardi, N., Allen, I., Demirov, E., Mey, P.D., Korres, G., Lascaratos, A., Traon, P.-Y.L.,

Maillard, C., Manzella, G., Tziavos, C., 2003. The Mediterranean ocean forecasting system: first phase of implementation (1998–2001). Ann. Geophys. 21, 3–20.

Pollard, R.T., Rhines, P.B., Thompson, R.O.R.Y., 1972. The deepening of the wind-mixed layer. Geophys. Astrophys. Fluid Dyn. 4, 381–404.

Pullen, J., Doyle, J.D., Signell, R.P., 2006. Two-way air–sea coupling: a study of the Adriatic. Mon. Weather Rev. 134, 1465–1483. http://dx.doi.org/10.1175/MWR3137.1.

Pullen, J., Doyle, J.D., Dorman, C., Signell, R.P., Haack, T., Lee, C.M., 2007. Bora event variability and the role of air–sea feedback. J. Geophys. Res. 112, C03S18. http://dx.doi.org/10.1029/2006JC003726.

Raicich, F., Malačič, V., Celio, M., Giaiotti, D., Cantoni, C., Colucci, R.R., Čermelj, B., Pucillo, A., 2013. Extreme air–sea interactions in the gulf of Trieste (north Adriatic) during the strong Bora event in winter 2012. J. Geophys. Res. Oceans 118, 5238–5250. http:// dx.doi.org/10.1002/jgrc.20398.

Renault, L., Chiggiato, J., Warner, J.C., Gomez, M., Vizoso, G., Tintoré, J., 2012. Coupled atmosphere–ocean–wave simulations of a storm event over the Gulf of Lion and Balearic Sea. J. Geophys. Res. Oceans 117. http://dx.doi.org/10.1029/2012JC007924 (n/a–n/a).

Russo, A., Coluccelli, A., Carniel, S., Benetazzo, A., Valentini, A., PAccagnella, T., Ravaioli, M., Bortoluzzi, G., 2013. Operational models hierarchy for short term marine predictions: the Adriatic Sea example. OCEANS-Bergen MTS/IEEE.

Sclavo, M., Benetazzo, A., Carniel, S., Bergamasco, A., Falcieri, F.M., Bonaldo, D., 2013. Wave-current interaction effect on sediment dispersal in a shallow semi-enclosed basin. J. Coast. Res. 65, 1587–1592. http://dx.doi.org/10.2112/SI65-268.1.

Shchepetkin, A.F., McWilliams, J.C., 2005. The regional oceanic modeling system (ROMS): a split-explicit, free-surface, topography-following-coordinate oceanic model. Ocean Model. 9, 347–404. http://dx.doi.org/10.1016/j.ocemod.2004.08.002.

Signell, R.P., Carniel, S., Cavaleri, L., Chiggiato, J., Doyle, J.D., Pullen, J., Sclavo, M., 2005. Assessment of wind quality for oceanographic modelling in semi-enclosed basins. J. Mar. Syst. 53, 217–233. http://dx.doi.org/10.1016/j.jmarsys.2004.03.006.

Skamarock, W.C., Klemp, J.B., Dudhia, J., Gill, D.O., Barker, D.M., Wang, W., Powers, J.G., 2005. A Description of the Advanced Research WRF Version 2.

Uchiyama, Y., McWilliams, J.C., Shchepetkin, A.F., 2010. Wave–current interaction in an oceanic circulation model with a vortex-force formalism: Application to the surf zone. Ocean Model. 34, 16–35.

Umlauf, L., Burchard, H., 2003. A generic length-scale equation for geophysical turbulence models. J. Mar. Res. 61 (2), 235–265. http://dx.doi.org/10.1357/002224003322005087. Wamdi Group, 1988. The WAM model-a third generation ocean wave prediction model.

J. Phys. Oceanogr. 18, 1775–1810. Warner, J.C., Sherwood, C.R., Arango, H.G., Signell, R.P., 2005. Performance of four turbulence closure models implemented using a generic length scale method. Ocean

Model. 8 (1–2), 81–113. http://dx.doi.org/10.1016/j.ocemod.2003.12.003. Warner, J.C., Armstrong, B., He, R., Zambon, J.B., 2010a. Development of a coupled ocean– atmosphere–wave–sediment transport (COAWST) modeling system. Ocean Model.

35, 230–244. http://dx.doi.org/10.1016/j.ocemod.2010.07.010. Winterbottom, H.R., Uhlhorn, E.W., Chassignet, E.P., 2012. A design and an application of a regional coupled atmosphere–ocean model for tropical cyclone prediction. 4. http://dx.doi.org/10.1029/2012MS000172.

Zambon, J.B., He, R., Warner, J.C., 2014a. Investigation of Hurricane Ivan using the coupled ocean–atmosphere–wave–sediment transport (COAWST) model. Ocean Dyn. 64 (11). http://dx.doi.org/10.1007/s10236–014-0777-7 (10/2014).

Zambon, J.B., He, R., Warner, J.C., 2014b. Tropical to extratropical: marine environmental changes associated with superstorm sandy prior to its landfall. Geophys. Res. Lett. http://dx.doi.org/10.1002/2014GL061357 (n/a–n/a).

2. Scratching beneath the surface while coupling atmosphere, ocean and waves : Analysis on Dense water formation

2.1. Overview

Cold Air Outbreaks (CAOs) over shallow seas may lead to dense water formation episodes, enhancing water, heat, nutrient and sediment exchanges across the continental margin, with associated seabed reshaping. During winter 2012, a CAO episode characterised by exceptional intensity stroke the northern Adriatic Sea, one of the most effective cool engines driving the Mediterranean circulation, providing a paramount opportunity for an integrated investigation of dense shelf water dynamics. In the present study, we describe this event using a fully coupled modeling approach exploring the effects of mutual interactions among atmosphere, ocean currents and sea surface waves, usually not completely accounted for, in the resulting dense water formation. Whilst atmospheric fields appear to be marginally affected by coupled dynamics in the present case, implications for sea surface elevation and circulation are far from negligible. Measurements collected in the northern Adriatic Sea showed that a physically consistent description of energy exchanges between ocean and atmosphere provides an improved estimate of heat fluxes and of air and sea temperatures. In addition, the explicit inclusion of wave action within the modeling system further enhances the modulation of air-sea exchanges and the propagation of its effect along the water column, resulting in a different intensity of northern Adriatic gyres and in different water fluxes flowing through the formation basin. Through these main controls on the water volume involved in the densification process and on the intensity of momentum input and cooling, a coupled modeling strategy accounting for atmosphere-waves-currents interactions can turn out to be crucial for improving the quantification of thermohaline properties and energy content, newly formed dense water mass, and provide a better description of its migration pathways and rates of off-shelf descent. Dense water dynamics are generally acknowledged as one of the main ocean drivers for large-scale circulation and deep sea ventilation around the world (Ivanov et al., 2004). Dense water downflow also acts as a major conveyor for sediment and nutrients off the continental shelf towards the deeper sea (Canals et al., 2006; Tesi et al., 2007; Turchetto et al., 2012; Carniel et al., 2016), thus playing a role in long-term segregation of organic carbon (Malanotte-Rizzoli et al., 2014). On the other hand, this can be seen as a part of a

broader cycle driving off-shelf transport along different morphological features of the continental slope (Carniel et al., 2016) and on-shelf flows due to canyon-induced upwelling (Connolly and Hickey, 2014), being a primary regulator for the seasonal migration of a number of biological species, with paramount ecological consequences on marine trophic networks (Boero, 2015). Furthermore, dense water dynamics and their interactions with large-scale circulation have been identified as a main factor for continental margin reshaping, giving rise to peculiar erosional and depositional bedform patterns (Verdicchio and Trincardi, 2006; Bonaldo et al., 2016).

2.2. Introduction

Dense water formation over continental shelf seas may occur as a response to severe weather events that, under a set of conditions generally identified as "preconditioning" (Vilibic´ and Supic´, 2005), can drastically modify the thermohaline properties of the basin. During these episodes, newly-formed dense water masses tend to sink and flow approaching a geostrophic equilibrium, progressively descending as bottom friction and external forcings (topography singularities, tides, internal waves, etc.) perturb the stream motion. While the mechanisms driving propagation and fate of these masses have been progressively better understood in the last decades (Smith et al., 1975; Griffiths 1986) up to the most recent efforts by Holland (2011), Benetazzo et al. (2014), and Bonaldo et al. (2016), the formation phase needs to be further elucidated. The estimated amount of dense waters produced is indeed rather variable (Herrmann et al., 2008 and Carniel et al., 2016), depending on the relative weight of river discharges, air and sea temperatures and wind-driven circulation (Hansen et al., 2004 and Ivanov et al., 2004) before and during the event. Therefore, this phase is clearly controlled by interacting dynamics involving air and sea, but the extent and the dominant direction of these interactions, as well as the role of waves in their modulation, is much less clear. In addition, modeling approaches commonly used for describing these events are generally based on a one-way coupling (i.e. without any feedback from the ocean to the atmosphere) between atmosphere and sea, resulting in a diagnostic computation of heat fluxes at the interface that does not warrant consistency of the energy budget in the two systems. This notwithstanding, recent efforts have been carried out towards a comprehensive description of air-sea interaction within a coupled modeling framework. By means of the Coupled Ocean-Atmosphere-Wave-Sediment Transport (COAWST, see Warner et al., 2010) modeling system, Renault et al. (2012) explored the implications of these aspects by implementing different modeling strategies for the description of a severe storm occurred in the Mediterranean Sea. As they assessed the effect of improved interface processes on wind fields, sea surface temperature and ocean vertical mixing, the lack of a coupling between ocean and wave models did not allow to

explicitly represent the effect of wave-current interaction, which can play a relevant role in the distribution of kinetic energy along the water column and in the modulation of advective processes at the sub-mesoscale (Carniel et al., 2009; Benetazzo et al., 2013; and Sclavo et al., 2013). In turn, Zambon et al. (2014) recently relied on the same modeling system for investigating the dynamics of a tropical storm evolving into an extratropical superstorm in the Atlantic ocean, in this case with a three-way, full coupling of ocean, atmosphere and waves. In that case, results indicated that there was a dominance of large-scale synoptic circulation over smaller-scale phenomena captured by model coupling in driving the process, implying a limited improvement of overall skills in response to model coupling. A paramount case study for dense water dynamics is provided by an exceptional cooling event that took place in winter 2012, when the intrusion of cold and dry Siberian air masses (a Cold Air Outbreak, CAO hereinafter) induced extremely low temperatures in the north-eastern epi-continental basin of the Mediterranean Sea, namely the Adriatic Sea (Davolio et al., 2015). This gave rise to the formation of an extensive mass of high-density water whose migration across the Adriatic basin was subsequently recorded on the shelf and along the continental margin (Mihanovic´ et al., 2013; Najdek et al., 2014; and Langone et al., 2016). After the work of Mihanovic´ et al. (2013), where heat fluxes resulting from operational models were briefly assessed against measurements, recent estimates on the Adriatic behavior during the 2012 CAO event have been achieved by Janekovic´ et al. (2014) and Benetazzo et al. (2014) based on one-way ocean-atmosphere coupled models (with atmospheric forcing provided respectively by ALADIN/HR and COSMO-I7 limited area models), allowing a deep insight on dense water dynamics at the basin scale. In that context, Benetazzo et al. (2014) highlighted the effect of wave-current interactions in modulating kinetic energy distribution along the water column, with major implications for circulation and advective processes. For the same event, most recent efforts made use of coupled modeling strategies for investigating the effect of explicitly describing air-sea interactions on the evaluation of heat fluxes and evaporation rates (Licˇer et al., 2016). After a first attempt to include the sea surface waves besides the atmospheric processes (Carniel et al., 2015), Ricchi et al. (2016) presented some results following the strategy proposed in this work, although focusing on the implications of different sea surface temperature descriptions for the reproduction of atmospheric dynamics, and validating the modeling tools mostly in the atmospheric compartment. In the present study, using the COAWST coupled atmosphere-wave-ocean modeling system we characterise the interface processes and their role in the mechanisms of dense water formation. In particular, we explore the role of coupled processes in terms of both air-sea exchanges and wave-modulated advective processes, in order to assess their impact on dense water formation rates and extent. In accordance with Warner et al. (2010), Zambon et al. (2014) and Licˇer et al. (2016), results presented here are not accounting for

the relative wind velocity with respect to sea surface currents when computing the surface heat fluxes. Although applied in a different area, the potential impact of surface currents in surface fluxes computations has been recently highlighted by Olita et al (2015), in a purely stand-alone hydrodynamic case. Although resulting effects may be reflecting into potentially relevant physical biological processes at sea as well (primary production, biomass redistribution and export, etc.), we suggest this modification to be included in state-of-the-art coupled modeling suites after careful analysis. Section 2 presents available observations and numerical experiments, results and discussions are grouped into Section 3, and some final considerations are presented in Section 4.

2.3. The 2012 CAO in the northern Adriatic Sea

2.3.1. Observations

The CAO event stroke the NA basin between January 25 and February 14, 2012 (Benetazzo et al., 2014). Although immediately after this period a series of monitoring activities was promoted in the region (see Mihanovic´ et al., 2013 for a complete list), during the proper CAO very few continuous measurements were available in NA, mostly resourcing to the operating coastal observatories (Mihanovic´ et al., 2013; Raicich et al., 2013) represented by the CNR-ISMAR "Acqua Alta" (AA) tower, located in a 17m deep area about 15 km off the town of Venice, and "Paloma" buoy (PB), located in the central part of the Gulf of Trieste, about 10 km west of the town of Trieste (Fig. 1). Whilst details on data acquisition and sensors are given in Mihanovic´ et al. (2013) and Raicich et al. (2013), here we recall the main observed features of this event. A long-lasting (more than 2 weeks) Bora storm, with observed wind speed exceeding 15 m s−1 and gusts up to 29 m s−1 in the northern Adriatic Sea (Davolio et al., 2015), was driven by a persistent pressure gradient associated to a stable anticyclone extending over north-eastern Europe and cyclonic conditions over the Mediterranean Sea. This resulted in cooling and mixing the whole water column and increasing the North Adriatic (NA) salinity, under the joint effect of augmented evaporation and salty water masses intrusion from the Levantine region. As a striking consequence of these meteorological conditions, an extremely rare event such as the partial freezing of the Venice lagoon was faced (Camuffo, 1987), while existing NA coastal observatories registered very low water temperatures. In the Gulf of Trieste this value was generally below 4.7°C, with a 3.9°C minimum observed at PB in the central part of the Gulf towards the end of the event (February 13 and 15, see Mihanovic´ et al., 2013). Along the western coast, a temperature drop down to 5.8°C was recorded at AA. Overall, satellite retrieved Sea Surface Temperature (SST) fields depicted a decrease of about 6°C during the whole span of the CAO.

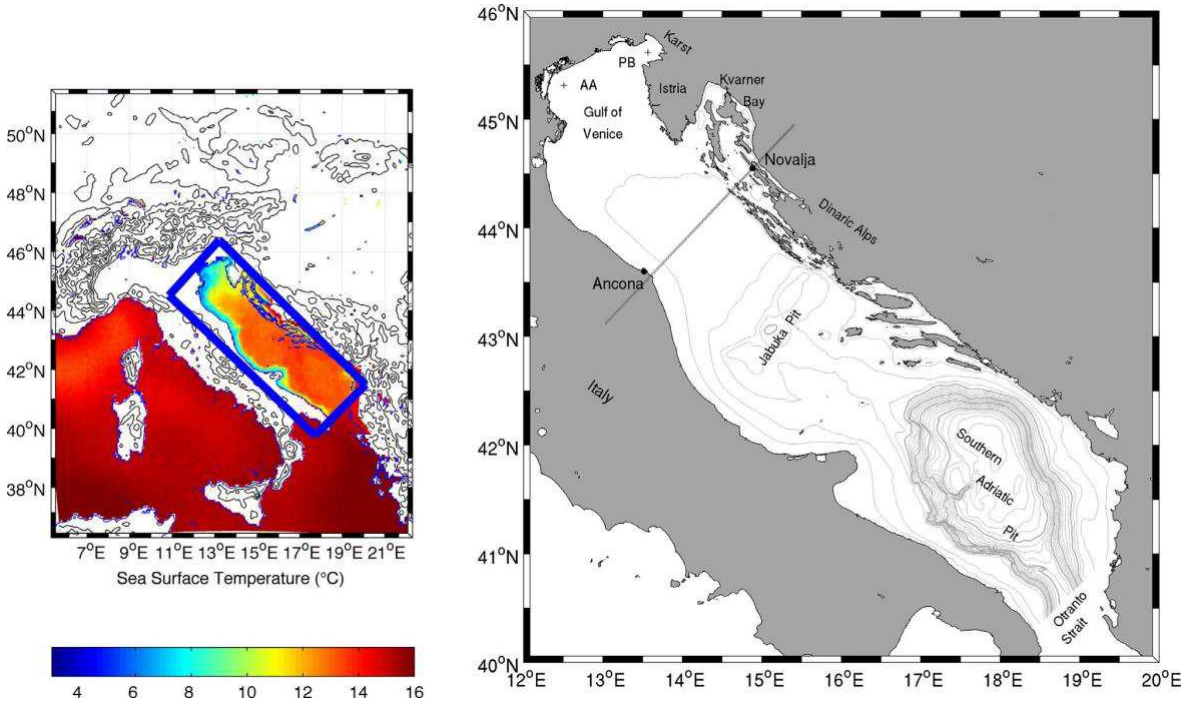

Fig. 1. Geographical setting of the study. Left panel: WRF (outer box) and ROMS (inner box) numerical domain and Sea Surface Temperature field (ROMS in the Adriatic Sea, radiometer in the Mediterranean) at the beginning of the event. Right: Adriatic Sea and Ancona-Novalja transect (reference cross section in the study, grey thick line) conventionally encompassing the "cooling" or "formation" basin. Thin (thick) grey contours represent 50 (250) m isobaths. AA and PB represent the position of Acqua Alta tower and Paloma Buoy respectively.

Thus, estimated turbulent heat fluxes at AA during the CAO were characterised by two peaks down to −800 W m−2 on February 3 and −700 W m−2 on February 11 (Fig. 2), whereas maximum heat loss reached 1000 W m−2 at PB (Raicich et al., 2013) and was estimated to largely exceed this value among the Croatian islands (Janekovic´ et al., 2014). The fact that in these papers slightly different bulk formulae parameterizations were used, is not changing the overall intense picture of the CAO; however it is worth pointing out that these values may be even larger in proximity of the core of the wind jets (Pullen et al., 2006). Furthermore, the small amount of riverine freshwater supplied during the CAO (a large amount of precipitation occurred as snowfall on the Po Valley, northern Italy, and accumulations of 60– 100 cm stayed on the ground for 15 days) was not sufficient for significantly diluting salty water of Levantine origin intruding along the eastern Adriatic coast, leading salinity to exceed 38.5 at AA and in the Gulf of Trieste. The concurrence of these factors gave rise to exceptionally high Potential Density Anomaly (PDA) values, exceeding 30 kg m−3 at AA and throughout the whole Gulf of Trieste, except nearby the mouth of the Isonzo river, up to record-

breaking of 30.59 kg m−3 (Mihanovic´ et al., 2013; Vatova, 1934). Based on this dataset, the modeling analysis carried out by Benetazzo et al. (2014) depicted a formation event taking place north of the ideal Ancona-Novalja transect (Fig. 1), with the strongest densification within a cyclonic gyre enclosed in the northern end of the basin, between Po river mouth and the Istrian peninsula. The ensuing spreading phase was characterised by a dense water vein flowing tidally-modulated and nearly geostrophically adjusted along the Italian coast, at a depth depending on the vein density and potential vorticity, and another dense mass spilling from the Croatian islands towards the mid-Adriatic pit. South of Ancona, the westernmost dense vein parted into two branches. A "shallow" one, flowing southwards close to the coast, approaches the continental margin off the Apulian coast, partly intercepted by the shelf break and downflowing towards the Southern Adriatic Pit (Bonaldo et al., 2016) and partly crossing the Otranto strait over the continental shelf. A "deep" stream, in turn, plunges into the mid-Adriatic pit and thence flows towards the southern basin across the Palagruža sill. Worth noting, in that case waves appeared to enhance kinetic energy injection during the generation phase and significantly increased the overall densification, influencing the subsequent migration pathways and, by consequence, the shelf edge efficiency in triggering dense water downflow (Carniel et al., 2016). In this framework, our analysis focuses on the generation phase, bracketing the period from January 23 to February 23, 2012, with particular emphasis to the investigation of the role and acting mechanisms of atmosphere-ocean-waves interactions.

2.3.2 Numerical model set-up

The modeling approach discussed in this paper explores the multiple model coupling possibilities provided by the COAWST system (Warner et al., 2010). Based on the Model Coupling Toolkit, COAWST enables the exchange of information among numerical models representing different processes of the meteo-oceanic system (WRF, Weather Research Forecasting model for atmosphere dynamics; SWAN, Simulating Waves Nearshore for wave motion; ROMS, Regional Ocean Modeling system for ocean currents, and the Community Sediment Transport Modeling System for sediment transport), thus allowing an explicit description of their interactions. WRF (Skamarock et al., 2005) is a non-hydrostatic, fully compressible atmospheric model in sigma vertical coordinates for the prediction, among others, of three-dimensional wind momentum components, air pressure distribution, relative humidity, dew point, heat fluxes and precipitation. SWAN (Booij et al., 1999) is a third generation, phase-averaged wave model computing spectral quantities of short-crested, wind-generated sea states by solving the radiative wave action equation. Several mechanisms of energy injection, transport, redistribution and dissipation (e.g. wind-driven wave generation, white-

capping, bottom friction, non-linear three and four-wave interactions, wave breaking) can be reproduced under arbitrary wind conditions. ROMS (Haidvogel et al., 2008), is a free-surface ocean model solving three-dimensional Reynolds Averaged Navier-Stokes equations in curvilinear coordinates under the hydrostatic approximation. After having performed four WRF "stand alone" runs in which the effects of different formulations for inputting SST into the atmospheric model were explored (Carniel et al., 2015; Ricchi et al., 2016), a WRF-ROMS one-way simulation is analyzed as a benchmark (ATM run, see Table 1). This represents a "classical" approach, where no feedbacks to the atmosphere are provided by the ocean model (ROMS), but momentum and heat fluxes are imposed by the meteorological model (WRF) via the COAWST ATM_FLUX option (Carniel et al., 2009). However, differently from Renault et al. (2012), where the off-line WRF model received no SST update (being kept constant and equal to the snapshot acquired at the beginning of the simulation), in order to provide the best description available for an uncoupled model, in this case SST fields are updated every 6 h. Fields were obtained from satellite-retrieved data obtained from the RTG_SST (Real Time Global SST Analysis) High Resolution dataset (Gemmill et al., 2007), provided by the National Center for Environmental Prediction (NCEP). As a second numerical test, the WRF-ROMS two-way coupled case (AO run) is proposed, where the models mutually exchange momentum and heat/moisture fluxes (air to sea), and SST (sea to air).

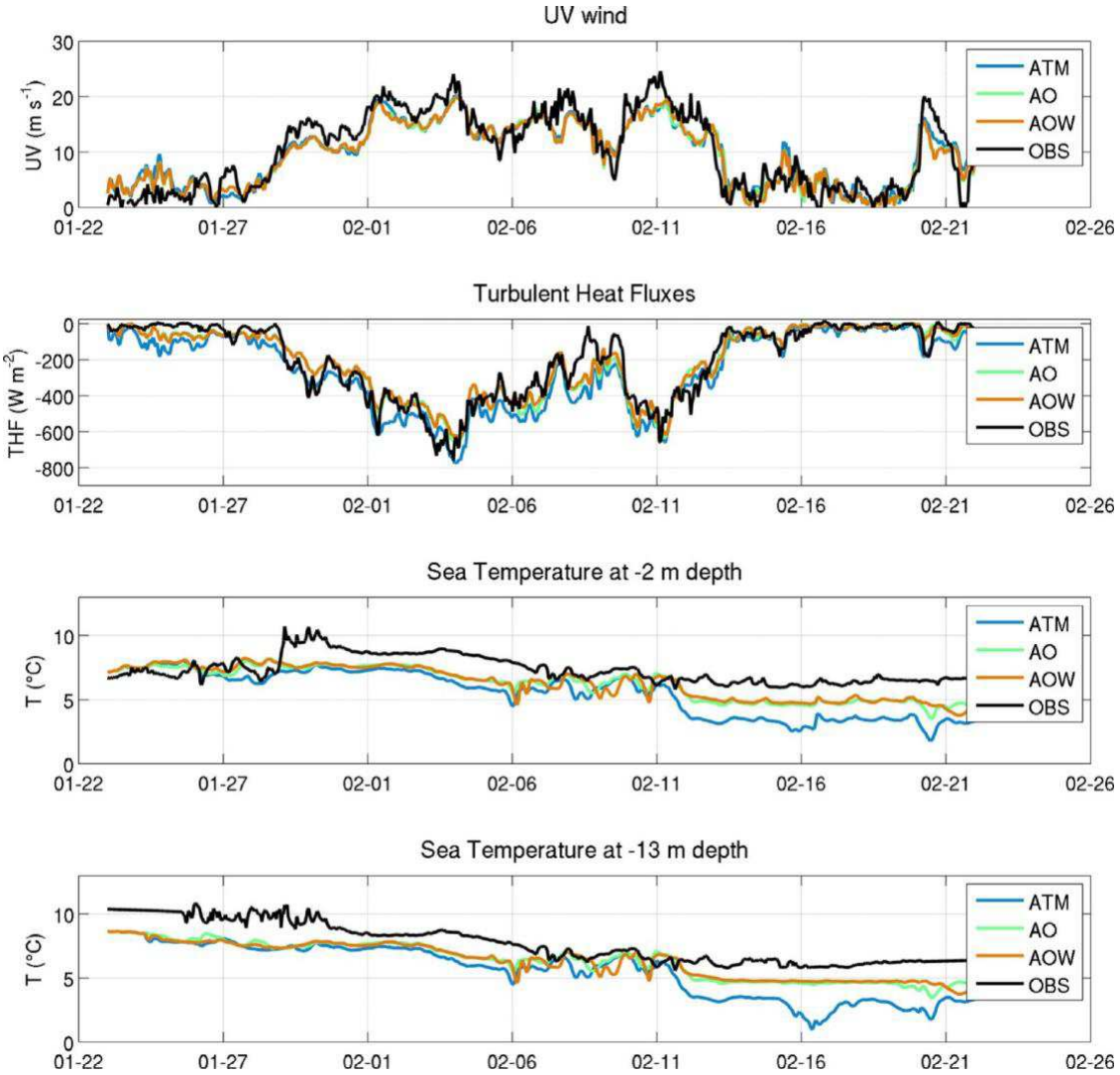

Fig. 2. Model results (color lines) and observations (black line) at the "Acqua Alta" tower. (For interpretation of the references to colour in this figure legend, the reader is referred to the web version of this article.)

Finally, the WRF-ROMS-SWAN two-way fully coupled case for waves-ocean-atmosphere is discussed (AOW run). For a graphical representation of the model interactions and detailed description of the variables exchanged, readers are referred to Appendix A and to Renault et al. (2012) and Zambon et al. (2014). It suffices here to say that in AO run the surface roughness is computed based on wind friction velocity according to Charnock et al. (1955), while in AOW run (where the atmospheric model provides the wind components to the wave model and receives back the wave parameters, from which it derives the surface roughness) the Oost et al. (2002) formulation was employed.

	UV wind ($m\,s^{-1}$)	T2 (°C)	SST (°C)	THF (Wm^{-2})	S	σ_θ (
ias	−0.73	0.14	−1.8	−55.00	0.21	0.41
MSD	0.44	0.55	1.20	0.89	0.75	0.61
C	0.90	0.85	0.68	0.94	0.73	0.86
ias	−0.85	−0.23	−1.05	−7.00	0.17	0.29
MSD	0.41	0.52	0.86	0.34	0.73	0.63
C	0.92	0.86	0.69	0.94	0.73	0.83
ias	−0.83	−0.28	−1.01	−2.71	0.19	0.29
MSD	0.40	0.50	0.91	0.32	0.72	0.63
C	0.92	0.91	0.66	0.94	0.72	0.82

Table 1. Model performances compared with AA observations for different implementations in the period January 23–February 23. ATM represents ROMS forced by WRF, AO two-way coupled ROMS and WRF, AOW full two-way coupling ROMS, SWAN and WRF. Correlation coefficients (CC) are expressed in dimensionless units.

Compared to other approaches implemented in the COAWST system (see Taylor and Yelland, 2001; Drennan et al., 2005), Oost formulation, based on wave age and (indirectly) on steepness, exhibited better performances for the considered sea state (Olabarrieta et al., 2012). Moreover, in AOW run the wave model provides the wave parameters to the ocean model, and ROMS gives back velocity components, surface height and bathymetric variation to the wave model (Benetazzo et al., 2013). The domain used for the meteorological model encompasses a larger region within Europe, ranging from 6°30′ to 22° E and 36°30′to 51° N, discretized into 60 vertical levels and with a uniform horizontal grid spacing of 7 km (see again Fig. 1). Following the works (Benetazzo et al 2012, Benetazzo et al 2013) the ROMS hydrostatic model, is suitable for the study of convective phenomena such as the formation of dense waters, both for the mixing schemes used and for the high number of vertical levels, thickened especially in the mixed layer. ROMS has 30 vertical levels, unevenly distributed in order to increase resolution close to the surface and close to the seabed, and runs on the 1 km by 1 km bathymetry adopted by Benetazzo et al. (2014), Bonaldo et al. (2016) and Carniel et

al. (2016). SWAN model horizontal resolution is also 1km, while the spectral space is discretized into 40 intrinsic frequencies and 36 equally spaced directions. Initial and boundary conditions for WRF model were provided by Global Forecasting System Final Analysis (GFS-FNL), whereas the ocean was initialized with 3D fields provided by the model discussed in Benetazzo et al. (2014), and calm sea state. Potential temperature, salinity, momentum and sea surface elevation at the southern open boundary (Otranto Strait) were provided by interpolated Mediterranean Forecasting System (Pinardi et al., 2003) fields and the tidal forcing was obtained from the Oregon State University Tidal Model (Egbert and Erofeeva, 2002); riverine inputs were not accounted for, in consideration also of the small freshwater discharge in the analyzed period (Mihanovic et al., 2013; Ricchi et al., 2016; and Benetazzo et al., 2014) and following the considerations on the plume structure presented by Falcieri et al. (2014)Common data fields shared among different models are exchanged by the coupling toolkit every 1200 s.

2.4. Results and discussion

2.4.1 Model performances: overview

Due to its position a few kilometers downstream of a mountainous coast exposed to the dominant Bora wind, atmospheric modeling at PB location undergoes a number of well-documented issues related for example to the representation of the orography in the model (Horvath et al., 2011) that may hamper the evaluation and comparison of the coupled/uncoupled models skills. Therefore, we will base our evaluations mostly on measurements collected at AA, far downstream of the dominant wind and more representative of the effects of air-sea interaction occurred along the NA. Generally speaking, winds are well reproduced in the proximity of AA in terms of peaks and timing (Fig. 2). The differences among the various numerical runs are not significant, with all simulations tending to underestimate the measured wind at AA (Table 1), and the air temperature time series are rather close to each other. For air temperature 2 m above the mean sea level (T2), ATM run is providing the warmest scenario. Likely due to the aforementioned topographic issues, the situation is reversed in the middle of the Trieste gulf, where PB registered faster winds with respect to modeled ones and, after a slight overestimation of air temperature that characterises mostly ATM, the trends are very close to each other, with AO providing the coldest scenario. Interestingly, at both stations in the last part of the CAO event, AO and AOW seem to depart from ATM in providing lower air temperatures, better matching with observations. This points out that model coupling may help overriding possible shortcomings related to limitations in available radiometer data, which in this case was providing a

SST value significantly higher than reality, missing mesoscale thermal patterns and colder coastal features (Carniel et al., 2015). As suggested in previous works (Mihanovic' et al., 2013 and Benetazzo et al., 2014), Turbulent Heat Fluxes (THF) computed from observed data during the CAO could reach the extreme values of -800 W/m^2. Once again (see Table 1) the trends of THF computed at AA via the COARE algorithm (Fairall et al., 2003) are overall satisfactorily captured by the three numerical runs, although some differences are to be noted. More specifically, at AA the ATM run, driven initially by a SST field provided by the radiometer, estimated much stronger (negative) THF. As the integration proceeds, this problem is progressively mitigated by the availability of new, more realistic, satellite fields before diverging again towards the end of the run. THF estimates at AA provide a synthetic outlook of the model skills in capturing the main features of the process evolution, with very similar correlations (0.94 for all three runs), standard deviations slightly better in the uncoupled case (0.99, 0.91, 0.88 W/m^2 for ATM, AO and AOW, respectively) and Root Mean Square Deviation (RMSD) again very similar for coupled case (0.34 W/m^2 for AO and 0.32 W/m^2 for AOW) and 0.89 W/m^2 for uncoupled case. This notwithstanding, the average spread between uncoupled and coupled estimates for THF is on the order of 50 W/m^2, with a -55 W/m^2 bias for the uncoupled ATM run against a -7 W/m^2 and around -3 W/m^2 bias for the coupled AO and AOW runs respectively. THF at PB show a RMSD of about 0.58 W/m^2 for run ATM, 0.38 and 0.36 W/m^2 for the run AO and AOW respectively, consistently with the results obtained for AA and with the different behavior observed in the various runs. The correlation coefficient at PB is 0.92 for ATM and 0.94 for cases AO and AOW. The Bias in THF at the PB station is -117 W/m^2 for the run ATM, around -22 W/m^2 for AO and -9 W/m^2 for AOW, again consistently with the findings obtained in AA. It is worth to note that the differences in model performances at PB are larger than those obtained at AA. This is attributable partly to a larger mismatch between radiometer-retrieved and sea-truth measured SST at PB, and partly to the effect of larger evaporation induced by the dry and very cold air coming from the hinterland and spilling over the sea just near the PB station as well as throughout the North Eastern part of NA.

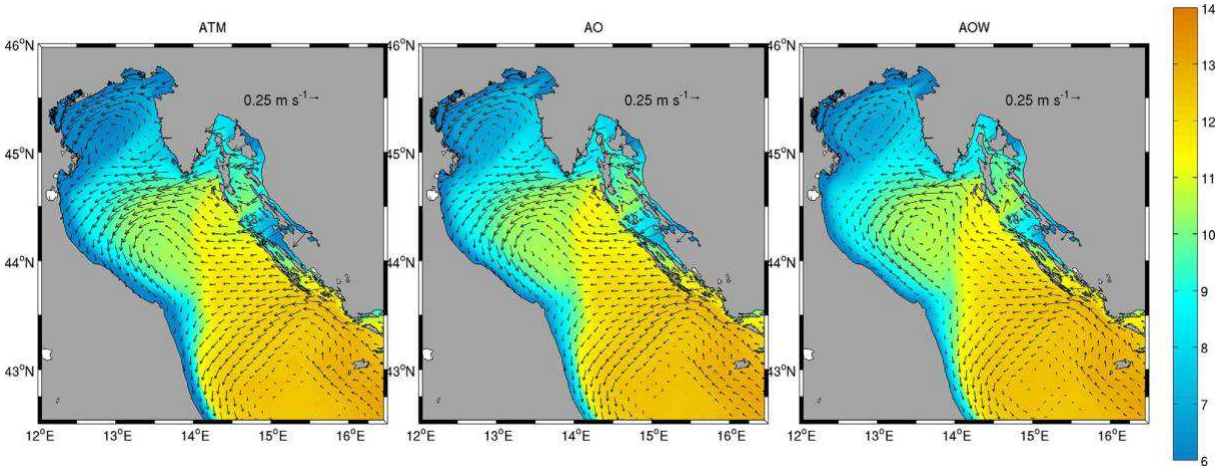

Fig. 3. Time-averaged (January 29–February 13) sea surface temperature and current velocity in the northern Adriatic Sea for different runs. Vectors related to current speed have been omitted.

Concerning model skills in terms of thermohaline properties, the extent of the bias, as reported for all runs in Table 1, is largely due to uncertainties in the initialization. This is indeed a well-acknowledged circumstance related to the drift of long-term operational models (Benetazzo et al., 2014 and Licˇer et al., 2016). Further validations of the modeling suite employed are presented by Ricchi et al. (2016), which discussed results from this configuration mostly focused on the atmospheric side. In their work a further station in central Italy (Ancona) was used to validate the surface fluxes, while the air temperatures in three different stations were used to validate the coupled approaches as well. Results showed that the AOW and AO setup were producing more realistic values (see for instance Table 2, Ricchi et al., 2016).

2.4.2. Sub-basin scale coupled dynamics

The small differences in the estimates of wind intensity and THF in the proximity of AA, being confined within a small percentage, appear as an indication of overall good model performances. However, this is not conclusive about the effect of the coupled system, since the variables explored until now do not necessarily provide complete direct information about the dynamical adjustment of the basin to the complex energy interplay of atmosphere, currents and waves. As shown by Sclavo et al. (2013) and Benetazzo et al. (2014), for instance, a two-way coupled description of wave-current interactions may generate energy and tracer transport adjustments that are not reflected at a single

point in terms of local budget, but can be nevertheless propagated into basin-wide patterns as a result of advective dynamics. Therefore, it may be helpful for our scopes to describe modeled physical patterns produced by the CAO, and subsequently summarize the main features of the process into a few global quantities referred to the region north of the Ancona-Novalja transect as a whole (see Fig. 1), namely the "formation basin" for 2012 Northern Adriatic Dense Water (NAdDW). As a response to the pattern of Bora jets blowing from the Dinaric Alps (with two main jets on the Karst, on the north-easternmost sector of the basin, and south of Istria), the typical mean ocean circulation pattern during the period is characterised by two major cyclonic gyres. A northernmost one is enclosed by the Po Delta (45° N, 12°30′ E) and the Istrian Peninsula, whilst another involves the region between the Po Delta, Ancona and the Kvarner Bay, with a net westward transport off the Kvarner Bay (44°45′N, 14°30′E) and south-eastwards along the Italian coast (Fig. 3). In between, a smaller anticyclonic gyre is established off the Istrian coast (called Rovinj gyre by Kuzmic´ et al., 2007; Bignami et al., 2007), partially promoting mass recirculation from the southern gyre towards the northern sub-basin (Fig. 3). In all cases, the cyclonic circulation is well established during the CAO, but the 2-way coupling with atmosphere and waves (AOW) provides the strongest recirculation in the Gulf of Venice and in the Po-Ancona-Kvarner gyre. The small riverine inflow during the event was shown to have limited implications (Mihanovic´ et al., 2013; Benetazzo et al., 2014; Ricchi et al., 2016) although Supic´ et al. (2012) and later on Kraus et al. 2015; Kraus et al., 2016 suggested that the variability of freshwater sources in circulation patterns may in principle relevantly affect the ratio of riverine water entrained into the gyre, and therefore its thermohaline properties and biological load. This difference is also associated to a few degree differential rotation of the mean wind stress and the intensity of the Bora-induced sea surface elevation gradients (Kuzmic´ et al., 2007), enhanced along the cross-basin (NE to SW) direction, due to the increased wave-induced transport. On the other hand, wind stress intensity in the three runs is rather similar (Fig. 4, top row), although temporary differences arise especially in early February peaks, both in global (sub-basin scale average, see Fig. 5) and local (point measurements, see Fig. 2) terms, on the order of up to 10%. In addition, ATM run provides the most intense (negative) heat fluxes throughout the whole cooling basin (Fig. 4, bottom row) and during the whole simulation (Fig. 5, second row), while AOW and AO implementations appear nearly overlapping and producing weaker THF, with a difference of about 10–20%. In this situation, a proxy of the overall dynamical state of the formation basin as a whole can be given by the evolution of its mean density and kinetic energy content (Fig. 5, lower panels). Run ATM produces the densest water, whereas the fully coupled run (AOW) the least dense of the set. In turn, it appears clear that ATM provides a low kinetic energetic scenario in spite of the largest wind stress value at the surface. If we look at the mean TKE distribution along the vertical, we can depict how run AOW

(with wave inclusion) describes the kinetic energy distribution along the water column in a different way with respect to other runs (Fig. 6). Wind velocity is indeed used by the wave model, that returns to the ocean a portion of the atmospheric energy in the form of additional conservative and non-conservative wave forces (Kumar et al., 2012), that now starts acting into the ocean modulating the penetration of momentum injection into the water column. Generally, a more effective transfer of kinetic energy along the water column, with a more uniform distribution of this quantity, can modify velocity profiles and net barotropic transport mechanisms, in this case favoring water accumulation along the northern Italian coast and the development of stable gyre circulation features. Thus, apparently small modifications on bulk dynamic variables, such as average wind stress, may be the sign of crucial differences in key processes governing circulation and transport patterns. In the following paragraph we will explore to what extent this can impact the formation, migration and the fate of dense waters.

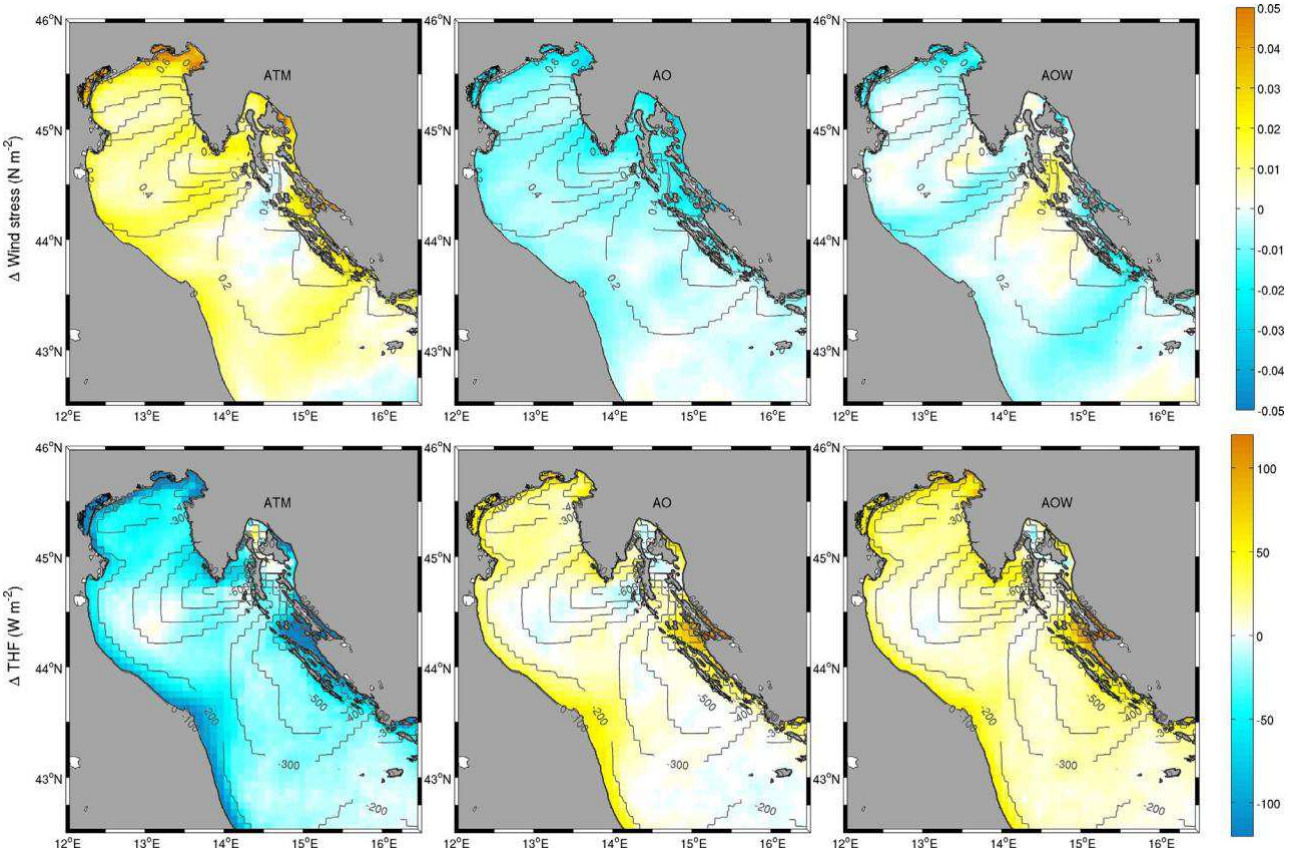

Fig. 4. Differences between time-averaged (January 29–February 14) fields of wind stress (top row) and heat fluxes (bottom row) at the sea surface for each run and the mean value from all three separate (ATM, AO, AOW) runs for the same period, identified by black contour lines.

2.4.2. Energy and mass fluxes and the fate of dense waters

Since in all model implementations the water fluxes induced by the CAO are comparable with the overall volume of the basin enclosed north of the Ancona-Novalja transect (Fig. 1), heat and dense water budgets should in principle account for the cooled water masses leaving the densification basin. More specifically, energy density extraction (i.e. energy extracted per unit mass) from the ocean is a function of THF and of the efficiency of circulation in flushing and renewing the cooling basin. In order to simplify the physical interpretation of the results though retaining the inter-comparability among different runs, all temperature, salinity and potential density values will be hereinafter discussed in terms of unbiased values. Such reference values are the biases affecting thermohaline quantities in the AOW case, chosen as a benchmark since this is the run characterised by the most complete physical description, providing −1.01°C in water temperature, +0.19 in salinity and +0.29 kg/m^3 in potential density. This approach, introduced and broadly discussed by Benetazzo et al. (2014) and followed by Bonaldo et al. (2016) and Carniel et al. (2016), allows a more realistic identification of water masses with given thermohaline properties such as NAdDW, and appears particularly effective in favoring the contextualization of the findings and their discussion in the framework of other studies. Thus, whilst Fig. 7 summarizes overall metrics of mass and heat fluxes irrespective of water density, Fig. 8 focuses on the effect of the cooling process in terms of density distribution with reference to unbiased results. Fig. 7 shows that time-averaged circulation during the CAO (January 29–February 13) in the AOW run provides larger masses of water leaving the cooling basin (Fig. 7, left panel) compared to wave-uncoupled runs, with a net export of 7.18E + 14 m^3 (6.51E + 14 m^3 and 6.74E + 14 m^3 in the AO and ATM case respectively), against an overall sub-basin volume of 1.23E + 15 m. In particular, Fig. 3 (top row) and Fig. 8 (second row) suggest that this surplus is due to an enhanced drawal of relatively warm and less dense waters from the southern Croatian coastal zone, subsequently trapped within the Po-Ancona-Kvarner gyre and leaving the basin along the Italian coast. In turn, due to the SST overestimate in the radiometer data, the ATM simulation is characterised by stronger surface heat extraction (1.81E + 19 J) compared to atmosphere-coupled runs (1.57E + 19 J and 1.54E + 19 J in AO and AOW respectively, see Fig. 7, middle panel), whilst the slight difference between AO and AOW is associated to a different calculation of the variables involved in air-sea interface exchanges and to the drawal of colder water from the vicinity of the Croatian islands (Fig. 3, first panel) into the northern basin (Fig. 8, second panel).

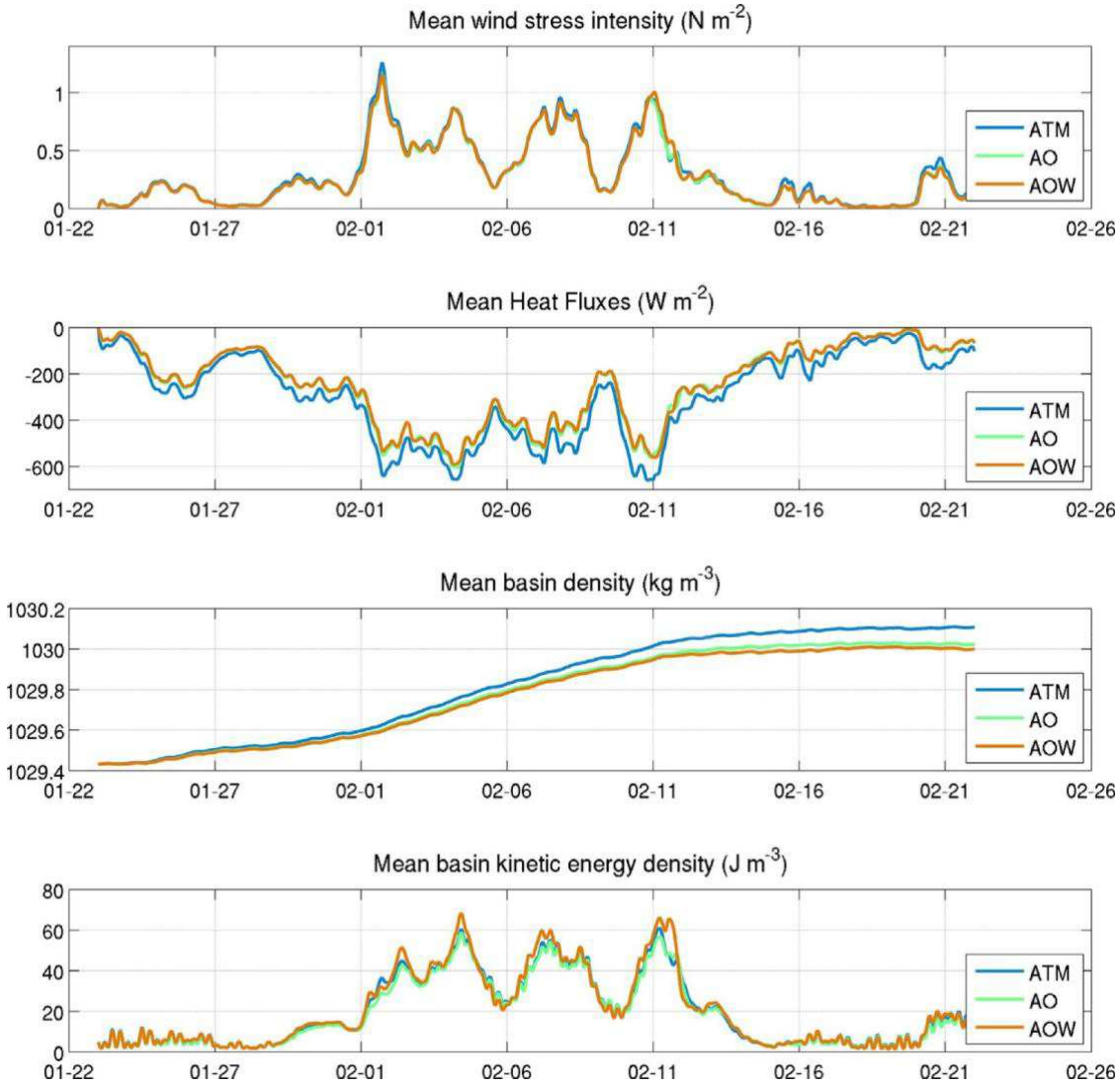

Fig. 5. Overall mean properties evolution in the formation basin during Winter 2012 event: surface momentum stress (top panel), turbulent heat flux (second panel), water potential density (third panel), kinetic energy (bottom panel).

Thus, the highest (9.5E + 3 J/kg , ATM run) and lowest (7.9E + 3 J/kg, AOW run) heat density (namely, heat per unit mass) extraction from the ocean, respectively correspond to a smaller volume of denser water and to a larger volume of less dense water. Circulation and advective transports provide a substantial contribution in controlling thermohaline properties, the amount of produced water volume and the export of dense water masses. Considering the water density distribution within the basin at the end of the CAO, it turns out that the extra-densification acting in the ATM run results in the production of a larger mass of dense (say, PDA > 28.8 kg/m^3) water (4.4E + 14 kg) compared to AO (2.9E + 14 kg) and AOW (2.6E + 14 kg), with overall higher values of PDA (Fig. 8, bottom panel). Worth noting, in the coupled cases (AO and AOW) the circulation pattern induces a relatively small export of newly formed water masses, while most of the outflow involves the lighter fraction, circulating south of the core of the densification basin and only partially hit by the cooling process. (Average PDA of the exported masses 29.42 and 29.39 kg kg/m^3 respectively). By contrast, uncoupled run (ATM) exports a larger amount of dense waters (Fig. 8, third panel) during the CAO. (Average PDA of the exported masses being 29.45 kg/m^3). The main implications of dense water formation are related to the potentiality of a partial or complete renewal of Mid-Adriatic (Jabuka) and South-Adriatic Pit (SAP, see Fig. 1) and to the reshaping of the continental margin seabed (Bonaldo et al., 2016). Benetazzo et al. (2014) identified some reference thresholds for dense water propagation along the Adriatic basin (see Fig. 28 in their paper). Following the generation of a PDA exceeding 30 kg/m^3 in the northern basin, Jabuka pit renewal takes place with PDA exceeding 29.6 kg/m^3, whereas dense water approaching the shelf break along the Southern Adriatic Margin has PDA around 29.4 kg/m^3, typically dropping to 29.2 kg/m^3 as the dense water vein descends the continental slope towards the abyssal plain. This means that dense water migration induces entrainment and mixing up to an overall potential density drop of 0.4 kg/m^3 from the generation basin to Jabuka pit, and of 0.8 kg/m^3 from the generation basin to the SAP. As a consequence, the newly formed core potentially available for direct (advection of water directly coming from the NA) or indirect (water masses entrainment out of the generation basin, which can be a large fraction of the overall volume, see Benetazzo et al., 2014) SAP renewal is 0.5E + 14 kg in the AO and AOW runs, and 1.5E + 14 kg in the ATM run.

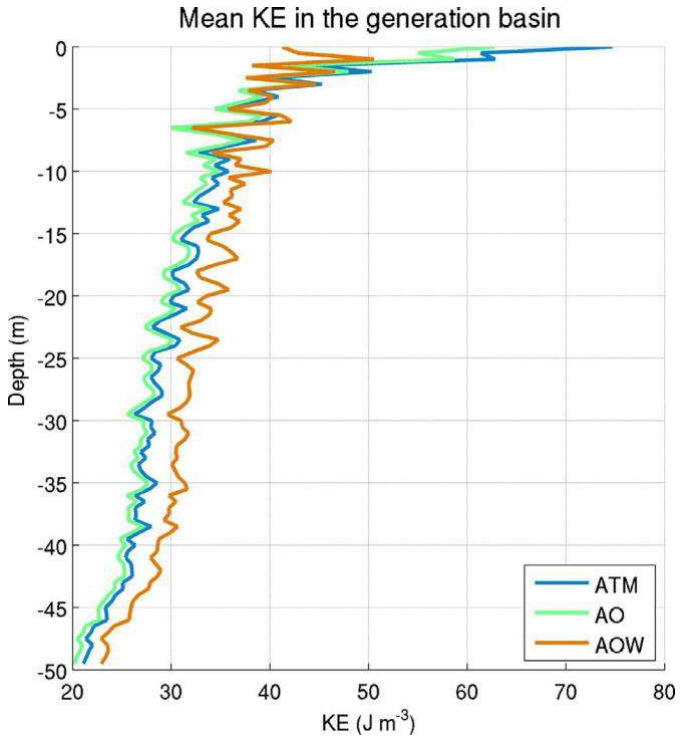

Fig. 6. Horizontally-averaged kinetic energy per unit volume profiles in the forma-tion basin for the three runs.

On the other hand, the actual continental slope flushing and pit ventilation are also function of the trajectory of the dense water stream, and in particular of the depth at which a dynamic geostrophic adjustment is established. For a given domain, this depth in turn is a function of the water density (proportional to −1/g', being g' the reduced gravity of the water mass) and of the initial velocity of the stream leaving the cooling basin (proportional to −v2; for a detailed treatise refer to Griffiths, 1986). Therefore, water masses leaving the basin with a smaller density and/or a higher current speed will likely have a smaller role in ventilating Jabuka pit and the SAP, and will tend to concentrate most of their effects (such as biogeochemical transport phenomena, seabed reshaping) on the coastal zone up to the outer continental shelf and upper slope. In turn, denser waters with smaller kinetic energy (ATM run) will generally tend to establish deeper pathways ending up in a higher interception rate from the shelf break (Carniel et al., 2016), with a significant role of the Jabuka pit in modulating and laminating the fluxes, thus smoothing part of the possible episodic energy peaks hitting the bottom and giving rise to erosional features. In this perspective (and in our implementation), uncoupling waves in an ocean-atmosphere coupled run (AO case) at the seasonal scale may lead to a slight increase in estimated dense water cascading volumes. This occurs as a consequence of a possibly smaller estimate of current intensity due to the incomplete description of atmosphere-ocean

momentum transfer, resulting in a less intense circulation and therefore in a longer cooling (especially for the water masses excluded from the gyre) and a deeper descent pathway. A major discrepancy may instead arise in the absence of a two-way coupling ocean and atmosphere, as in the case of the ATM run. In general, inconsistencies related to the lack of a feedback between these fields eventually propagate a number of possible shortcomings related to initialization and forcings throughout the modeling chain, without a dynamic response of the system as a whole and virtually enhancing the extent of a possible drift in its energetic properties. In the case of the ATM run, an overestimation of the SST due to a poor radiometer rendering (see Ricchi et al., 2016 for a discussion) led the atmospheric model to partially overestimate surface heat fluxes intensity giving rise to an excess in basin densification. In addition, the different circulation induced by kinetic energy distribution along the water column can strongly influence the main features of the densification process (overall mass involved, density distribution, maximum density) and the dynamic properties of the dense water mass, thus affecting the extent, timing and pathway of dense water migration and the renewal of the Adriatic depressions.

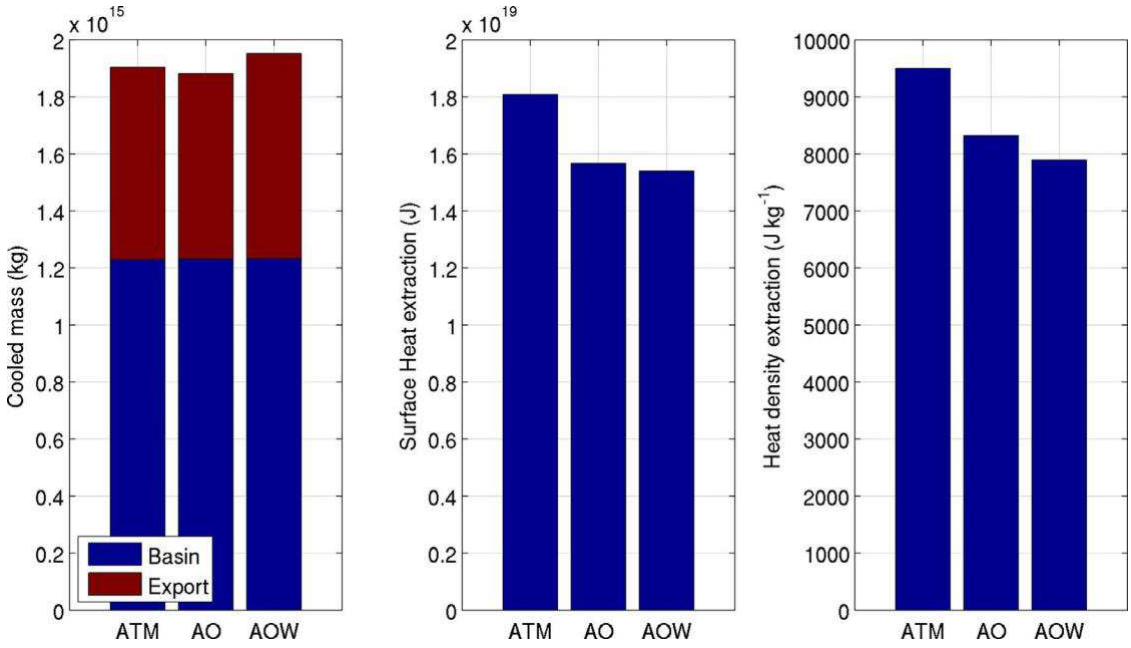

Fig. 7. Key metrics for dense water formation, January 29–February 14. Left: total water mass involved in the densification process as a sum of water masses passing through the formation basin and eventually exported (red) and overall mass of the formation basin. Middle: Total surface heat extraction during the event. Right: Total surface extraction per unit mass (note that positive values for surface heat and heat density extraction mean heat directed from the ocean to the atmosphere). (For interpretation of the references to colour in this figure legend, the reader is referred to the web version of this article.)

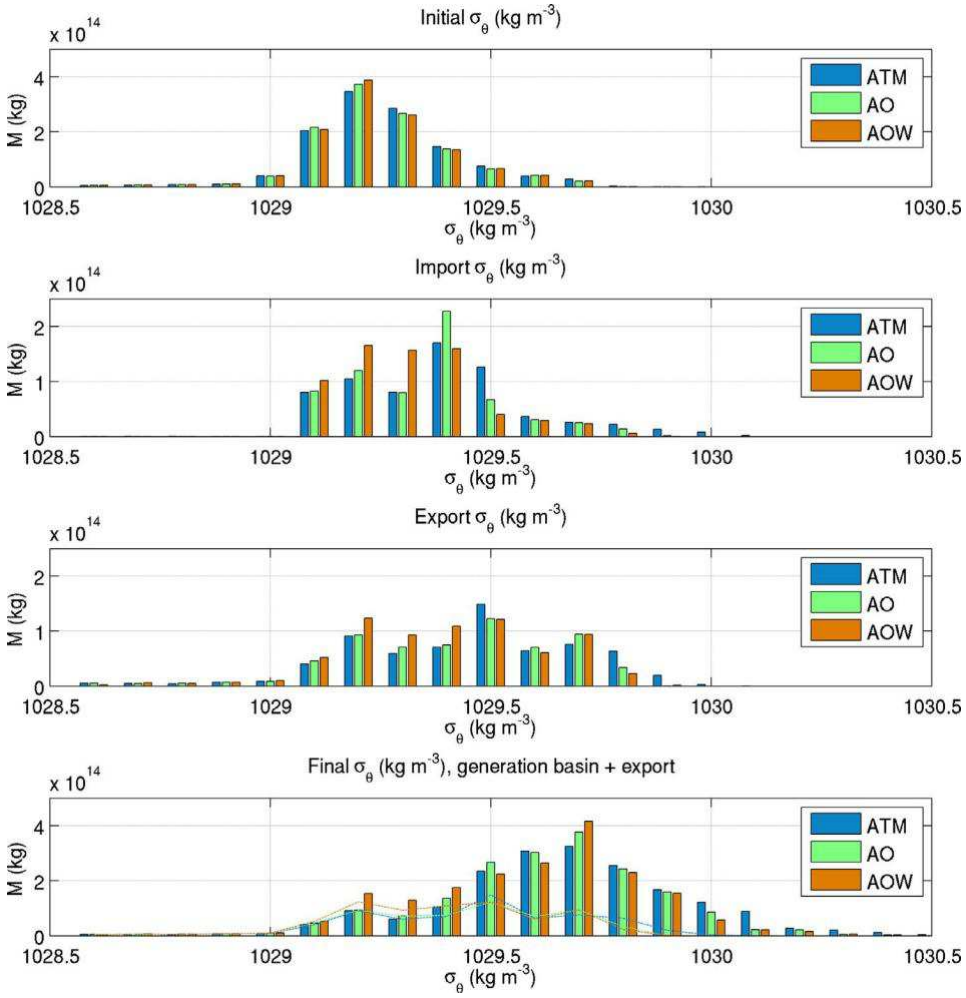

Fig. 8. Potential density composition of the water masses involved in the cooling event (unbiased values): initial (January 29, 2012) condition of the cooling basin (top panel), time-integrated inflow (second panel), time-integrated outflow (third panel), final (February 14, 2012) condition in the generation basin, including total export (bottom panel, thick lines representing the export depict its relative contribution to the overall mass involved in the process

2.5. Concluding remarks

The work aims at evaluating the different contributions of the interplay between ocean-atmosphere and waves in a semi-enclosed basin during a strong CAO event, focusing on the implications of the description of these processes on dense shelf water formation and deeper sea ventilation. In the wake of a set of previous ocean-atmosphere(e.g.Pullenetal.,2006 and Licˇer et al., 2016) or wave-currents (e.g. Benetazzo et al., 2013) coupling experiments, to our best knowledge this study (together with the preliminary atmosphere-focused example by Ricchi et al., 2016 and Carniel et al., 2015) represents the first example of a fully two-way coupled approach to wave, atmosphere and ocean dynamics in the NA basin. Interactive ocean feedback produces improved heat fluxes and air temperatures estimates compared to those of a stand-alone atmospheric model forced with persisting SST anomalies (see Ricchi et al., 2016). Our findings indicate that skill metric tendentially improved (especially in the case of THF, with a bias improvement from −55 to −7 W/m^2) in the coupled version (AO run), with respect to the one-way atmosphere-ocean version (ATM run), which still represents a widely accepted approach in the field. Improvements are related with the dynamic SST prediction brought into the system by the oceanic part, while the fully coupling with surface waves (AOW run) further improves the figures, albeit to a lesser extent (THF bias improving from −7 to around −3 W/m^2). Moreover, the evolution of the mean kinetic energy of the basin certifies that, although AOW run produces surface momentum stresses that only slightly differ from ATM and are very similar to the ones produced in the AO case, the explicit inclusion of wave effect in atmosphere-ocean interactions provides a different dynamical characterization of the basin. Overall, it appears that coupling ocean and atmosphere, even in a sub-region of the model domain, may significantly modify the water circulation and characteristics in a much larger area, in spite of their apparently small extent. This can strongly affect the volume of water involved in the cooling process within the whole NA basin, its density and its kinetic energy, actually conditioning its potential contribution in deep sea ventilation. In this context, the role of waves lies substantially in modulating air-sea exchanges and energy distribution along the water column. By explicitly accounting for additional momentum terms in the ocean, a wave-ocean coupling in the absence of a feedback to the atmosphere (not considered in this study but performed and discussed by Benetazzo et al., 2014) may basically induce a kinetic energy surplus into the system, with relevant implications for basin-scale circulation and densification processes.

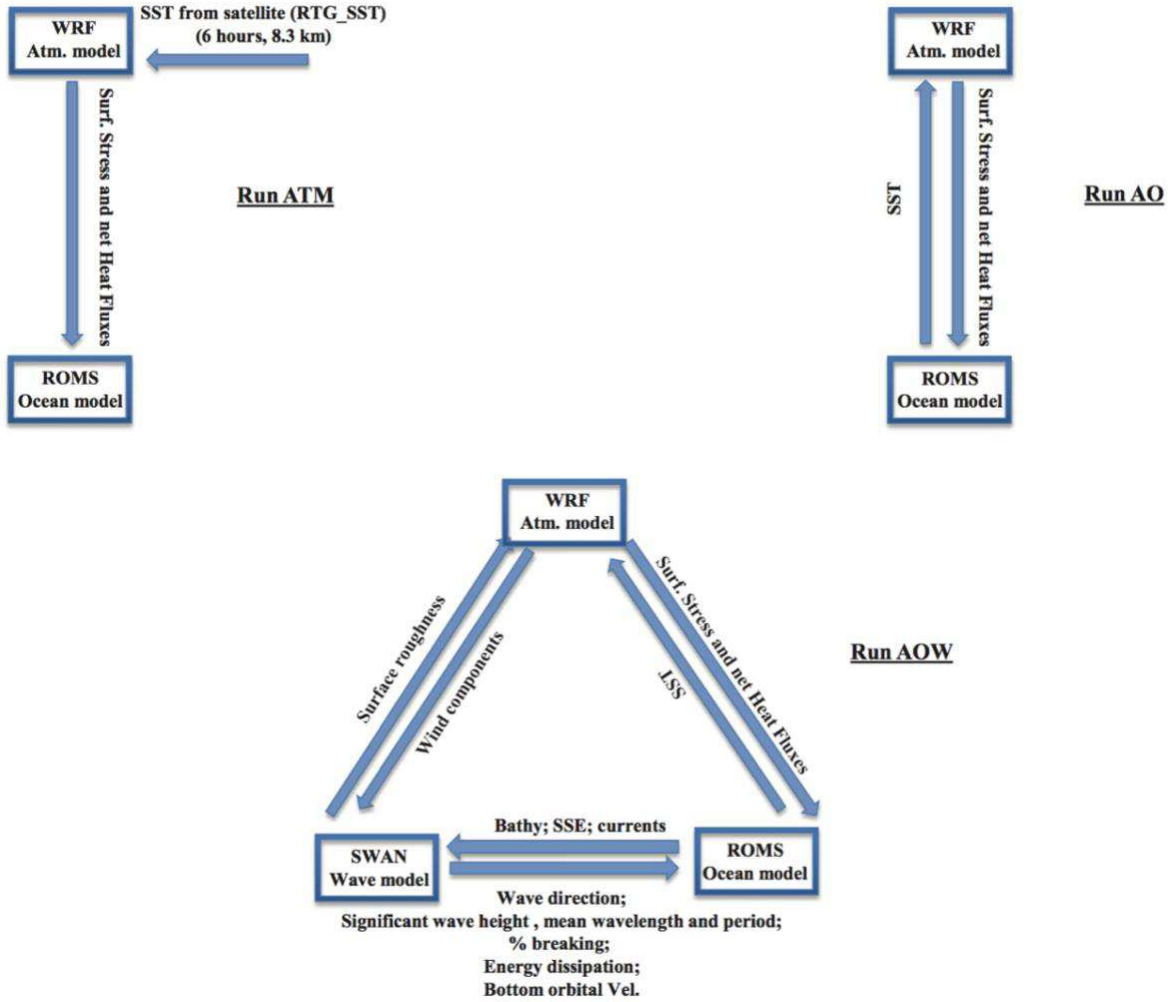

Fig. A.1. Schematic representation of the proposed COAWST experiments (ATM, AO, AOW). The arrows represent the coupling direction with in evidence the exchanged variables. SST is the Sea Surface Temperature, SSE the sea surface elevation.

Last but not least, we should recall that parameterizations for most state-of-art models have been calibrated and consolidated in a long time for mimicking observed dynamics in the absence of an explicit coupling within a complete wave-current-atmosphere system. Besides an undoubted improvement in the physical insight, the benefits of a shift towards a coupled approach in terms of model performances are therefore expected to appear progressively, as a further fine-tuning is carried out based on the new modeling framework. For this reason, it is not presently straightforward to widely generalize an evaluation of coupled models skills compared to uncoupled ones, and an extensive systematic comparison against observational evidences is still required. In particular, evidences presented in this study highlight the importance of choosing basin-scale quantities and their patterns as indicators for the quality of the process description, warning about possible misleading hints that can result from point or bulk analysis alone.

Reference

Benetazzo, A., Bergamasco, A., Bonaldo, D., Falcieri, F.M., Sclavo, M., Langone, L., Carniel, S., 2014. Response of the Adriatic Sea to an intense cold air outbreak: Dense water dynamics and wave-induced transport. Prog. Oceanogr. 128, 115– 138. doi:10.1016/j.pocean.2014.08.015.

Benetazzo, A., Carniel, S., Sclavo, M., Bergamasco, A., 2013. Wave–current interaction: Effect on the wave field in a semi-enclosed basin. Ocean Model. 70, 152–165.

Bergamasco, A., Benetazzo, A., Carniel, S., Falcieri, F., Minuzzo, T., Signell, R.P., Sclavo, M., 2012. Knowledge discovery in large model datasets in the marine environment: The THREDDS Data Server example. Adv. Oceanogr. Limnol 3 (1), 41–50. doi:10.1080/19475721.2012.669637.

Bignami, F., Sciarra, R., Carniel, S., Santoleri, R., 2007. The variability of the Adriatic sea coastal turbid waters from SeaWiFS imagery. J. Geophys. Res. Oceans 112, C03S10. doi:10.1029/2006JC003518.

Booij, N., Ris, R.C., Holthuijsen, L.H., 1999. A third-generation wave model for coastal regions: 1. Model description and validation. J. Geophys. Res. 104 (C4), 7649. doi:10.1029/98JC02622. 112 S. Carniel et al./Ocean Modelling 101 (2016) 101–112

Bonaldo, D., Benetazzo, A., Bergamasco, A., Campiani, E., Foglini, F., Sclavo, M., Trincardi, F., Carniel, S., 2016. Interactions among Adriatic continental margin morphology, deep circulation and bedform patterns. Mar. Geol. doi:10.1016/j. margeo.2015.09.012.

Boero, F., 2015. The future of the Mediterranean Sea Ecosystem: Towards a different tomorrow. Rend. Fis. Acc. Lincei 26, 3–12. doi:10.1007/s12210-014-0340-y. Camuffo, D., 1987. Freezing of the Venetian Lagoon since the 9th century AD in comparision to the climate of western Europe and England. Climatic Change 10, 43–66.

Canals, M., Puig, P., de Madron, X.D., Heussner, S., Palanques, A., Fabres, J., 2006. Flushing submarine canyons. Nature 444 (7117), 354–357. doi:10.1038/ nature05271.

Carniel, S., Warner, J.C., Chiggiato, J., Sclavo, M., 2009. Investigating the impact of surface wave breaking on modelling the trajectories of drifters in the Northern Adriatic Sea during a wind-storm event. Ocean Model. 30, 225–239. doi:10.1016/ j.ocemod.2009.07.001.

Carniel, S., Barbariol, F., Benetazzo, A., Bonaldo, D., Falcieri, F.M., Miglietta, M.M., Ricchi, A., Sclavo, M., 2015. On the use of ocean-atmosphere-wave models during an extreme CAO event: The importance of being coupled. In: EGU General Assembly Conference Abstracts, 17, 2015 EGU General Assembly.

Carniel, S., Trincardi, F., Bonaldo, D., Benetazzo, A., Bergamasco, A., Boldrin, A., Falcieri, F.M., Langone, L., Sclavo, M., 2016. Off-shelf fluxes across the Southern Adriatic Margin: Factors controlling dense water-driven transport phenomena. Mar. Geol. doi:10.1016/j.margeo.2015.08.016.

Charnock, H., 1955. Wind stress on a water surface. Quart. J. Roy. Meteorol. Soc 81, 639–640.

Connolly, T.P., Hickey, B.M., 2014. Regional impact of submarine canyons during seasonal upwelling. J. Geophys. Res: Oceans 119 (2), 2121–2128. doi:10.1002/jgrc. 20224.

Davolio, S., Stocchi, P., Benetazzo, A., Bohm, E., Riminucci, F., Ravaioli, M., Li, X.-M., Carniel, S., 2015. Exceptional Bora outbreak in winter 2012: Validation and analysis of high-resolution atmospheric model simulations in the northern Adriatic area. Dyn Atmos Oceans 71, 1–20. doi:10.1016/j.dynatmoce.2015.05.002.

Drennan, W.M., Taylor, P.K., Yelland, M.J., 2005. Parameterizing the sea surface roughness. J. Phys. Oceanogr. 35, 835–848. doi:10.1175/ JPO2704.1.

Egbert, G.D., Erofeeva, S.Y., 2002. Efficient inverse modeling of barotropic ocean tides. J. Atmos Oceanic Technol. 19 (2), 183–204.

Fairall, C.W., Bradley, E.F., Hare, J.E., Grachev, A.A., Edson, J.B., 2003. Bulk parameterization of air-sea fluxes: Updates and verification for the COARE algorithm. J. Climate 16 (4), 571–591.

Falcieri, F.M., Benetazzo, A., Sclavo, M., Russo, A., Carniel, S., 2014. Po River plume pattern variability investigated from model data. Cont. Shelf Res. 87, 84–95. doi:10.1016/j.csr.2013.11.001.

Gemmill, W., Katz, B., Li, X., 2007. Daily real-time global SST-high-resolution analysis: RTG_SST_HR, NOAA/NCEP. NOAA/NWS/NCEP/MMAB Office Note Nr 260, 39 http://polar.ncep.noaa.gov/sst/.

Griffiths, R.W., 1986. Gravity currents in rotating systems. Ann. Rev. Fluid Mech. 18, 59–89.

Haidvogel, D.B., Arango, H., Budgell, W.P., Cornuelle, B.D., Curchitser, E., Di Lorenzo, E., Fennel, K., Geyer, W.R., Hermann, A.J., Lanerolle, L., Levin, J., McWilliams, J.C., Miller, A.J., Moore, A.M., Powell, T.M., Shchepetkin, A.F., Sherwood, C.R., Signell, R.P., Warner, J.C., Wilkin, J., 2008. Ocean forecasting in terrain-following coordinates: Formulation and skill assessment of the Regional Ocean Modeling System. J. Comput. Phys. 227, 3595–3624. doi:10.1016/j.jcp. 2007.06.016.

Hansen, B., Østerhus, S., Quadfasel, D., Turrell, W., 2004. Already the day after tomorrow? Science 305 (August), 953–954.

Herrmann, M., Estournel, C., Déqué, M., Marsaleix, P., Sevault, F., Somot, S., 2008. Dense water formation in the Gulf of Lions shelf: Impact of atmospheric interannual variability and climate change. Cont. Shelf Res. 28 (15), 2092–2112. doi:10.1016/j.csr.2008.03.003.

Holland, P.R., 2011. Oscillating dense plumes. J Phys. Oceanogr. 41 (8), 1465–1483. doi:10.1175/2011JPO4532.1.

Horvath, K., Bajic´, A., Ivatek-Šahdan, S., 2011. Dynamical downscaling of wind speed in complex terrain prone to bora-type flows. J. Appl. Meteorol. Climatol. 50, 1676–1691. doi:10.1175/2011JAMC2638.1.

Ivanov, V.V., Shapiro, G.I., Huthnance, J.M., Aleynik, D.L., Golovin, P.N., 2004. Cascades of dense water around the world ocean. Prog. Oceanogr. 60, 47–98. doi:10.1016/j.pocean.2003.12.002.

Janekovic´ , I., Mihanovic´ , H., Vilibic´ , I., Tudor, M., 2014. Extreme cooling and dense water formation estimates in open and coastal regions of the Adriatic Sea during the winter of 2012. J. Geophys. Res. Oceans 119, 3200–3218. doi:10.1002/ 2014JC009865.

Kraus,R.,Supic´,N.,Lucˇic´,D.,Njire,J.,2015.Impactofwinteroceanographicconditions on zooplankton abundance in northern Adriatic with implications on Adriatic anchovy stock prognosis. Estuarine and Coastal Shelf Science 167, 56– 66. doi:10.1016/j.ecss.2015.10.008.

Kraus, R., Supic´, N., Precali, R., 2016. Factors favouring phytoplankton blooms in the northern Adriatic: Towards the northern Adriatic empirical ecological model. Ocean Sci. 12 (1), 19–37. doi:10.5194/os-12-19-2016.

Kumar, N., Voulgaris, G., Warner, J.C., Olabarrieta, M., 2012. Implementation of the vortex force formalism in the coupled ocean-atmosphere-wave-sediment transport (COAWST) modeling system for inner shelf and surf zone applications. Ocean Model. 47, 65–95. doi:10.1016/j.ocemod.2012.01.003.

Kuzmic´, M., Janekovic´, I., Book, J.W., Martin, P.J., Doyle, J.D., 2007. Modeling the northern Adriatic double-gyre response to intense bora wind: A revisit. J. Geophys. Res.: Oceans 112 (3), 1–27.

Langone, L., Conese, I., Miserocchi, S., Boldrin, A., Bonaldo, D., Carniel, S., Chiggiato, J., Turchetto, M., Borghini, M., 2016. Sediment transport to the western margin of the Southern Adriatic: Processes involved in transferring particulate matter to the deep basin. Mar. Geol. doi:10.1016/j.margeo.2015.09.004.

Licˇer,M.,Smerkol,P.,Fettich,A.,Ravdas,M.,Papapostolou,A.,Mantziafou,A.,Strajnar, B., Cedilnik, J., Jeromel, M., Jerman, J., Petan, S., Malacˇicˇ, V., Sofianos, S., 2016. Modeling the ocean and atmosphere during an extreme bora event in northern Adriatic using one-way and two-way atmosphere–ocean coupling. Ocean Sci. 12, 71–86. doi:10.5194/os-12-71-2016.

Malanotte-Rizzoli, P., et al., 2014. Physical forcing and physical/biochemical variability of the Mediterranean Sea: A review of unresolved issues and directions for future research. Ocean Sci. 10, 281–322. doi:10.5194/os-10-281-2014.

Mihanovic´, H., Vilibic´, I., Carniel, S., Tudor, M., Russo, A., Bergamasco, A., Bubic´, N., Ljubešic´, Z., Vilicˇic´, D., Boldrin, A., Malacˇicˇ, V., Celio, M., Comici, C., Raicich, F., 2013. Exceptional dense water formation on the Adriatic shelf in the winter of 2012. Ocean Sci. 9, 561–572.

Najdek, M., Paliaga, P., Šilovic´, T., Batistic´, M., Garic´, R., Supic´, N., Ivancˇic´, I., Ljubimir, S., Korlevic´ , M., Jasprica, N., Hrustic´ , E., Dupcˇic´ Radic´ , I., Blažina, M., Orlic´, S., 2014. Picoplankton community structure before, during and after convection event in the offshore waters of the southern Adriatic Sea. Biogeosciences 11, 2645–2659.

Olabarrieta, M., Warner, J.C., Armstrong, B., Zambon, J.B., He, R., 2012. Ocean– atmosphere dynamics during Hurricane Ida and Nor'Ida: An application of the coupled ocean–atmosphere–wave–sediment transport (COAWST) modeling system. Ocean Model. 43-44, 112–137. doi:10.1016/j.ocemod.2011.12.008.

Olita, A., Iermano, I., Fazioli, L., Ribotti, A., Tedesco, C., Pessini, F., Sorgente, R., 2015. Impact of currents on surface flux computations and their feedback on dynamics at regional scales. Ocean Sci. 11, 657–666. doi:10.5194/os-11-657-2015.

Oost, W.A., Komen, G.J., Jacobs, C.M.J., Van Oort, C., 2002. New evidence for a relation betweenwind stress and wave age from measurements during ASGAMAGE. Bound.-Layer Meteorol 103, 409–438.

Pinardi, N., Allen, I., Demirov, E., De Mey, P., Korres, G., et al., 2003. The Mediterranean ocean forecasting system: First phase of implementation (1998-2001). Ann. Geophys. 21 (1), 3–20.

Pullen, J., Doyle, J.D., Signell, R.P., 2006. Two-way air-sea coupling: A study of the Adriatic. Mon. Weather Rev. 134, 1465–1483. doi:10.1175/MWR3137.1.

Raicich, F., Malacˇicˇ, V., Celio, M., Giaiotti, D., Cantoni, C., Colucci, R.R., Cˇermelj, B., Pucillo, A., 2013. Extreme air-sea interactions in the Gulf of Trieste (North Adriatic) during the strong Bora event in winter 2012. J. Geophys. Res. Ocean. 118, 5238–5250.

Renault, L., Chiggiato, J., Warner, J.C., Gomez, M., Vizoso, G., Tintoré, J., 2012. Coupled atmosphere-ocean-wave simulations of a storm event over the Gulf of Lion and Balearic Sea. J. Geophys. Res. Ocean. 117 (C9).

Ricchi, A., Miglietta, M.M., Falco, P.P., Benetazzo, A., Bonaldo, D., Bergamasco, A., Sclavo, M., Carniel, S., 2016. On the use of a coupled ocean-atmosphere-wave model during an extreme Cold Air Outbreak over the Adriatic Sea. Atmos. Res. 172-173, 48–65. doi:10.1016/j.atmosres.2015.12.023.

Sclavo, M., Benetazzo, A., Carniel, S., Bergamasco, A., Falcieri, F.M., Bonaldo, D., 2013. Wave-current interaction effect on sediment dispersal in a shallow semi-enclosed basin. J. Coastal Res. (65) 1587–1592.

Skamarock, W.C., Klemp, J.B., Dudhia, J., Gill, D.O., Barker, D.M., Wang, W., and Powers, J.G., 2005. A Description of the Advanced Research WRF Version 2.

Signell, R.P., Carniel, S., Chiggiato, J., Janecovic, I., Pullen, J., Sherwood, C., 2008. Collaboration tools and techniques for large model datasets. J. Mar. Syst. 65, 154– 161. doi:10.1016/j.jmarsys.2007.02.013.

Smith, P.C., 1975. A streamtube model for bottom boundary currents in the ocean. Deep-Sea Res. 22, 853–873.

Supic´ , N., Kraus, R., Kuzmic´ , M., Paschini, E., Precali, R., Russo, A., Vilibic´ , I., 2012. Predictability of northern Adriatic winter conditions. J. Mar. Syst. 90, 42–57.

Tesi, T., Miserocchi, S., Goñi, M.A., Langone, L., Boldrin, A., Turchetto, M., 2007. Organic matter1020 origin and distribution in suspended particulate materials and surficial sediments from the1021 western Adriatic Sea (Italy). Estuarine, Coastal and Shelf Science 73, 431–446. doi:10.1016/j.ecss.2007.02.008.

Taylor, P.K., Yelland, M.J., 2001. The dependence of sea surface roughness on the height and steepness of the waves. J. Phys. Oceanogr. 31, 572–590.

Turchetto, M., Boldrin, A., Langone, L., Miserocchi, S., 2012. Physical and biogeochemical processes controlling particle fluxes variability and carbon export in the Southern Adriatic. Cont. Shelf Res. 44, 72–82. doi:10.1016/j.csr.2011.05.005.

Vatova, A., 1934. L'anormale regime fisico-chimico dell'Alto Adriatico nel 1929 e le sue ripercussioni sulla fauna (in Italian). Thalassia I 8, 1–49.

Verdicchio, G., Trincardi, F., 2006. Short-distance variability in slope bed-forms along the Southwestern Adriatic Margin (Central Mediterranean). Mar. Geol. 234 (1-4), 271–292. doi:10.1016/j.margeo.2006.09.007.

Vilibic´, I., Supic´, N., 2005. Dense water generation on a shelf: The case of the Adriatic Sea. Ocean Dyn 55, 403–415.

Warner, J.C., Armstrong, B., He, R., Zambon, J.B., 2010. Development of a Coupled Ocean-Atmosphere-Wave-Sediment Transport (COAWST) Modeling System. Ocean Model 35, 230–244.

Zambon, J.B., He, R., Warner, J.C., 2014. Investigation of hurricane Ivan using the coupled ocean–atmosphere–wave–sediment transport (COAWST) model. Ocean Dyn. 1535–1554. doi:10.1007/s10236-014-0777-7.

3. Sensitivity of Mediterranean Tropical-Like Cyclone to different model configuration and coupling strategy

3.1. Abstract

In November 2011, an Atlantic depression affected the Mediterranean basin, eventually evolving into a Tropical-Like Cyclone (TLC or Mediterranean Hurricane, usually designated as Medicane). In the region affected by the Medicane, mean sea level pressures down to 990 hPa, wind speeds of hurricane intensity close to the eye (around 115 km/h) and intense rainfall in the prefrontal zone were reported. The intensity of this event, together with its long permanence over the sea, suggested its suitability as a paradigmatic case for investigating the sensitivity of a numerical modeling system to different configurations, air-sea interface parameterizations and coupling approaches. Toward this aim, a set of numerical experiments with different parameterization schemes and levels of coupling complexity was carried out within the Coupled Ocean Atmosphere Wave Sediment Transport System (COAWST), which allows the description of air-sea dynamics by coupling an atmospheric model (WRF), an ocean circulation model (ROMS), and a wave model (SWAN). The sensitivity to different initialization times and Planetary Boundary Layer (PBL) parameterizations was firstly investigated by running a set of WRF standalone (atmospheric-only) simulations. In order to better understand the effect of coupling on the TLC formation, intensification and trajectory, different configurations of atmosphere-ocean coupling were subsequently tested, eventually including the full coupling among atmosphere, ocean and waves, also changing the PBL parameterization and the formulation of the surface roughness. Results show a strong sensitivity of both the trajectory and the intensity of this TLC to the initial conditions, while the tracks and intensities provided by the coupled modeling approaches explored in this study do not introduce drastic modifications with respect to those resulting from a fine-tuned standalone atmospheric run, though they provide by definition a better physical and energetic consistency. Nevertheless; the use of different schemes for the calculation of the surface roughness from wave motion, which reflects the description of air-sea interface processes, can significantly affect the results in the fully coupled runs.

3.2. Introduction

With the advent of remote sensing, some peculiar vortices having characteristics very similar to tropical cyclones have been detected over the Mediterranean Sea (Ernst et al 1983; Moscatello et al 2008) and hence are named Tropical Like Cyclones (TLCs), or Medicanes (Mediterranean Hurricanes). Although there is still an open debate in the literature about what should be exactly considered as a Medicane, these vortices are usually characterized from satellites by spiral-like cloud bands elongated from the center, a calm "eye" without cloud coverage, and intense wind speed maxima some tens of km far from the center of the cyclone. From a dynamic point of view, they are characterized by an axi-symmetric structure with the vertical alignment of the pressure minima at different levels, weak vertical wind shear and deep warm anomaly. TLCs have a typical diameter of 100–300 km (Aktar et al 2014; Tous et al 2013), while the associated surface wind speeds can occasionally reach hurricane 1 strength according to Saffir-Simpson scale. These cyclones may last for several days, although the presence of tropical characteristics may be limited to a few hours (Miglietta et al 2013; Emanuel 2005; Fita et al 2007) . They form predominantly during the end of summer or during autumn, when the latent and sensible heat fluxes are more intense (Cioni et al 2016) due to the relatively high sea surface temperatures (SSTs) combined with upper-level cold-air intrusions (Miglietta et al 2011). They originally develop in baroclinic environments, associated with the cut-off (Emanuel 2005) of an Atlantic depression in the Mediterranean, sometimes associated with the high vorticity in the low level associated with an orographic depression (Moscatello et al 2008). A typical feature of Medicanes is the presence of a warm core developing over the whole extension of the troposphere, associated with the release of latent heat caused by the convection around the pressure minimum (Akhtar et al 2014; Miglietta et al 2011). The intensity of surface heat fluxes can be very important mainly during the intensification of TLC; for this reason, the SST plays a key role in the Medicanes evolution (Cioni et al 2016). Sensitivity examination of both the initial conditions and parameterization schemes reveals that microphysics and convection may affect the simulation results, but the main sensitivity is to the initial conditions (Davolio et al 2012; Miglietta et al 2015). Due to the central role of air-sea interaction, the interplay between atmosphere and ocean in generating and maintaining these Mediterranean hurricanes should be properly modeled, in a way similar to what is actually performed for hurricanes. In fact, the latter have been studied considering the feedback between the two environments with the aid of numerical coupled atmosphere-ocean (-wave) models (Warner et al 2010; Olabarietta et al 2012). Results achieved in these studies have shown that the coupling between atmosphere and ocean can be important for simulating properly some of these cyclones (Olabarrieta et al 2012), while in other cases it does not provide significant improvements with respect to standalone simulations (Zambon et al 2014). The purpose of this work

is to explore the sensitivity to different configurations of a coupled modeling system (COAWST; Coupled Ocean Atmosphere Wave Sediment Transport System), applied to the study of an intense Mediterranean cyclone. Results can be used for research purposes, such as model fine-tuning to obtain deeper physical insights into the genesis and evolution of these processes, as well as for operational scopes, dealing with the prediction of severe events and the definition of emergency response strategies. The modeling activity proposed here was performed using three different configurations. Following an approach similar to (Zambon et al 2014; Ricchi et al 2016), in the first implementation we used "standalone" runs, using only the atmospheric WRF model (Weather Research and Forecasting System). In these runs three different approaches for the description of SST (Sea Surface Temperature) and two different PBL (Planetary Boundary Layer) schemes (that implement the coupling of waves in the atmospheric model) were adopted. The second configuration couples bi-directionally WRF and the ROMS (Regional Oceanic Modelling System) ocean model. The last and most complex numerical approach is based on the full coupling among WRF, ROMS, and the SWAN (Simulating WAves in Nearshore) wave model. In addition, we also analyzed the effect of different roughness schemes which include wave characteristics in their calculation. The paper is organized as follows. Section 2 shows an overview of the event at the synoptic scale. In Section 3 we describe the numerical modeling systems and the numerical approach. Section 4 describes the numerical results and some conclusions are drawn in Section 5.

3.3. Case Study: Medicane ROLF

In this work, we study the TLC named ROLF (official name provided by the University of Berlin, the institution in charge to name the cyclones over the European area), selected as a "reference" case study among several events described in (Miglietta et al 2013) due to the long persistence (more than 48 h) of its tropical features. ROLF developed from a cut-off low over Spain on 3 November 2011 (Miglietta et al 2013), associated with a large and deep Atlantic depression centered to the west of England, while a high-pressure area affected eastern Europe (Figure 1 panel (a)). The Atlantic depression was "locked" between the high over central Europe and the Azores high. The meridional stretching of the Atlantic depression (Figure 1 panel (b)) induced the baroclinic wave to "cut-off" over the Gulf of Lion and to form a pressure minimum (on 6 November 2011 around 1000 hPa) (Figure 1 panel (c,d)). The depression was isolated from the synoptic circulation and was tilted with respect to the vertical axis, showing the typical characteristics of an extra-tropical cyclone (Hart et al 2003). On 7 November the pressure minima at sea level and at 500 hPa were aligned, e.g., the geopotential cut-off was located over the SLP (Sea Level Pressure) minimum (Figure 1 panel (e)),

while the cyclone crossed the Balearic Islands and moved to the east (Figure 2 panels (a,b)). On the following day, it moved slowly northward towards the Gulf of Lion: in this phase, the TLC reached its highest intensity, with 10 m wind speed up to 30 m s−1 and the lowest estimated pressure of around 985 hPa. Landfall occurred on 9 November (around 12 UTC) near the east coast of the Gulf of Lion (Figure 2 panel (d)). During this period, ROLF reached 10 m wind speeds of around 30 m s−1, generated significant wave heights up to 8 m high, and a large rainfall amount, particularly in coastal areas. Following (Miglietta et al 2013), the estimated maximum wind speed at 900 hPa was approximately 46 m/s, the maximum radius was around 150 km and the phase with tropical characteristics lasted for approximately 2 days and half. As shown in Figure 3, the SST anomaly in the area of generation and transit of the Medicane was about +3 ◦C, and approximately +2 ◦C in the entire western Mediterranean basin, except from the coastal areas where some negative anomaly was recorded, mainly due to the intense coastal upwelling, which is very frequent in the area (Millot et al 1999; Renault et al 2012). The Satellite Service Division of the National Oceanic and Atmospheric Administration (NOAA) carried out a preliminary analysis of the TLC (NOAA-NESDIS), identifying its trajectory, estimating the minimum pressure and the maximum wind around the eye. This analysis was carried out during the event based on readily available data, aiming at a real-time assessment of the evolution of the TLC for operational purposes, but suffered from some inconsistencies as emerges from comparison with the ASCAT (Advanced SCATterometer) wind data (e.g., Figure 4). For this reason, in this work we estimated the trajectory of the cyclone by identifying the position of the eye, based on a set of georeferenced hourly-spaced satellite images (Eumetsat infrared datasets).

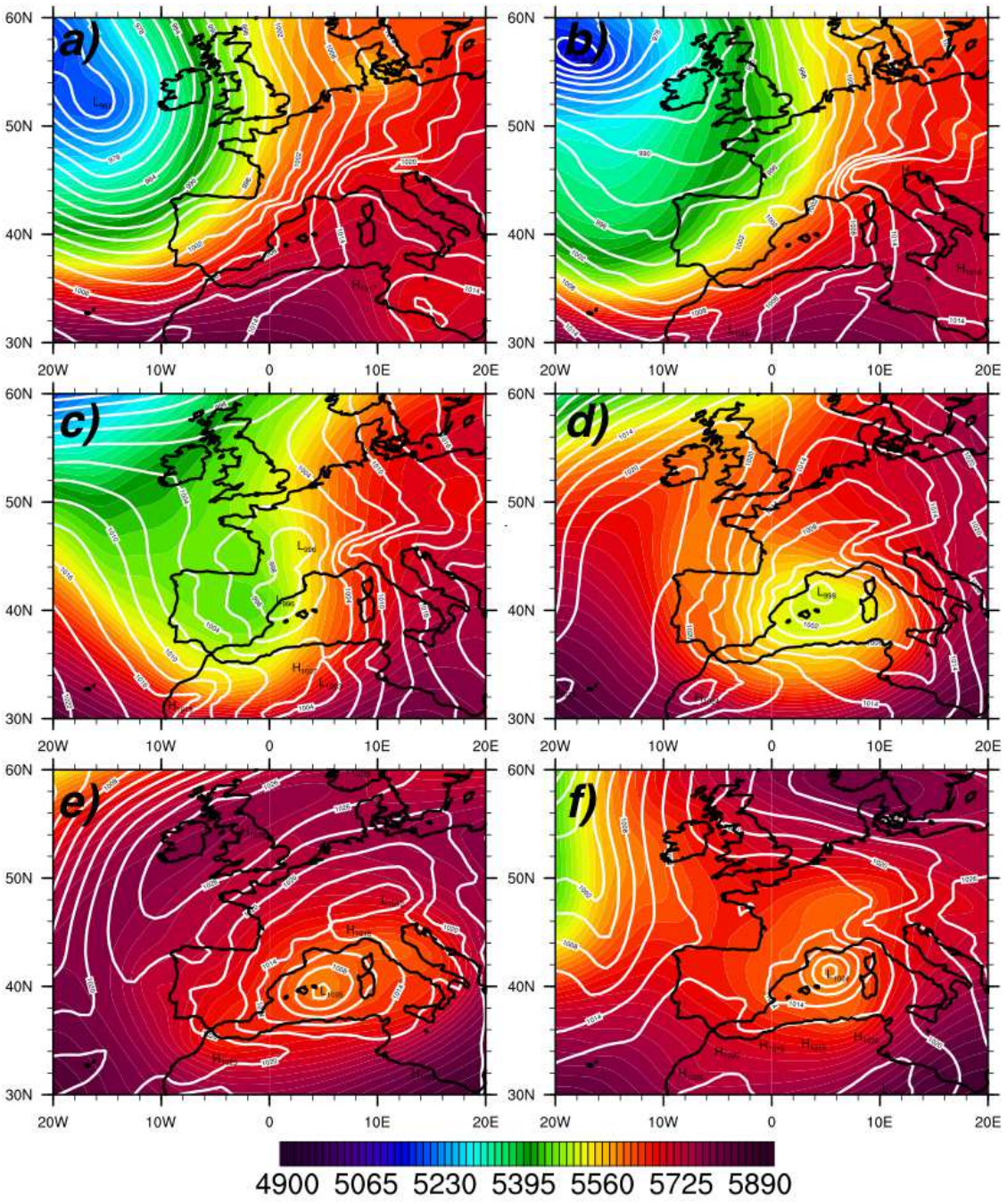

Figure 1. Snapshots of surface pressure (white lines; c.i. = 3 hPa), and 500 hPa geopotential height (colors) on 3 November 2011, 00 UTC (panel (a)) and 4 November 2011, 00 UTC (panel (b))—during the transit of the Atlantic baroclinic wave over Spain, close to the Balearic Sea-, 5 November 2011, 00:00 UTC (panel (c))—during the formation of the ROLF depression over Spain-, on 6 November 2011, 00:00 UTC (panel (d))—during the cut-off low over the Balearic sea-, on 7 November 2011, 00:00 UTC (panel (e)) and 8 November 2011, 00:00 UTC (panel (f)). Data are from ECMWF ERA-40 (European Center for Medium range Weather Forecasting).

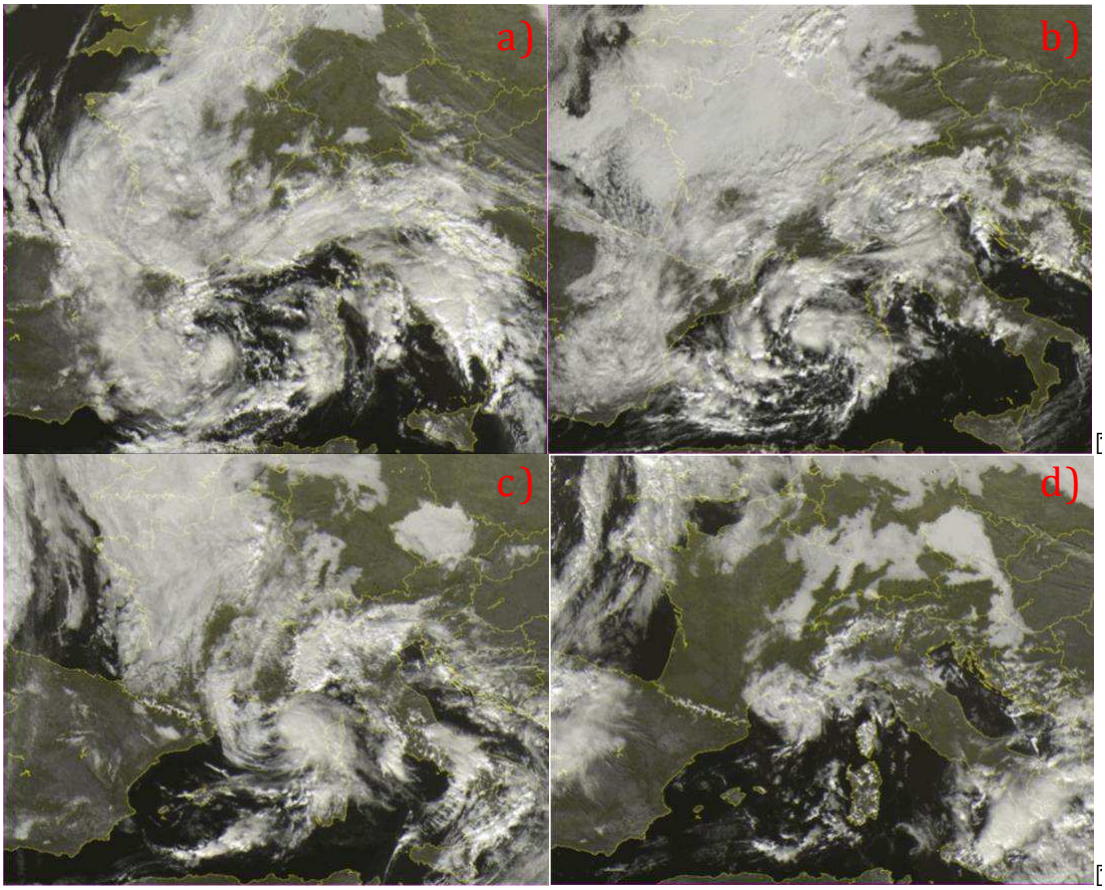

Figure 2. Visible channel of Meteosat Satellite images on 6 November 2011, 12:00 UTC (panel (a)), 7 November 2011, 12:00 UTC (panel (b)), 8 November 2011, 12:00 UTC (panel (c)) and 9 November 2011, 12:00 UTC (panel (d)) (source: www.sat24.com; copyright: EUMETSAT). In panel (a) we can see the formation of the TLC, whereas in the panel (b) the TLC is formed and in panel (c) ROLF is still well identified. In panel (d) the landfall of cyclone is shown.

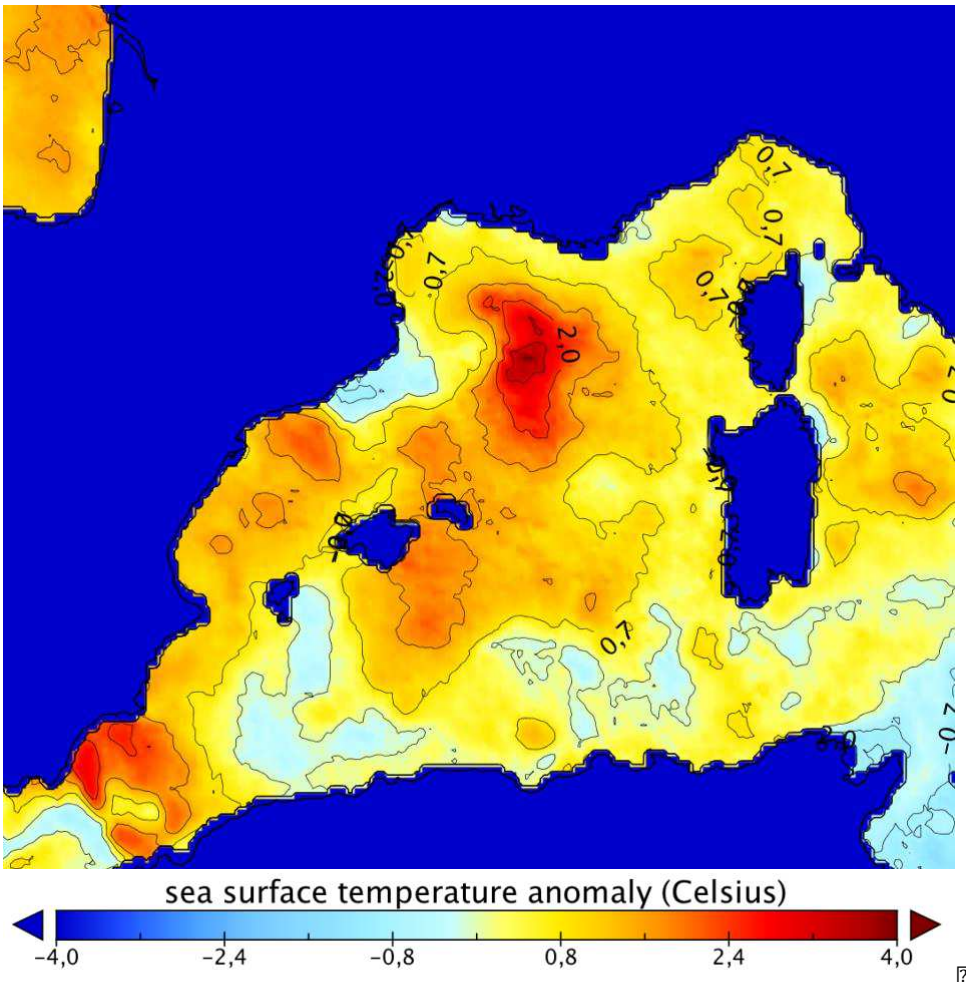

Figure 3. SST anomaly produced by the Mediterranean Forecasting System (MFS INGV, [24]) on 8 November 2011, consisting of the difference between analysed SST from MFS and the climatology 1955–2004 supplied by the Nucleus for European Modelling of the Ocean (NEMO), with a variational data assimilation scheme (OceanVAR) for temperature and salinity vertical profiles and satellite Sea Level Anomaly along track data. The model horizontal grid resolution is 1°/16° (ca. 6–7 km) and the unevenly spaced vertical levels are 72 (Pinardi et al 2003). In this figure, we can see the positive SST anomaly in the western Mediterranean Sea, between 1–3.7 °C, in particular over the formation area of the TLC.

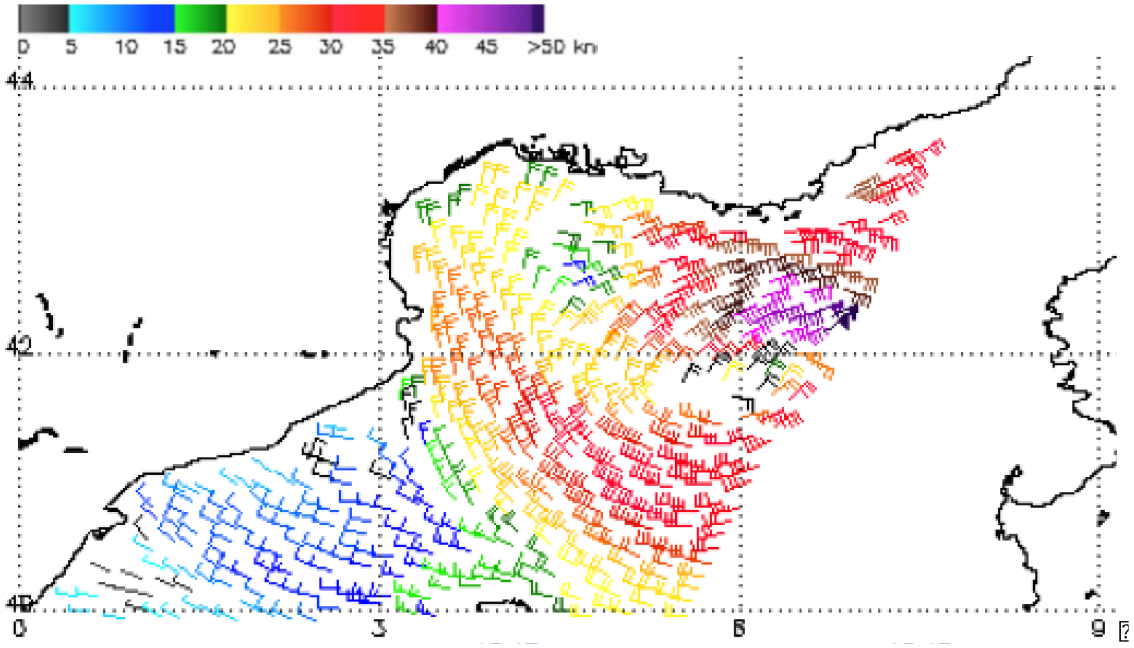

Figure 4. Wind speed and direction from the Advanced Scatterometer Wind data (ASCAT) shown on 8 November 10:00 UTC at 25 km of resolution. In the proximity of the pressure minimum, wind speed is approximately 25–28 ms−1 (50–55 knots). The area with maximum intensity is located on the northern side of TLC.

3.4 Numerical Modelling and Approach

3.4.1. The COAWST Modeling Suite

COAWST is a complex system that manages different numerical models and allows feedbacks at the air-sea interface, through the interaction among SST, marine circulation, waves and atmospheric dynamics. The COAWST infrastructure is shown in Figure 5, where the models implemented in the system are represented: WRF for the atmosphere, ROMS for the ocean, and SWAN for the generation and propagation of wind waves. In COAWST, the coupling is performed with the use of two tools responsible for the organization and communication of the information among different models. The tool that provides the data flow management is the Model Coupling Toolkit (MCT (Larson et al 2005)), which is a dedicated library tool interfacing with the models, responsible for the exchange, transmission and processing of numerical data among the models using coupled and parallel approach by means of MPI libraries (Warner et al 2008). The exchange of variables takes place with a user-defined time step (300 s in this work). To allow the exchange of variables among the grids of the different models, COAWST relies on the Spherical Coordinate Remapping Interpolation Package (SCRIP (Jones et al 1999)) to compute interpolation weights overcoming the possible differences in resolution, rotation and spatial coverage among the grids.

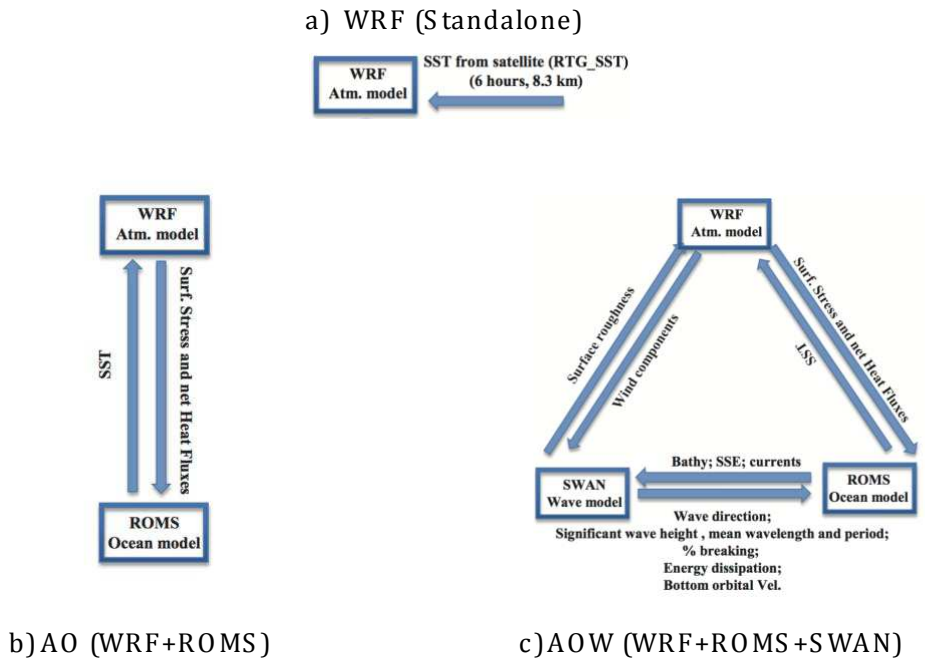

Figure 5 he three different configurations adopted in this study. Panel (a): WRF run: atmosphere standalone (WRF uses the SST data from the RTG_SST dataset, every 6 h). Panel (b): AO (Atmosphere-Ocean) run: coupling between atmosphere and ocean (WRF receives the SST from ROMS model, at 1 km resolution, every 300 s, and exchanges the turbulent heat fluxes with ROMS). Panel (c): AOW (Atmosphere-Ocean-Wave) run: full atmosphere-ocean-wave coupling (WRF and ROMS exchange SST and fluxes; WRF and SWAN exchange the wind fields and the wave parameters; ROMS and SWAN exchange currents fields and wave parameters).

3.4.2. Atmospheric Model

WRF is a mesoscale numerical weather prediction model, serving a wide range of meteorological applications across scales from tens of meters to thousands of kilometers. WRF is a finite-difference numerical model over an Arakawa-C grid in σ (terrain-following) coordinate, fully compressible and non-hydrostatic (Skamarock et al 2008). The use of coupled models within COAWST requires that the atmospheric model domain fully encloses the ocean model grid, which in turn encompasses the whole Mediterranean basin. In addition, the need for a proper characterization of the large-scale dynamics, especially over the Atlantic Ocean, where the system comes from, led to the extension of the atmospheric model domain significantly to the west and north of the TLC position. For these reasons, WRF is configured over a large "mother" grid with 350 × 250 points spaced by 25 × 25 km2, centered at latitude 47.5° N and longitude 7.5° E, ranging from northern Norway to the Sahara Desert, and from the central Atlantic ocean to the western Caspian Sea. This grid provides the boundary conditions to a nested grid with 5 km horizontal spacing and 970 × 708 grid points, using a one-way nesting technique, ranging from the north-eastern Atlantic to the whole Mediterranean and Black Sea (Figure 6) with 55 vertical levels, the lowest one located 12 m above the ground. The topographic dataset is USGS (30″ resolution on inner domain) interpolate, at the resolution of the grid. The ratio 1:3 and 1:5 (used in this work), between child and parent domain, are suggested in WRF model user guide.

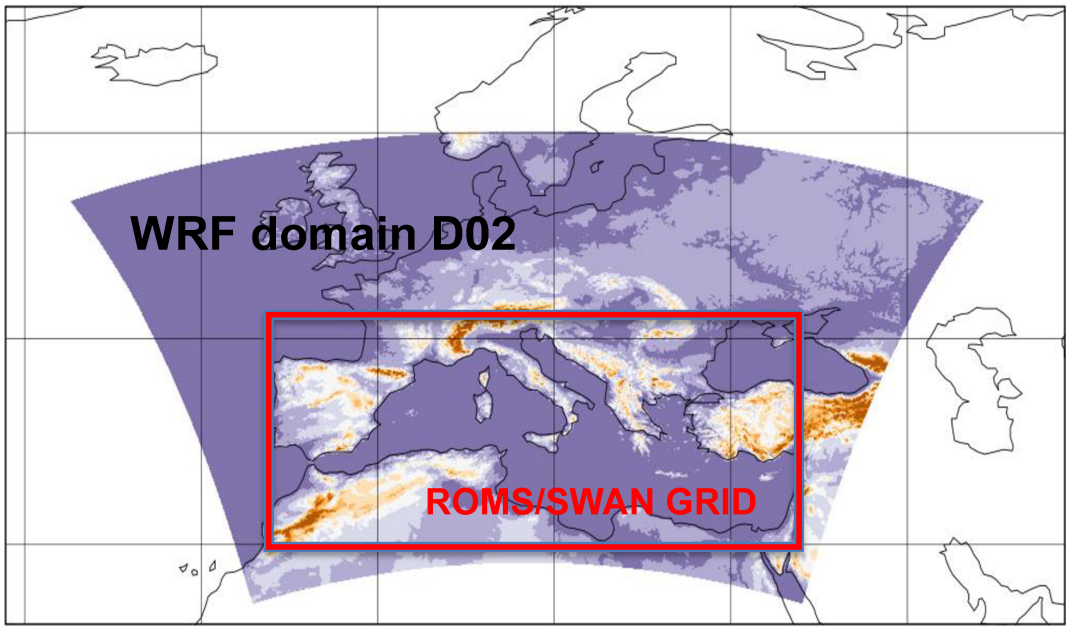

Figure 6. The nested WRF domain and, delimited by the red line, the computational domain used for ROMS-SWAN which included the whole Mediterranean Sea.

3.4.3. Ocean Model

ROMS is a hydrostatic, finite differences, split-explicit, free-surface numerical model for ocean circulation and thermohaline processes (Shchepetkin et al 2005). It solves the RANS (Reynolds Average Navier-Stokes) equations in a horizontal Arakawa-C grid and s-coordinate (σ terrain-following coordinate is a special case of s-coordinate) in vertical (Shchepetkin et al 2005; Shchepetkin et al 2009; Haudvogel et al 2008;). In this work, we ran ROMS simulations over a grid with 5 km horizontal resolution (for consistency with the atmospheric model) and 30 vertical levels, using GEBCO bathymetry at 30″. The grid has 532 × 264 grid points and covers the entire Mediterranean basin (Figure 6, red box) in order to prevent possible interpolation noise on an open sea boundary. The grid is closed at the Dardanelles and at the Strait of Gibraltar. As good practice, we ran a 15-day spin-up, initializing ROMS with MF-STEP fields retrieved from MyOcean (now CMEMS - http://marine.copernicus.eu) data referred to 20 October 2011 at 00:00 UTC. The spin-up was performed with the coupling technique between atmosphere and ocean (run AO, described further on) in order to achieve consistency with the dynamic atmospheric fields, with the use of the GFS-FNL dataset for initial and boundary conditions. In these simulations, ROMS used the Generic Length Scale mixing scheme as in (CMEMS)

3.4.4. Wave Model

The computation of wind wave dynamics in the Mediterranean Sea within the COAWST system relied on SWAN (Simulating WAves Nearshore), a third-generation wave model that computes wind-generated waves in offshore and coastal regions (Booji et al 1999). This model describes the generation, evolution and dissipation of the wave action variance density spectrum $E(\omega,\theta)$, with ω the wave angular frequency, and θ the wave direction. SWAN solves a radiative time-dependent transport equation in $E(\omega,\theta)$, accounting for the wind input, the wave-wave interactions, and several dissipation terms both in deep and shallow waters. From $E(\omega,\theta)$, various wave parameters can then be estimated at any point of the computational domain. Typical output fields are the significant wave height, hereafter denoted as Hs, the peak and mean wave periods, and the mean wave propagation direction. In our simulations covering the whole Mediterranean Sea, we used a consolidated configuration for the coupled use of SWAN in the COAWST system, as discussed in (Carniel et al 2016; Ricchi et al 2016; Booij et al 1999; Benetazzo et al 2014). In detail, SWAN has been implemented with the same horizontal resolution adopted for ROMS (in order to be coupled in COAWST, SWAN and ROMS models must use the same grid), being the wave action spectrum discretized with 36 equally spaced

directions and 24 geometrically distributed frequencies f, such that fn= fn + 1/1.1, with fn = 0.05 Hz. The SWAN model runs in non-stationary mode, namely with E(ω,θ) evolving in time, with a wind input from WRF every 300 s and the output saved every 3600 s.

3.5. Model Coupling in COAWST

As mentioned before, COAWST allows various levels of coupling among models, according to the degree of complexity in the implementation and the number of variables that are exchanged (as shown in Figure 5). The atmospheric model, the wave model and the ocean current model can then be mutually connected or excluded, as in the experiments described hereinafter.

3.5.1. WRF-Only Experiments

First, the simulations using WRF in standalone mode (WRF1-10 experiments, see Table 1 and Figure 5 panel (a)), i.e., without any coupling to other models, are considered. As discussed in (Ricchi et al 2016), the initial SST forcing can be represented in different ways. In this work, we have chosen the RTG_SST satellite dataset (Benetazzo et al 2014) available every 24 h with 8.3 km horizontal resolution. The configuration of the model in the control run is based on the same setup used in (Miglietta et al 2013). Kain-Fritsch formulation (Kain 2004) was used for cumulus scheme, while Thompson scheme (Kain et al 2004) was adopted for cloud physics and RRTMG (Thompson et al 2008) for short and long wave radiation schemes. The initialization data of the standalone simulations are provided by the global model reanalyses GFS-FNL (Final Reanalysis of the Global Forecasting System https://www.ncdc.noaa.gov/data-access/model-data/model-datasets/global-forcast-system-gfs) with a resolution of 1° × 1°. The same data were used for the boundary conditions, updated every 6 h. Seven simulations were performed using different initialization times (shifting the starting time every 12 h from 4 November, 00 UTC, to 7 November, 00 UTC) in order to test the sensitivity to the initial condition (run WRF1-7) and to identify the one leading to the best model performances. The role of the Planetary Boundary Layer (PBL) scheme is also analyzed, using both schemes available in COAWST (WRF5 and WRF8), namely "Mellor-Yamada-Janjic" MYJ (Mlawer et al 1997) and Mellor-Yamada-Nakanishi-Niino MYNN2.5 (Compo et al 2011), starting from the initial condition providing the best results (i.e., 00 UTC, 6 November—WRF5 and WRF8). All of these different configurations are shown in Table 1, for a total of 10 experiments using the WRF standalone configuration. The numerical formulation for surface roughness is taken from (NOAA GFS-FNL),

used by default in WRF, with: z0 = zch*u*2/g, where z0 is the roughness length, zch is the Charnock constant (0.0011), and u* the friction velocity. Also, since we speculate about the importance of the air-sea interactions in the development of the cyclone, the sensitivity to SST is analyzed by reducing the initial SST by 3 °C all over the domain in the control run (WRF9). In this way, the SST anomaly, present at moment of TLC formation, is removed and the experiment is performed with the average values of SST; the comparison of the two allows to disentangle the effect of a warmer sea surface. An additional run (WRF10) was forced using the same high-resolution SST provided by ROMS to initialize the coupled experiments (the boundary SST is also provided by the ROMS field every 6-h). This simulation bridges the conceptual gap between uncoupled and coupled runs and allows to discriminate the effects of coupling from the effect of using the same initial/boundary conditions without coupling.

3.5.2. AO (Atmosphere – Ocean Coupling) Experiments

The second set of simulations employs a two-way coupling of WRF and ROMS. In this configuration, the ROMS model sends the SST data to WRF every 300 s, while the WRF model uses the received SST data (Figure 5 panel (b)) as the boundary condition, and in turn sends the turbulent heat fluxes to ROMS (which does not need to recalculate them). The substantial difference between the WRF standalone case and the AO run is that in the latter, the SST provided by ROMS is at high resolution and updated frequently in a dynamically consistent way. In fact, the heat fluxes that WRF sends to ROMS are based on the SST that WRF receives from ROMS, therefore providing a consistent approach for energy and momentum (Carniel et al 2016, Ricchi et al 2016; Warner et al 2008; Janjic 1994). In standalone configurations, the fluxes are calculated offline independently by the atmospheric and the ocean models, generating inconsistencies between the two representations. The surface roughness is parameterized using the Charnock algorithm in both models. As shown in Table 1, two different experiments are employed in the AO configuration, using respectively the MYJ (AO1 experiment) and MYNN 2.5 (AO2 experiment) PBL schemes. As in the standalone WRF case, we decided to use these two PBL calculation schemes because they are the only ones that implement the coupling with the wave in this COAWST version.

3.5.3. AOW (Atmosphere Ocean Wave Coupling) Experiments

The most complete COAWST coupling configuration includes the two-way interaction of air, ocean and wind waves, described by the exchange of information among the three different models: WRF, ROMS, SWAN (Figure 5 panel (c)). Differently from the case AO, the WRF model sends the wind components also to the SWAN wave model, that provides the wave parameters with which WRF calculates the surface roughness and the heat fluxes at the air-sea interface. ROMS and SWAN also communicate with each other, exchanging the components of the current along the water column and the wave parameters (Warner et al 2010; Booij et al 1999; Nakanishi et al 1955). Two PBL schemes, widely used in the scientific community (MYJ and MYNN, mainly differing in their order of closure, respectively 1.5 and 2.5), are available in COAWST in its fully coupled configuration. Also, COAWST has the possibility to compute the surface roughness following 3 different formulations. The first one is TY, from a work by Taylor and Yelland (Charnock et al 1955), who proposed a wave steepness-dependent ocean roughness, relying on three datasets representing sea-state conditions ranging from strongly forced to shoaling (Small et al 2011)

$$\frac{z_0}{H_s} = 1200\left(\frac{u_*}{L_p}\right)^{4.5} \qquad (1)$$

where z_0 is the roughness length, Lp is the peak period and Hs is the significant wave height computed by SWAN. The scheme by Drennan (Kumar et al 2012), the DRE parameterization, uses a wave age-based formula for the ocean roughness:

$$\frac{z_0}{H_s} = 3.35\left(\frac{u_*}{C_p}\right)^{3.4} \qquad (2)$$

where Cp is the wave phase speed at the peak frequency and where u_* is the friction velocity.

The OOST (Taylor and Yelland 2001) parameterization is a wave-age dependent scheme based on the 1996 ASGAMAGE experiment, expressed as:

$$\frac{z_0}{L_p} = \frac{25.0}{\pi}\left(\frac{u_*}{C_p}\right)^{3.4} \qquad (3)$$

To analyze the effect that the two PBL schemes and the three roughness formulations may have on the coupled model, a set of simulations is performed by changing the PBL and the surface roughness.

The resulting experiments with the AOW configurations (two using respectively the MYJ-AOW1 run and MYNN-AOW2 run PBL schemes, and three varying the surface roughness—with the MYJ scheme-), are listed in Table 1.

Run Name	Coupl.	ROMS	SWAN	SST	Roughness	PBL	Initialization Time
WRF1–7	NO	NO	NO	RTG_SST	CHA	MYJ	4–7 November 2011, every 00 UTC and 12 UTC (7 runs)
WRF8	NO	NO	NO	RTG_SST	CHA	MYNN	6 November 2011 00 UTC
WRF9	NO	NO	NO	RTG_SST decrease by 3 °C	CHA	MYJ	6 November 2011 00 UTC
WRF10	NO	NO	NO	SST MFS System	CHA	MYJ	6 November 2011 00 UTC
AO1	YES	YES	NO	ROMS 5 km	CHA	MYJ	6 November 2011 00 UTC
AO2	YES	YES	NO	ROMS 5 km	CHA	MYNN	6 November 2011 00 UTC
AOW1	YES	YES	YES	ROMS 5 km	OOST	MYJ	6 November 2011 00UTC
AOW2	YES	YES	YES	ROMS 5 km	OOST	MYNN	6 November 2011 00 UTC
AOW3	YES	YES	YES	ROMS 5 km	TY	MYJ	6 November 2011 00 UTC
AOW4	YES	YES	YES	ROMS 5 km	DRE	MYJ	6 November 2011 00 UTC

Table 1. Summary of all performed runs and their numerical setup. Acronyms used: CHA = Charnock (1955) (Charnock et al 1956); OOST = Oost et al. (2002)]; TY: Taylor and Yelland et al. (2001) ; DRE: Drennan et al. (2005) [. MYI: Mellor-Yamada-Janjic' ; MYNN: Mellor Yamada.

3.6. Results

In this section we discuss the results of the sensitivity experiments to different initialization times, to the PBL scheme, to the type of coupling between the atmosphere, ocean and wave models; the effect of PBL schemes and of the roughness formulations in the case of coupling are analyzed separately. While a thorough investigation of the physical processes and their modeling characterization is left to a dedicated forthcoming paper, here we focus on some key quantities of interest for operational forecasting and emergency management, such as the trajectory and intensity of the pressure minimum, and the wind speed. In particular, the quality of modeled trajectories (retrieved following (Olabarietta et al 2010; Drennan et al 2003; Oost et al 2002)) has been quantified in terms of geometrical distance from that retrieved from satellite data (Section 2, Figures 7 and 12).

3.6.1 Uncoupled Simulation

3.6.1.1. Initialization Time

The first analysis aimed at identifying the most suitable initial time and at assessing the model sensitivity to this (runs WRF1-7 in Table 1). The trajectories in the runs initialized on 4 November 2011 are shown respectively in Figure 7 panel (a) (00:00 UTC) and in Figure 7 panel (b) (12:00 UTC).The simulation starting at 00:00 UTC produces a shallow depression, which does not evolve into a TLC. The initialization at 12:00 UTC, 4 November (WRF2) also produces a weak depression in the early stage of the simulation, but the pressure minimum intensifies earlier, at about 09:00 UTC, 6 November, as shown in Figure 7 panel (b). The depression remains weak as the minimum pressure is generally above 1000 hPa (Figure 8 panel (a)), while the landfall occurs in the center of the Gulf of Lion, about 12 h before the observations. In this case, the average distance from the observed trajectory is 59 km (Table 1). Figure 7 panels (c,d) show the trajectories produced by the WRF3/WRF4 runs, initialized respectively at 00:00 UTC and 12:00 UTC, 5 November. Both trajectories are rather far from the satellite-retrieved track (average distance respectively of 71 and 58 km); also, the run initialized at 00:00 UTC develops a pressure minimum of around 995 hPa, while the run initialized at 12:00 UTC produces a much deeper pressure minimum of 983 hPa (Figure 8 panel(a)). The depression generated by WRF3 fills-up over the sea, while the cyclone in the WRF4 does end up with a landfall, although its occurrence is anticipated by about 21 h compared to the observations. Figure 7 panels (e,f) show the trajectories of the runs WRF5 and WRF6 initialized on 6 November respectively at 00:00 UTC (panel (e)) and at 12:00 UTC (panel (f)). These two simulations represent similar trajectories, which differ only in the last part of the TLC lifetime, but have different intensity during the entire evolution of the cyclone. In terms of trajectory, the run initialized at 00:00 UTC is slightly better, with an average distance of around 50 km, while for the other initializations we have a minimum distance of around 55–60 km (except for the WRF8 case, where the average distance is less than in WRF5 but the time evolution is anticipated compared to WRF5 and the observations). Also, the cyclone is more intense and reaches values of pressure minimum and wind speed very close to observations (Figure 8 panel (a)). On the other hand, the run initialized at 12:00 UTC has a better trajectory but does not deepen sufficiently and produce an unrealistically fast evolution of the TLC, in particular during the central part of the trajectory (Figure 8 panel (a). The simulation initialized at 00:00 UTC on 7 November (WRF7, Figure 7 panel (g)) provides the worst trajectory with an average distance of around the 90–100 km, and the depression does not reach pressure and wind speeds comparable with that provided by NOAA (Figure 8 panel (a,b)).

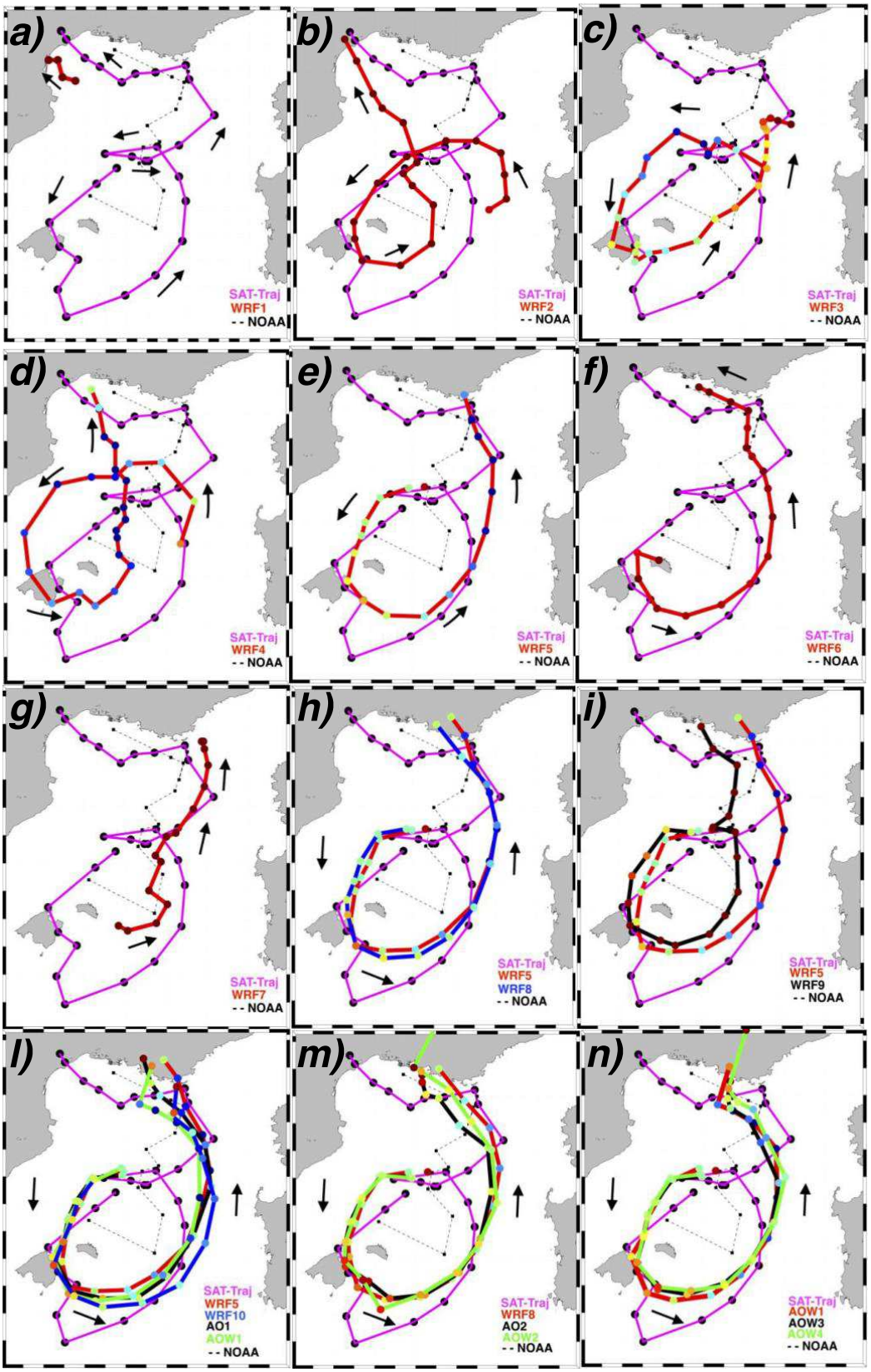

Figure 7. Trajectory and intensity of the cyclone for all simulations. In purple the trajectory estimated using observations from geo-referenced satellite image, which starts at 00:00 UTC, 6 November 2011, and ends at 12:00 UTC, 9 November 2011. The trajectory identifies the minimum pressure of ROLF every 3 h. Values of pressure minimum are highlighted by the color of the dots. The black arrows show the direction of propagation of the Medicane. In the different panels we

can observe the trajectories resulting from the various runs, compared with the trajectory obtained from the satellite, and the trajectory proposed by the NOAA. Panels (a-g): runs WRF1-7 (atmosphere standalone). Panel (h): runs WRF5 and WRF8 (MYJ and MYNN PBL). Panel (i): runs WRF5 (with MYJ) and WRF9 (WRF with SST decreased by 3 °C). Panel (l): runs WRF5, WRF10 (with high resolution SST from MFS-system), AO1 and AOW1 (AO and AOW with MYJ PBL scheme). Panel (m): runs WRF8, AO2 and AOW2, using MYNN PBL scheme. Panel (n): runs AOW1, AOW3, AOW4 using the different surface roughness schemes (OOST, TY, DRE)

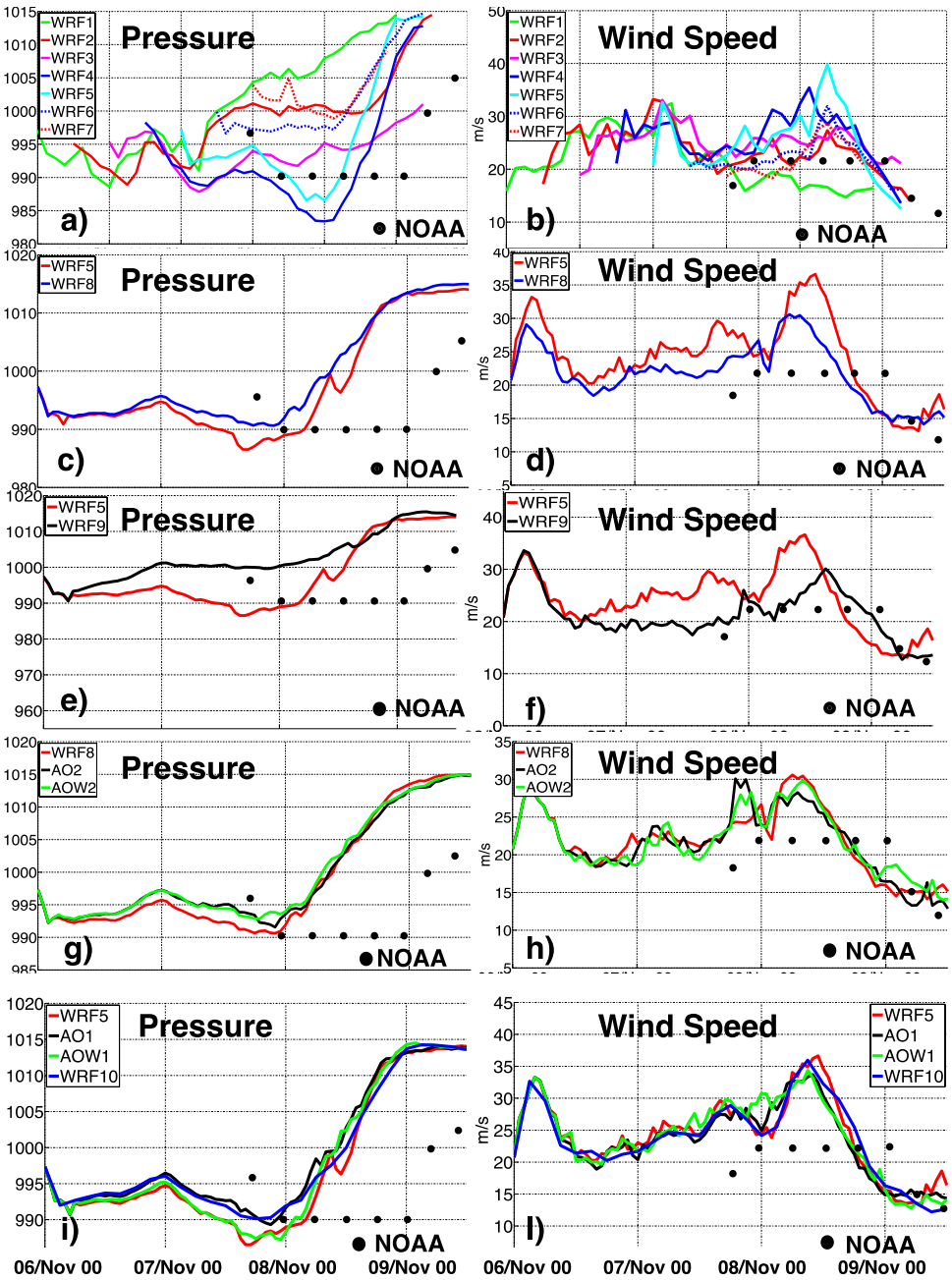

Figure 8. Time evolution of the pressure minimum (in hPa) and the maximum wind speed (m/s) around the eye, as resulting from different experiments. Black dots represent estimated NOAA data for the pressure minimum of the cyclone and wind speed around the minimum. Panels (a) and (b): comparison between the evolutions of the various WRF1-7 runs

for the pressure minimum and wind intensity. Panels (c) and (d): comparison between WRF5 and WRF8 (using, respectively, MYJ and MYNN PBL schemes). Panels (e) and (f): results from WRF5 and WRF9 (SST spectrum radiometer and SST +3 ° C). Panels (g) and (h): comparison among runs WRF8, AO2, AOW2, with MYNN PBL scheme. Panels (i) and (l): results for runs WRF5, WRF10, AO1, AOW1.

In conclusion, a significant sensitivity of the simulations to the initial condition is apparent both in terms of intensity and track. No simulation appears able to capture completely the observed evolution of the cyclone, in particular the timing in the central part of trajectory, when the cyclone makes a ring-like rotation addressing the difficulty in simulating correctly this category of events (see also Davolio et al 2009; Chanoureau et al 2012; Miglietta et al 2015). Apparently, the most accurate simulations are those that do not start neither too early (when the cyclone is still developing and the model cannot capture the development processes of the storm) nor too late (since the model needs a spin-up time to downscale the low-resolution global model FNL data to high-resolution model simulations). In conclusion, the best runs start during the cyclone mature stage; among these, the best is WRF5.

3.6.1.2 PBL Scheme

Next, we compare the effect of two different schemes of PBL considering only the initialization time that produced the best results (WRF5 run). The PBL schemes are used to parameterize the unresolved vertical turbulent fluxes of heat and momentum in the lower levels of the atmosphere (Drennan et al 2003). Results obtained when the PBL scheme is changed (WRF8 is implemented as run WRF5, initialized on 6 November at 00 UTC, but using MYNN2.5) are shown in Figure 7 panel (h) (blue line). The different PBL scheme does not lead to significant changes in the trajectories compared to WRF5 (red line), except from the last few hours, when the simulate trajectory is closer to the observed track near the landfall point. Comparing the two simulations, we note that the MYNN2.5 scheme generates a less intense cyclone in terms of pressure and wind speed (Figure 8 panels (c,d)). In conclusion, the advantage of using the updated MYNN scheme appears limited in the present case in terms of track, and even detrimental in terms of cyclone depth.

3.6.1.3. SST Variation

During the genesis of ROLF, the western Mediterranean sub-basin between the Balearic Islands, Sardinia and the Gulf of Lion was characterized by a SST anomaly of around +3 °C with respect to the climatology 1955–2004 produced by the Mediterranean forecasting System (MFS INGV, (Pinardi et al 2003)) (Figure 3). Since the TLC ROLF was generated in this area, we decided to evaluate how relevant the observed anomaly of 3 °C may be for the cyclone generation and evolution, also in order to test the relevance of the sea surface fluxes for the cyclone development. To assess this, we decreased the SST by 3 °C, in a way similar to (Miglietta et al 2011). As shown in Figure 7 panel (i), the trajectory shows some variations, but it remains relatively close (around 50 km far) to that retrieved from satellite images. In the simulation WRF9 (where the SST was decreased by 3 °C), the pressure does not fall below 1000 hPa (Figure 8 panel (e)). As a consequence, during most of the simulation, the run WRF9 produces a less intense wind, by about 5 m/s, with respect to the run where the SST remained unchanged (Figure 8 panels (e,f)). Finally, the same high-resolution SST provided by ROMS to initialize the coupled experiments (the boundary SST is also provided by the ROMS field every 6-h) is used in the experiment WRF10. This simulation provides a more detailed and physically consistent SST, but without coupling. The WRF10 experiment performance in terms of trajectory description is comparable to WRF5 (and, as will be shown, to the AO and AOW runs) (Figures 7 and 12), although with a worse response in terms of geometrical distance (around 8 km worse compared to WRF5), and spatially characterized by a track covering a wider region.

3.6.2. Coupled Runs

The interaction between the atmosphere and the ocean takes place at their interface through heat and momentum fluxes. Fluxes are influenced respectively by the difference between SST and the air temperature, and by the surface roughness, which over the sea depends on the wave geometry. To explore the interaction among atmosphere-ocean-wave (runs AO and AOW), we chose as initialization time 00:00 UTC, 6 November 2011, the time of the best standalone simulation (WRF5). The 2-way coupling between the atmosphere and the ocean is activated first; next, we include also the wave dynamics. With these two coupled approaches, we explore the effect of SST and the effect of the waves on the energy exchanges. Both PBL schemes implemented in COAWST, i.e., MYJ and MYNN2.5, have been tested (see Table 1). The present experiments will also shed some light on the opportunity of using a coupled modeling system, not only for long simulation (as it is normally considered for climate simulations), but also over a short time range. The present cyclone, which persists over the sea for several hours, appears particularly attractive to address this issue.

3.6.2.2. PBL Scheme

Trajectories using the coupled system are shown in Figure 7 panel (m) (run AO1 and AOW1, for MYJ) and Figure 7 panel (l) (run AO2 and AOW2, for MYNN) and are compared with the results of the tests using the same implementation but in standalone configuration (WRF5 and WRF8). In the MYNN experiment panel (l), the effect of coupling is not significant in the early stages of the cyclone lifetime and is apparent only in the final phase of the storm, near the coast, where the trajectories in the coupled runs are directed westward and are closer to the observed track. However, the differences in the tracks are of the order of only 2–3 h and of about 50 km. The intensity of the TLC does not change significantly, being slightly weaker in the coupled simulations compared to the WRF standalone run in term of wind speed (Figure 8 panel (g)) and pressure (Figure 8 panel (h)). The second set of coupled simulations was performed using the MYJ PBL parameterization. Even in this case, the tracks in the coupled runs (AO1 and AOW1) are directed more westward near landfall when compared to the run WRF5. This effect is more pronounced in AOW1, which also simulates a slightly slower cyclone especially in the central part of the track, likely related to the higher roughness in this run (not shown). Differently from the runs using the MYNN PBL, the cyclone is deeper in WRF5 and in AOW1 (Figure 8 panel (i)) reaching 987 hPa as pressure minimum than in run AO1 (pressure minimum of 990 hPa). To complete the comparison, Figure 9 presents pressure and wind speed for all the coupled runs retaining the same PBL scheme, but changing the roughness parameterization. Going back to Figure 8, results obtained with MYJ appear more consistent with previous works (see for example, (Oost et al 2002)) when compared to MYNN. In fact, the effects of the change in roughness appear to be properly transferred to the whole modeling system in the run AOW1: the higher roughness in AOW1 (Figure 10 panel (c)) compared to WRF5 and AO1 runs (Figure 10 panels (a, b)), due to the inclusion of the waves in the calculation, produces higher fluxes and weaker winds than WRF5 (Figure 8 panel (l)) because of the increased drag, but deeper pressure minima than AO1 (Figure 8 panel (i)) because of higher amount of energy transferred to the atmosphere. Thus, in the following subsections, we will consider only the runs using the MYJ PBL scheme.

3.6.2.2. Surface Roughness Schemes

The effect of the surface roughness in the coupled runs using the MYJ PBL scheme is analyzed here. The heat fluxes are calculated with the surface roughness based on the geometric parameters calculated by the wave model SWAN. As mentioned above, the three schemes available in COAWST for parameterization of the surface roughness are: Oost (OOST), Taylor-Yelland (TY), and Drennan (DRE). To better understand the effect of roughness, the results of the different modeling approaches used in this work are analyzed here. Figure 10 panels (a–c) show the surface roughness after 36 h of simulation, for the three runs WRF5, AO1, AOW1. Results for WRF5 and AO1 are similar since both use the (NOAA GFS-FNL) scheme for the calculation of roughness. Run AOW1 uses (Taylor and Yelland 2001) and produces a higher roughness, in particular around the pressure minimum, where the waves are higher and steeper. Panels (d–f) and (g–i) in Figure 10 show the surface roughness generated by the fully coupled runs, comparing the results for the different calculation schemes of roughness (Oost in AOW1, Taylor Yelland in AOW3, Drennan in AOW4). Results refer to 36 and 48 h of simulation, when the cyclone respectively reaches its maximum intensity and approaches the coast. The OOST scheme (AOW1) generates smaller roughness, giving rise to the maximum intensity in the neighborhood of the pressure minimum. The "discontinuous" distribution of the surface roughness in the other two schemes is due to the discretization of the peak frequencies (i.e., the frequency corresponding to the maximum energy component of the wave spectrum) that produce highly peaked periods. This depends on the spatial pattern variability of the wave-induced roughness and on the way the wave features are implemented within the OOST scheme. Indeed, since this scheme depends on wave age and the waves around the minimum are generally associated with a generative sea state, steeper waves (shorter period and greater height) can be expected, with greater influence in terms of roughness computation. Figure 7 panel (n) shows that the trajectories of the cyclone in the simulations carried out with the three roughness schemes are close to each other, especially in the initial and central phase of the event, while some differences come out in the final stages of the cyclone lifetime (Figure 7 panel (l)). This divergence is probably caused by the highest difference in the surface roughness reached in the final part of the run, when the maximum wind intensity and significant wave height are simulated (not shown). After the cyclone begins to intensify, the run AOW1 (Figure 7 panel (n), red line) produces a much slower cyclone compared to the other two simulations. The distance between AOW1 and AOW3/AOW4 increases with time and reaches a maximum in the most intense phase of the cyclone. Figures 10 panels (d–i) show that the highest roughness is produced by the OOST scheme (AOW1). This suggests that a higher roughness slows down the evolution of the cyclone, and slightly changes its trajectory (with an effect that increases with time); indeed, at the end of the simulation, the runs AOW3 and AOW4 are 6 h ahead compared

to run AOW1. As shown in Figure 9 panel (a), the runs AOW3 and AOW4 show a cyclone with similar pressure minima, but less intense when compared to the run AOW1 (using OOST) by nearly 5 hPa. We speculate that this is due to the increased roughness in AOW1, which increases the heat fluxes and the energy available to the cyclone. However, the wind speed (Figure 9 panel (b)) is comparable in all the three runs in most of the lifetime (in some stages AOW1 produces the most intense wind speed), probably because the effect of the greater pressure gradient in run AOW1 is compensated by the more intense roughness around the eye of cyclone (Figure 9 panel (b)).

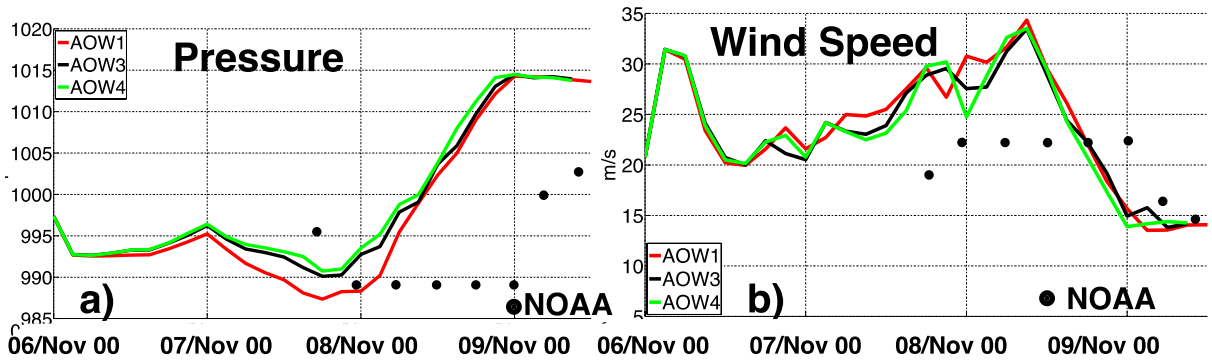

Figure 9. Panel (a): time evolution of the pressure minimum (hPa). Panel (b): maximum wind intensity (m/s) around the eye, for runs AOW1, AOW3 and AOW4. The black dots refer to the real-time estimation given by NOAA.

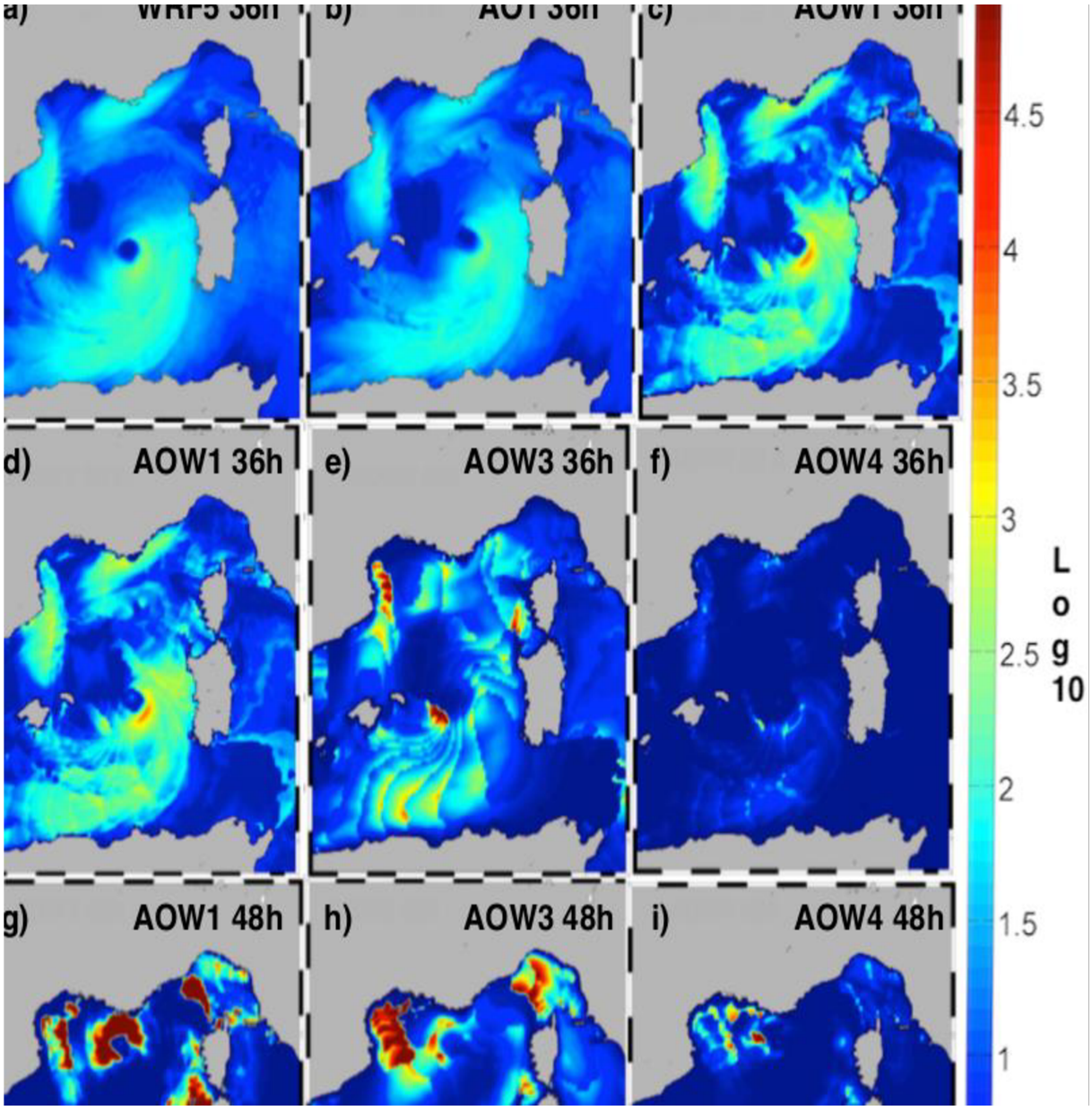

Figure 10. Surface roughness values (log10) in different runs. Panels (a-c): values for runs WRF5, AO1 (using Charnock 1955 scheme) and AOW1 (using the OOST scheme), on 7 November 2011, 12:00 UTC (36 hours after the start of simulation). Panels (d-f): values for runs AOW1 (OOST scheme), AOW3 (TY scheme) and AOW4 (DRE scheme), on 7 November 2011, 12:00 UTC. Panels (g-i): values for runs AOW1, AOW3 and AOW4, on 9 November 2011, 00:00 UTC.

3.6.2.3. SST Analysis and Comparison

As described in (Ricchi et al 2016; Warner et al 2008; Picornell et al 2002), the way the SST is handled in coupled models plays a fundamental role in describing possible feedbacks between the atmosphere and ocean. In this work, we used different approaches. In most of the standalone runs (WRF1-9, therefore including WRF5 itself), the SST was provided by a low-resolution (8.3 km) radiometer, which may suffer from several errors due mainly to the limited resolution in coastal areas and to the observational holes caused by weather (cloudy) conditions (see for instance (Carniel et al 2016)). In the coupled runs, the ROMS model at 5 km resolution provides SST directly to the atmospheric model (whose wind in turn forces the oceanic circulation) after initialization by MFS modeled fields. Conceptually in the middle of these two approaches, MFS SST fields were also used as initial condition for WRF10 experiment, allowing to distinguish to what extent the results of AO and AOW runs actually depend on model coupling or they simply descend from the use of a different initial/boundary condition. To evaluate the two different SST fields, we compare our results with the Meteo France #61002 buoy (http://www.ndbc.noaa.gov/station_page.php?station=61002), located in the gulf of Lion. As shown in Figure 11 panels (a–c), spatial differences of SST between the standalone run and the coupled runs are significant for example in the Gulf of Lion, being the standalone run warmer by about 1–1.5 °C. In the sub-basin affected by the TLC, the SST of the standalone run is overestimated by about 2 °C (Figure 11 panels (a–c)). It is worth noting that the satellite data cannot reproduce coastal structures such as the coastal upwelling in the eastern Sardinia or the cold water circulating near the Catalan coast. A further confirmation comes from the analysis of the simulation results near the #61002 buoy, where the coupled run reproduces better the SST evolution compared to the standalone run. Despite that SST in the two approaches is initially similar, during the TLC evolution, only the coupled runs reduce the initial difference from the observation. During the passage of the TLC near the buoy, the run AOW1 further improves the model performance due to the effect of mixing induced by the waves (see also (Hu et al 2010)). The decrease in SST is greater by about 0.1–0.3 °C compared to AO1 run, but it is too weak to affect significantly the development of the TLC. It is worth noting, although within a relatively narrow range of variation, the slight difference of WRF10 results from those of WRF5 and of the coupled runs (Figure 12) suggests that most of the features characterizing coupled experiments discussed so far are in fact mainly controlled by coupling instead of being the result of a different initial condition. On the other hand, Figure 8 shows that WRF10 and AO1 experiments produce comparable results in terms of timing and intensity of the cyclone.

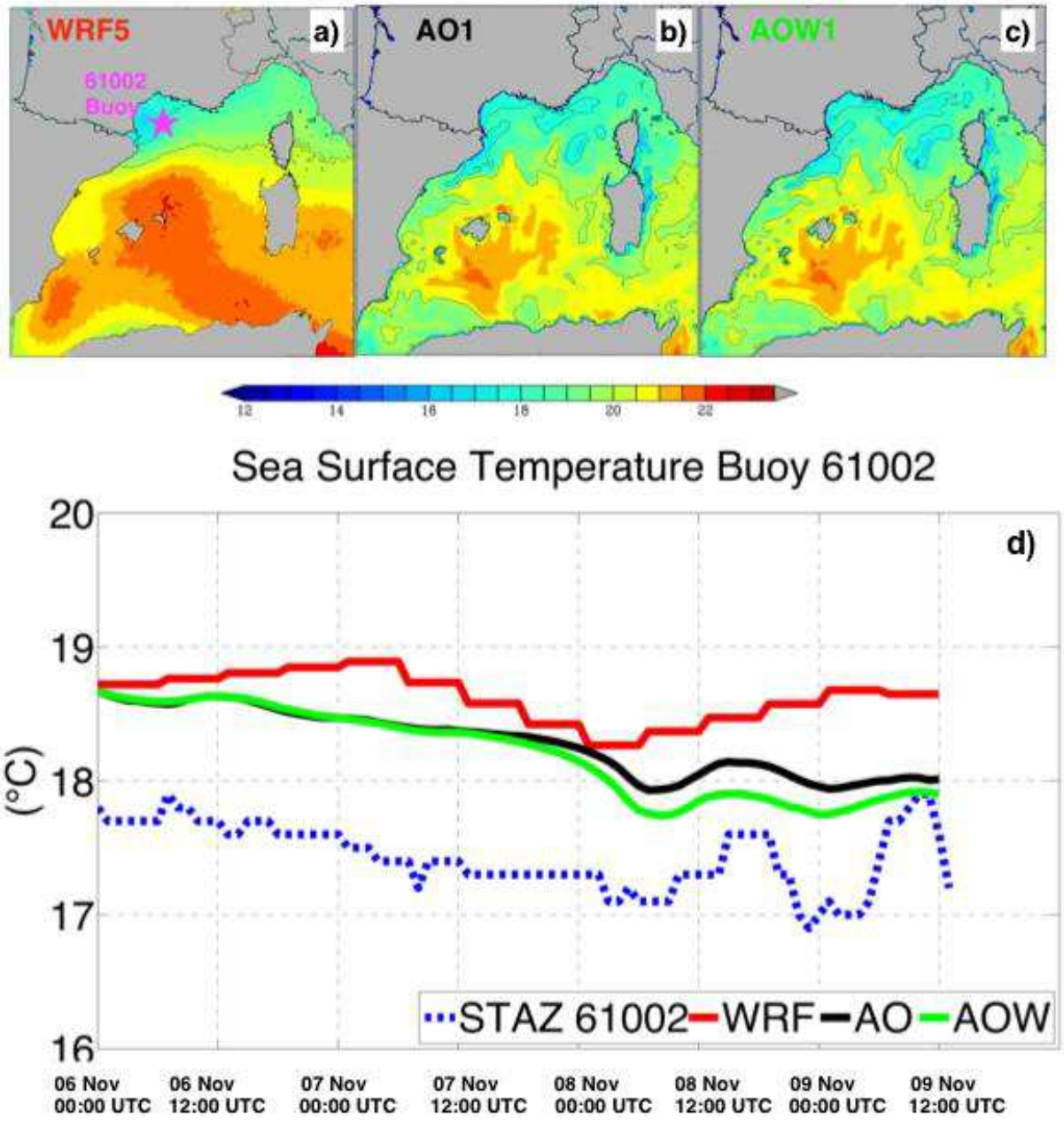

Figure 11. SST fields for the day 9 November 2011 at 12 UTC, for run WRF5 (a), AO1 (b), AOW1 (c). In panel (a) the position of the buoy #61002 (Meteo France) is shown. From the time series (panel (d)), we can notice that the three modeling approaches provide to the atmospheric model a very different SST field and only the coupled runs reproduce the variation of SST correctly, in particular the run AOW1, due to the additional effect of wave mixing [54]. It is colder than 1 °C, compared to the value from which the models are initialized (reanalysis). This is because the buoy is located in a sea zone characterized by the thermal front, composed of cold water masses, produced in the Gulf of Lions, and warmer water masses typical of the Balearic Sea.

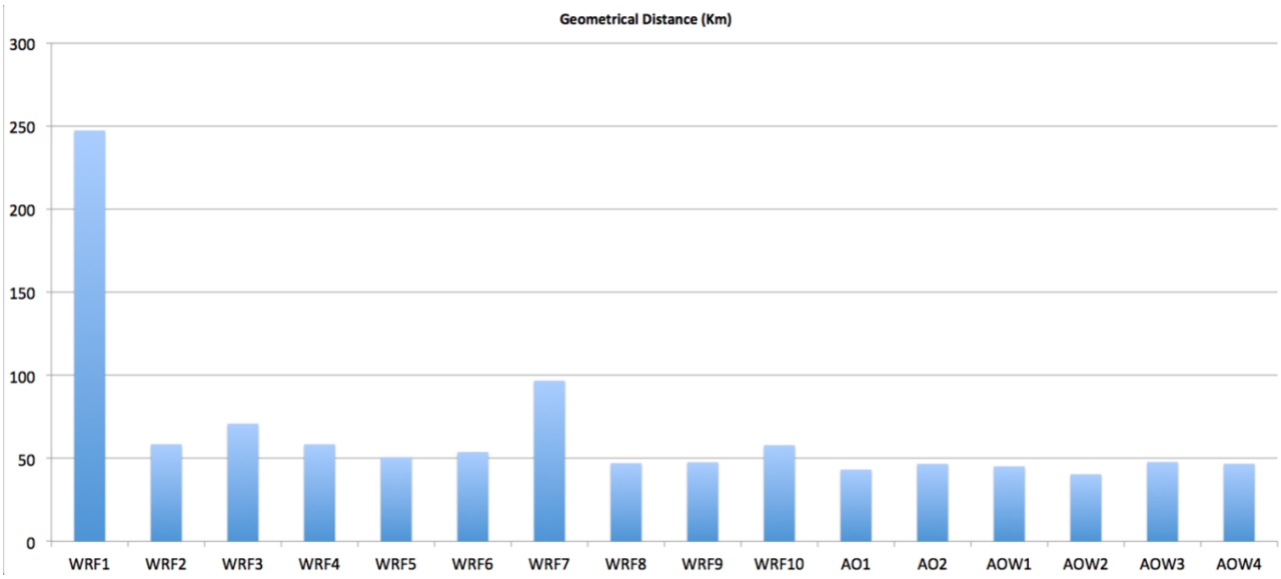

Figure 12. Average geometric distance between simulated and observed trajectories (km).

3.7. Discussion and Conclusions

By means of a coupled atmosphere-ocean-wave modeling suite (COAWST), the goal of this work is to explore the sensitivity of the numerical simulation of Tropical Like Cyclone ROLF, by comparing trajectory, pressure and wind speed obtained using different levels of coupling and different numerical approaches. ROLF has been a particularly intense TLC and, throughout its lifetime, has caused extensive damage even considerably far away from its pressure minimum (Renault et al 2012)). Indeed, the SST anomaly of about 3 °C in the central basin of the Balearic Islands (Figure 3) and the intensity and duration of the event allow consideration of ROLF as a paradigmatic case for disentangling the role of air-sea interactions on a cyclone evolution. Several studies have focused on the assessment of the SST role during TLC development. In particular, (Cioni et al 2016) showed how the use of more resolved and realistic SST fields (as in our case WRF10) with respect to the adoption of remotely sensed SST satellite fields with low spatial and temporal resolution (as our case WRF5) can play an important role to achieve better results in terms of trajectory and intensity of the cyclone. Other studies have focused on the identification of the physical factors that led to the formation and maintenance of this TLC (Davolio et al 2015). In this study, we evaluate the sensitivity to initial conditions, resolution of the SST and to different levels of coupling, starting with a standalone WRF setup (with different initialization times), then employing a coupled atmospheric-ocean (AO) approach and finally a fully coupled implementation including waves (AOW). The effects of the PBL schemes in both uncoupled and coupled runs, as well as the effects of different surface roughness parameterization techniques, have been also explored. The first set of results shows a strong sensitivity to the chosen initialization time (see also Davolio et al 2009; Chaboureau et al 2012; Miglietta et al 2015). These tests confirmed that it is not sufficient to generally initialize the model close to the date of the event, but it is extremely important to explore which specific initialization produces the best result in terms of intensity and trajectory. When doing this, it is necessary to arrange a buffer time in which the PBL of the atmospheric model can settle down on the new SST structure that the satellite or the circulation model provide to the atmosphere. Furthermore, we observed that it is better to avoid a choice of initial conditions too close to the TLC spin-up period, to allow a proper adjustment. For this reason, we have chosen as the best initialization time 00:00 UTC on 6 November 2011, which provided good results in terms of trajectory and intensity. Following other examples (Miglietta et al 2011), we also tested the decrease of SST over the whole domain, choosing to modify these conditions by 3 °C, since this is about the anomaly characterizing the Mediterranean basin near the cyclone on 8 November 2011. Finally, an uncoupled run initialized and forced with MFS SST was carried out, in order to investigate the effect of a high-resolution SST forcing without coupling before interpreting the results of coupled runs. The resulting differences in

terms of pressure minima show the importance of a correct distribution of the SST field, not only on the area affected by the phenomenon, but on the whole computational domain. The effect of SST reflects the different amount of energy transferred to the cyclone, and consequently its intensity (Figure 8 panels (e,f)). In addition, WRF10 experiment suggests that the implementation of an uncoupled model forced by a high-resolution SST can lead to modeled storm intensity not dissimilar to those produced by coupled models (in particular AO case). In addition, the strategy adopted in case WRF10, besides not being energetically consistent between sea and atmosphere, cannot be generally applied for operational purposes, since realistic SST forecasts are rarely available, while the easiest field estimates are provided by satellite data. This is also an indirect confirmation that in some cases it is therefore necessary to use a coupled approach, since in this case the temperature on the ocean side is then provided by a high-resolution circulation model and not by satellite images. As far as the effects of selected PBL are concerned, in the current COAWST release only the MYJ and MYNN2.5 schemes can be used when using the fully coupled atmosphere-ocean-wave model setup. We therefore performed a comparison among the standalone WRF model and the coupled runs (experiments WRF8-AO2-AOW2, WRF5-AO1-AOW1). The comparison shows that a change of the PBL scheme slightly affects the trajectory in the early and middle part of the run, but that this modification becomes larger in the final part, when the TLC approaches the coast. Indeed, the two PBL schemes have limited effects when the cyclone moves over the sea, and probably the different interactions between the atmosphere and the ocean due to the different distribution of SST fields take several hours to develop across the atmosphere. More specifically, looking at Figure 12 it can be seen that the total geometric distances obtained by the two runs using different PBL schemes are comparable; however, the difference increases when the TLC approaches the coast, and this can also explain the slight discrepancy resulting in the final landfall timing. We can further discuss the most significant differences in terms of intensity. As shown in the Figure 8 panels (g-l), run WRF5 produces a cyclone that is always more intense with respect to that produced by the coupled runs, because the satellite SST data are slightly warmer than the ROMS modeled surface temperature, and this produces an intensive development by approximately 5 hPa. In this case the choice of the PBL scheme becomes also crucial, as the PBL MYJ generates more intense heat fluxes (not shown) with respect to the MYNN2.5 scheme. We have therefore chosen the run with MYJ PBL as control run. In the coupled runs, differences emerge especially with the use of MYJ PBL. In this case, the run AOW1 is more intense than run AO1 (Figure 8 panels (i,l)) only in terms of atmospheric pressure and not in wind speeds. This could be attributed to the effect of the surface roughness calculated with the OOST scheme in run AOW1. This choice indeed generates a larger roughness around the pressure minimum (Figure 10 panels (a–c)), which induces an increase in the fluxes leading to an intense

development of the cyclone, similarly to what WRF5 run produced (where higher SST generated intense heat fluxes). The higher surface roughness also increases friction and, therefore, tends to limit the intensification of the 10m wind, as shown in Figure 8 panel (i). Moreover, the parameterization scheme adopted for the surface roughness has another crucial role, as shown in both Figures 9 and 10; among these schemes, the one that performs better is OOST (see Figure 12), which generates a consistent and homogeneous surface roughness, if compared with other simulations that use the Charnock scheme. Figure 11 helps us to understand how the use of coupled models can turn out to be important also on the oceanographic side. The SST data in Figure 11 panels (a–c) show the differences in the analysis among the WRF5, AO1, AOW1 runs, while panel (d) shows a temperature time series for the three models compared to data provided by the close by Meteo France buoy #61002. Results clearly show that the spectro-radiometer overestimates the SST especially in areas close to the coast, where the cloudiness effect is greater; also because of the low resolution of the satellite, the meandering and small-scale structures are not resolved. Further, by comparing runs AO1 and AOW1, it can be seen that in the latter the wave mixing effects induce a larger cooling of the sea surface (Carniel et al 2016; Hu et al 2010). Generally speaking then, at least in this specific TLC case the use of coupled models improved the reliability of the results in terms of heat and momentum fluxes (Carniel et al 2016; Ricchi et al 2016), which are more consistent thanks to a better description of the SST fields. Also, in this specific study, the TLC was shown to be more sensitive to the initialization than to the coupling strategy. Considering the fundamental role played by the roughness parameterization and the PBL scheme, we suggest to select them on the basis of specific tests, given that the responses may be very different depending on the phenomena and the type of waves that generate the roughness. Last but not least, as already mentioned, if it is true that the use of coupled models strategy can be beneficial for modeling TLCs, it should be recalled that it also leads to an increase of complexity on the informatics side. In addition to this, model coupling may emphasize some problems typical in all numerical approaches, such as the sensitivity to boundary conditions in atmospheric models (especially when dealing with temperature and soil type). In particular, it should be reminded that the SST fields must be prescribed very carefully, since they may be significantly different from that originally used in the global model adopted to produce the initialization. As a final remark, a critical aspect is represented also by the initialization time of the TLC where possible help may be sought for invariational assimilation techniques (3Dvar-4Dvar), although care must be taken in approaches (e.g., “hot-start”) that have to be shared by all the employed models.

Reference

Ernst, J.A.; Matson, M. A Mediterranean Tropical Storm? *Weather* **1983**, *38*, 332–337.

Moscatello, A.; Miglietta, M.M.; Rotunno, R. Observational Analysis of a Mediterranean "Hurricane" over Southeastern Italy. *Weather* **2008**, *63*, 306–311.

Akhtar, N.; Brauch, J.; Dobler, A.; Béranger, K.; Ahrens, B. Medicanes in an ocean—Atmosphere coupled regional climate model. *Nat. Hazards Earth Syst. Sci.* **2014**, *14*, 2189–2201.

Miglietta, M.M.; Laviola, S.; Malvaldi, A.; Conte, D.; Levizzani, V.; Price, C. Analysis of tropical-like cyclones over the Mediterranean Sea through a combined modeling and satellite approach. *Geophys. Res. Lett.* **2013**, *40*, 2400–2405. *Atmosphere* **2017**, *8*, 92 21 of 23

Cavicchia, L.; von Storch, H. The simulation of medicanes in a high-resolution regional climate model. *Clim. Dyn.* **2012**, *39*, 2273–2290.

Tous, M.; Romero, R. Meteorological environments associated with medicane development. *Int. J. Climatol.* **2013**, *33*, 1–14.

Emanuel, K. Genesis and maintenance of "Mediterranean hurricanes". *Adv. Geosci.* **2005**, *2*, 217–220.

Fita, L.; Romero, R.; Luque, A.; Emanuel, K.; Ramis, C. Analysis of the environments of seven Mediterranean tropical-like storms using an axisymmetric, nonhydrostatic, cloud resolving model. *Nat. Hazards Earth Syst. Sci.* **2007**, *7*, 41–56.

Cioni, G.; Malguzzi, P.; Buzzi, A. Thermal structure and dynamical precursor of a Mediterranean tropical-like cyclone. *Q. J. R. Meteorol. Soc.* **2016**, *142*, 1757–1766.

Miglietta, M.M.; Moscatello, A.; Conte, D.; Mannarini, G.; Lacorata, G.; Rotunno, R. Numerical analysis of a Mediterranean "hurricane" over south-eastern Italy: Sensitivity experiments to sea surface temperature. *Atmos. Res.* **2011**, *101*, 412–426.

Moscatello, A.; Miglietta, M.M.; Rotunno, R. Numerical Analysis of a Mediterranean "Hurricane" over Southeastern Italy. *Mon. Weather Rev.* **2008**, *136*, 4373–4397.

Davolio, S.; Miglietta, M.M.; Moscatello, A.; Pacifico, F.; Buzzi, A.; Rotunno, R. Numerical forecast and analysis of a tropical-like cyclone in the Ionian Sea. *Nat. Hazards Earth Syst. Sci.* **2009**, *9*, 551–562.

Chaboureau, J.-P.; Pantillon, F.; Lambert, D.; Richard, E.; Claud, C. Tropical transition of a Mediterranean storm by jet crossing. *Q. J. R. Meteorol. Soc.* **2012**, *138*, 596–611.

Miglietta, M.M.; Mastrangelo, D.; Conte, D. Influence of physics parameterization schemes on the simulation of a tropical-like cyclone in the Mediterranean Sea. *Atmos. Res.* **2015**, *153*, 360–375.

Warner, J.C.; Armstrong, B.; He, R.; Zambon, J.B. Development of a Coupled Ocean-Atmosphere-Wave Sediment Transport (COAWST) Modeling System. *Ocean Model.* **2010**, *35*, 230–244.

Olabarrieta, M.; Warner, J.C.; Armstrong, B.; Zambon, J.B.; He, R. Ocean-atmosphere dynamics during Hurricane Ida and Nor'Ida: An application of the coupled ocean-atmosphere-wave-sediment transport (COAWST) modeling system. *Ocean Model.* **2012**, *43*, 112–137.

Zambon, J.B.; He, R.; Warner, J.C. Investigation of hurricane Ivan using the coupled ocean-atmosphere-wave sediment transport (COAWST) model. *Ocean Dyn.* **2014**, *64*, 1535–1554.

Carniel, S.; Benetazzo, A.; Bonaldo, D.; Falcieri, F.M.; Miglietta, M.M.; Ricchi, A.; Sclavo, M. Scratching beneath the surface while coupling atmosphere, ocean and waves: Analysis of a dense water formation event. *Ocean Model.* **2016**, *101*, 101–112.

Ricchi, A.; Miglietta, M.M.; Falco, P.P.; Benetazzo, A.; Bonaldo, D.; Bergamasco, A.; Sclavo, M.; Carniel, S. On the use of a coupled ocean-atmosphere-wave model during an extreme cold air outbreak over the Adriatic Sea. *Atmos. Res.* **2016**, *172*, 48–65.

Hart, R.E. A Cyclone Phase Space Derived from Thermal Wind and Thermal Asymmetry. *Mon. Weather Rev.* **2003**, *131*, 585–616.

Millot, C. Circulation in the Western Mediterranean Sea. *J. Mar. Syst.* **1999**, *20*, 423–442.

Renault, L.; Oguz, T.; Pascual, A.; Vizoso, G.; Tintore, J. Surface circulation in the Alborán Sea (western Mediterranean) inferred from remotely sensed data. *J. Geophys. Res. Oceans* **2012**, *117*.

NOAA National Oceanic and Atmospheric Administration. NESDIS National Environmental Satellite, Data and Information Service). Tropical Bulletin Archive. 2011. Available online: http://www.ssd.noaa. gov/PS/TROP/2011/bulletin/archive.html (accessed on 15 January 2016).

Pinardi, N.; Allen, I.; Demirov, E.; Mey, P.D.; Korres, G.; Lascaratos, A.; Traon, P.L.; Maillard, C. Annales Geophysicae The Mediterranean ocean forecasting system: First phase of implementation (1998–2001). *Ann. Geophys.* **2003**, *21*, 3–20.

Oddo, P.; Adani, M.; Pinardi, N.; Fratianni, C.; Tonani, M.; Pettenuzzo, D. A nested Atlantic-Mediterranean Sea general circulation model for operational forecasting. *Ocean Sci.* **2009**, *5*, 461–473.

Larson, J.; Jacob, R.; Ong, E. The Model Coupling Toolkit: A New Fortran90 Toolkit for Building Multiphysics Parallel Coupled Models. *Int. J. High Perform. Comput. Appl.* **2005**, *19*, 277–292.

Warner, J.C.; Sherwood, C.R.; Signell, R.P.; Harris, C.K.; Arango, H.G. Development of a three-dimensional, regional, coupled wave, current, and sediment-transport model. *Comput. Geosci.* **2008**, *34*, 1284–1306. *Atmosphere* **2017**, *8*, 92 22 of 23

Jones, P.W. SCRIP Manual. 1999. Available online: oceans11.lanl.gov/svn/SCRIP/trunk/SCRIP/doc/ SCRIPusers.pdf (accessed on 20 October 2016).

Skamarock, W.C.; Klemp, J.B. A time-split nonhydrostatic atmospheric model for weather research and forecasting applications. *J. Comput. Phys.* **2008**, *227*, 3465–3485.

Shchepetkin, A.F.; McWilliams, J.C. The regional oceanic modeling system (ROMS): A split-explicit, free-surface, topography-following-coordinate oceanic model. *Ocean Model.* **2005**, *9*, 347–404.

Shchepetkin, A.F.; McWilliams, J.C. Computational Kernel Algorithms for Fine-Scale, Multiprocess, Longtime Oceanic Simulations. In *Handbook of Numerical Analysis*; Elsevier: Oxford, UK, 2009; pp. 121–183.

Haidvogel, D.B.; Arango, H.; Budgell, W.P.; Cornuelle, B.D.; Curchitser, E.; Di Lorenzo, E.; Fennel, K.; Geyer, W.R.; Hermann, A.J.; Lanerolle, L.; et al. Ocean forecasting in terrain-following coordinates: Formulation and skill assessment of the Regional Ocean Modeling System. *J. Comput. Phys.* **2008**, *227*, 3595–3624.

Copernicus Marine Environment Monitoring Service (CMEMS). Mediterranean Sea Physics Reanalysis Model. Available online: http://marine.copernicus.eu (accessed on 10 January 2016).

Carniel, S.; Warner, J.C.; Chiggiato, J.; Sclavo, M. Investigating the impact of surface wave breaking on modeling the trajectories of drifters in the northern Adriatic Sea during a wind-storm event. *Ocean Model.* **2009**, *30*, 225–239.

Booij, N.; Ris, R.C.; Holthuijsen, L.H. A third-generation wave model for coastal regions: 1. Model description and validation. *J. Geophys. Res. Ocean.* **1999**, *104*, 7649–7666.

Benetazzo, A.; Fedele, F.; Carniel, S.; Ricchi, A.; Bucchignani, E.; Sclavo, M. Wave climate of the Adriatic Sea: A future scenario simulation. *Nat. Hazards Earth Syst. Sci.* **2012**, *12*, 2065–2076.

Benetazzo, A.; Bergamasco, A.; Bonaldo, D.; Falcieri, F.M.; Sclavo, M.; Langone, L.; Carniel, S. Response of the Adriatic Sea to an intense cold air outbreak: Dense water dynamics and wave-induced transport. *Prog. Oceanogr.* **2014**, *128*, 115–138.

Gemmill, W.; Katz, B.; Li, X. *Daily Real-Time, Global Sea Surface Temperature, High-Resolution Analysis: RTG_SST_HR*; NOAA/NWS/NCEP/MMAB Office Note; National Centers for Environmental Prediction: Camp Springs, MD, USA, 2007; p. 39.

Kain, J.S. The Kain-Fritsch Convective Parameterization: An Update. *J. Appl. Meteorol.* **2004**, *43*, 170–181.

Thompson, G.; Field, P.R.; Rasmussen, R.M.; Hall, W.D. Explicit Forecasts of Winter Precipitation Using an Improved Bulk Microphysics Scheme. Part II: Implementation of a New Snow Parameterization. *Mon. Weather Rev.* **2008**, *136*, 5095–5115.

Mlawer, E.J.; Taubman, S.J.; Brown, P.D.; Iacono, M.J.; Clough, S.A. Radiative transfer for inhomogeneous atmospheres: RRTM, a validated correlated-k model for the longwave. *J. Geophys. Res.* **1997**, *102*.

Compo, G.P.; Whitaker, J.S.; Sardeshmukh, P.D.; Matsui, N.; Allan, R.J.; Yin, X.; Gleason, B.E.; Vose, R.S.; Rutledge, G.; Bessemoulin, P.; et al. The Twentieth Century Reanalysis Project. *Q. J. R. Meteorol. Soc.* **2011**, *137*, 1–28.

NOAA National Oceanic and Atmospheric Administration; National Centers for Environmental Information. GFS-FNL (Final Reanalysis of the Global Forecasting System). Available online: https://www.ncdc.noaa. gov/data-access/model-data/model-datasets/global-forcast-system-gfs (accessed on 10 January 2016).

Janjic´, Z.I. The Step-Mountain Eta Coordinate Model: Further Developments of the Convection, Viscous Sublayer, and Turbulence Closure Schemes. *Mon. Weather Rev.* **1994**.

Nakanishi, M.; Niino, H. An Improved Mellor–Yamada Level-3 Model: Its Numerical Stability and Application to a Regional Prediction of Advection Fog. *Bound.-Layer Meteorol.* **2006**, *119*, 397–407.

Charnock, H. Wind stress on a water surface. *Q. J. R. Meteorol. Soc.* **1955**, *81*, 639–640.

Small, R.J.; Campbell, T.; Teixeira, J.; Carniel, S.; Smith, T.A.; Dykes, J.; Chen, S.; Allard, R. Air-Sea Interaction in the Ligurian Sea: Assessment of a Coupled Ocean-Atmosphere Model Using In Situ Data from LASIE07. *Mon. Weather Rev.* **2011**, *139*, 1785–1808.

Kumar, N.; Voulgaris, G.; Warner, J.C.; Olabarrieta, M. Implementation of the vortex force formalism in the coupled ocean-atmosphere-wave-sediment transport (COAWST) modeling system for inner shelf and surf zone applications. *Ocean Model.* **2012**, *47*, 65–95.

Taylor, P.K.; Yelland, M.J. The Dependence of Sea Surface Roughness on the Height and Steepness of the Waves. *J. Phys. Oceanogr.* **2001**.

Olabarrieta, M.; Medina, R.; Castanedo, S. Effects of wave-current interaction on the current profile. *Coast. Eng.* **2010**, *57*, 643–655.

Drennan, W.M.; Graber, H.C.; Hauser, D.; Quentin, C. On the wave age dependence of wind stress over pure wind seas. *J. Geophys. Res.* **2003**, *108*, 8062.

Oost, W.A.; Komen, G.J.; Jacobs, C.M.J.; Van Oort, C. New evidence for a relation between wind stress and wave age from measurements during ASGAMAGE. *Bound.-Layer Meteorol.* **2002**, *103*, 409–438.

Picornell, M.A.; Carrassi, N.A.; Jansá, A. A study on the forecast quality of the mediterranean cyclones. In Proceedings of the 4th EGS Plinius Conference, Mallorca, Spain, 2–4 October 2002.

Hu, X.-M.; Nielsen-Gammon, J.W.; Zhang, F. Evaluation of Three Planetary Boundary Layer Schemes in the WRF Model. *JAMC* **2010**.

Renault, L.; Chiggiato, J.; Warner, J.C.; Gomez, M.; Vizoso, G.; Tintoré, J. Coupled atmosphere-ocean-wave simulations of a storm event over the Gulf of Lion and Balearic Sea. *J. Geophys. Res. Oceans* **2012**, *117*.

Davolio, S.; Stocchi, P.; Benetazzo, A.; Bohm, E.; Riminucci, F.; Ravaioli, M.; Li, X.-M.; Carniel, S. Exceptional Bora outbreak in winter 2012: Validation and analysis of high-resolution atmospheric model simulations in the northern Adriatic area. *Dyn. Atmos. Oceans* **2015**, *71*, 1–20.

NOAA National Oceanic and Atmospheric Administration, Nationa Data Buoy Center. Station 61002, Meteorological ad Waves Buoy Owned and Maintained by "Meteo France". Available online: http://www. ndbc.noaa.gov/station_page.php?station=61002 (accessed on 15 January 2016).

Benetazzo, A.; Carniel, S.; Sclavo, M.; Bergamasco, A. Wave-current interaction: Effect on the wave field in a semi-enclosed basin. *Ocean Model.* **2013**, *70*, 152–165.

Cassola, F.; Ferrari, F.; Mazzino, A.; Miglietta, M.M. The role of the sea on the flsh floods events over Liguria (Italy). *Geophys. Res. Lett.* **2016**, *43*, 3534–3542.

Miglietta, M.M.; Cerrai, D.; Laviola, S.; Cattani, E.; Levizzani, V. Potential vorticity patterns in Mediterranean "hurricanes". *Geophys. Res. Lett.* **2017**.

4. Preliminary result about: Describing a flash-flood event over the north-east Italy using a very-high resolution atmosphere-ocean-wave coupled model

4.1 Overview

An extremely intense precipitation event hit the Venice Lagoon and the neighboring coastal zone in the early hours of September 26, 2007, with precipitations exceeding 340 mm recorded in the Venetian mainland during the short period between 06 UTC and 12 UTC. This phenomenon, classified as a flash-flood, was the result of a mesoscale convective system formed in a convergence area between a north-easterly wind coming from the Alps and a south-easterly one over the Adriatic basin (Eastern Mediterranean Sea). In this study the flash-flood event is described by means of a set of runs using the modeling suite COAWST (Coupled Ocean Atmosphere Wave Sediment Transport system), in which different coupling configurations among ocean (ROMS), wave (SWAN), and atmosphere (WRF) models allowed to explore the importance of different components of the ocean-atmosphere system and the effects of their interactions. Preliminary results suggest that the use of high-resolution Sea Surface Temperature (SST) is crucial to realistically simulate this type of events, as the over/under estimation of the SST in the basin area affects the winds intensity and consequently the spatial localization of the event, together with the precipitation intensity. In the face of the generally poor performance of satellite data in capturing thermal patterns in coastal regions, a properly calibrated ocean model can provide a more realistical SST distribution in these systems. Furthermore, a coupled description of atmosphere and ocean dynamics warrants the energetic consistency between the two systems and modifies the distribution of heat and humidity in the Planetary Boundary Layer (in particular when the coupling with the wave model is also activated). Besides supporting a deeper insight in the physical processes underlying these intense phenomena, in the considered event the use of model coupling led to an unprecedented performance in reproducing recorded precipitation patterns and intensity.

4.2 Flash-Flood event description

Many studies in the recent years have focused on the SST role and effect in convective and highly-localized intense events that originate nearby coastal areas. This specific case study deals with a "flash-flood" event that took place in the Venice lagoon region on September 26, 2007, between 06 and 12 UTC. As described by Davolio et al. (2009), the whole event was due to the convergence between dry and cold air coming from the Alps with warmer and more humid air traveling from the south Adriatic (sirocco winds). The clash of these two different air masses happened to be near the coast line (see Figure 1) and activated an intense thunderstorm (Figure 2) and a strong wind-shear between the soil and the higher parts of the atmosphere. The storm activity persisted in the generation area for about 5 hours, presenting the typical V-shape and an estimated temperature of about -55 °C at 12 km (Davolio et al., 2009). This caused intense precipitations localized within an area of about 10 km2 and accumulated rainfall of 340 mm (ARPAV data) in the cities of Marghera and Mestre. Remarkably, both operational models employed in the region and those available from the Hymex campaign were not bale to reproduce the accumulated rain fall that resulted from the event. The timing of the storm and the positioning of the cell were not forecasted adequately either. These were the main reasons that prompted us to investigate the effects that the adoption of different SST fields (in lower/higher atmosphere and in the whole air-column) in numerical models may have in terms of rainfall, humidity and winds. In order to do this, we used the COAWST modeling suite in 4 different configurations. In the first one (WRF-RTG) we used the WRF model without any coupling approach, feeding the SST from the NOAA database (RTG_SST). It is a temperature filed available from satellite passages at 8.3 km resolution, updated every 6 hours. The second numerical experiment (WRF-ROMS) we implemented the SST at high resolution (1 km) as resulting from the spin-up of ROMS ocean model, initialized 25 days before the event. This case allows to analyze the effect of the new SST, still without having a coupling approach. In the third numerical set up (AO) the atmosphere and ocean were mutually coupled, while in the fourth case we also added the mutual feedback with waves (case AOW, see Figure 3). Numerical runs of WRF have been performed on a nested grid, ranging from 25 to 5 to 1 km, having 55 vertical levels. ROMS and SWAN models have been run on their specific grid at 1 km resolution and covering the whole Adriatic basin.

4.3 Preliminary results

We present here preliminary results that are still in needs of further analysis. Namely, we are now undergoing a verification versus radar reflectivity data (DbZ) acquired by the radar located in Teolo (80 km away). Besides, the thermodynamic causes that are most likely at the basis of the differences presented by the different numerical configurations still need to be properly assessed. Having this caveat in mind, we can surely state that the SST variation (Figure 4) affects the wind field intensity, particularly over marine regions (Figure 5). Area where the SST is exhibiting a larger variability are also characterized by stronger winds. As a consequence, the WRF-RTG run produces a weaker winds when compared to other runs. Among the coupled numerical models, the AO generates a stronger wind on the sea compared to AOW (although results in terms of SST are very similar). The origin of this difference is due to the fact that in run AOW the presence of waves increases the surface roughness, which on turn limits the wind growth. As far as rainfall rates are concerned, although the convergence line is positioned more or less in a similar area in all the numerical tests (Figure 5), forecasted values are different. Actually, only coupled numerical models are capable of forecasting the timing, location and total accumulation of rain, as can be depicted in Figure 6. Besides, only coupled numerical runs can reproduce vertically both the deep convection process that characterize the event (showing high vertical velocities even in the higher atmosphere) and the reflectivity high values, structured in a single cell in the area of the event. Humidity in higher levels (Figure 8) suggests that uncoupled runs maintain a moisture distribution above the PBL characterized by a dry-air tongue, that limits the convection. Differently, in the coupled runs not only the humidity distribution above the BL is evident, but values within the PBL as well are well marked. We can therefore conclude that coupled numerical models can represent a valid support for the accurate forecast of such extreme events, at least in proximity of coastal regions. They can indeed provide a more energetically consistent system, capable of transferring more heat and moisture in the lower and medium atmosphere. However, further analysis are required to confirm the findings here discussed.

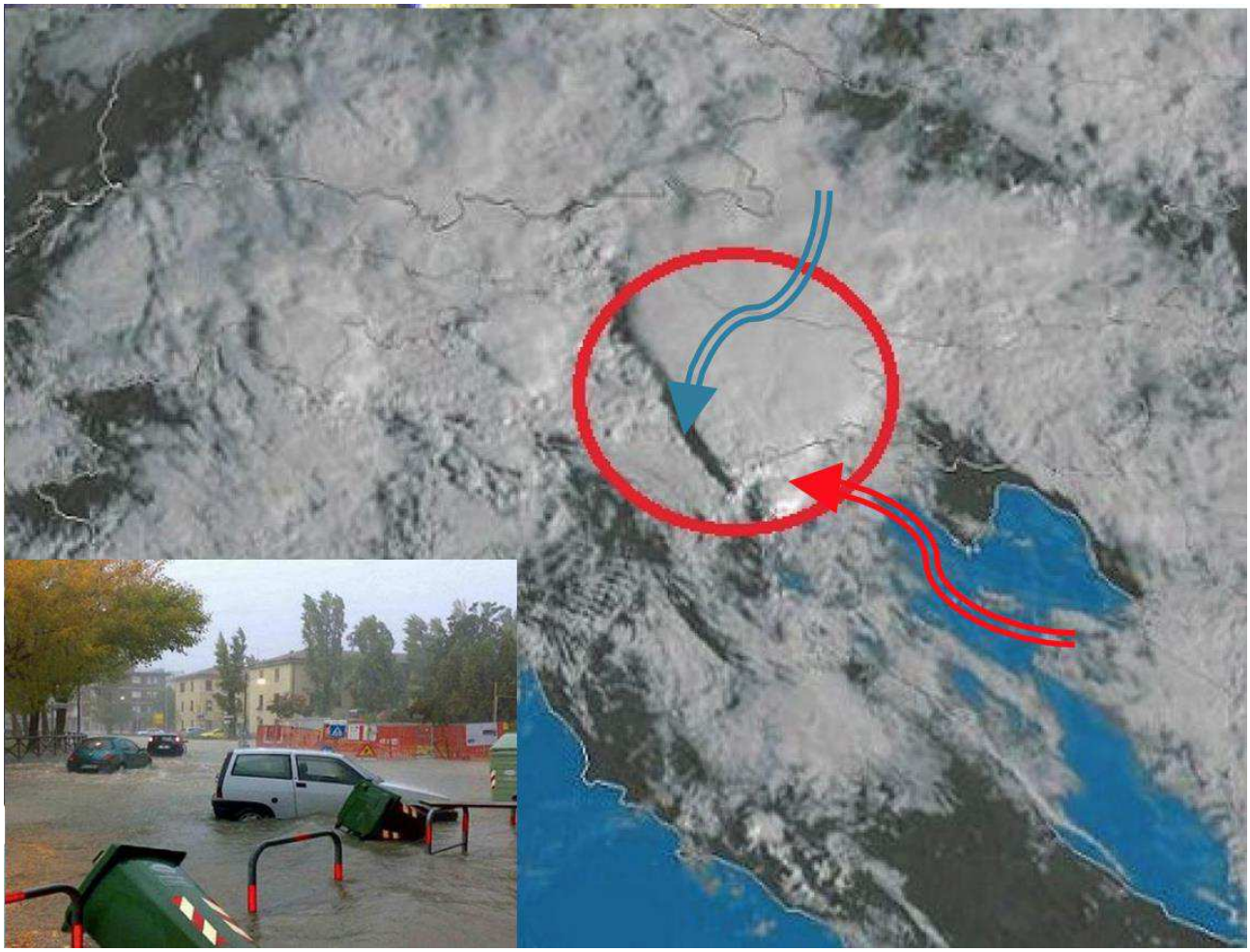

Figure 1. Satellite image that show the V-shape of thunderstorm developed over Venice Lagoon.

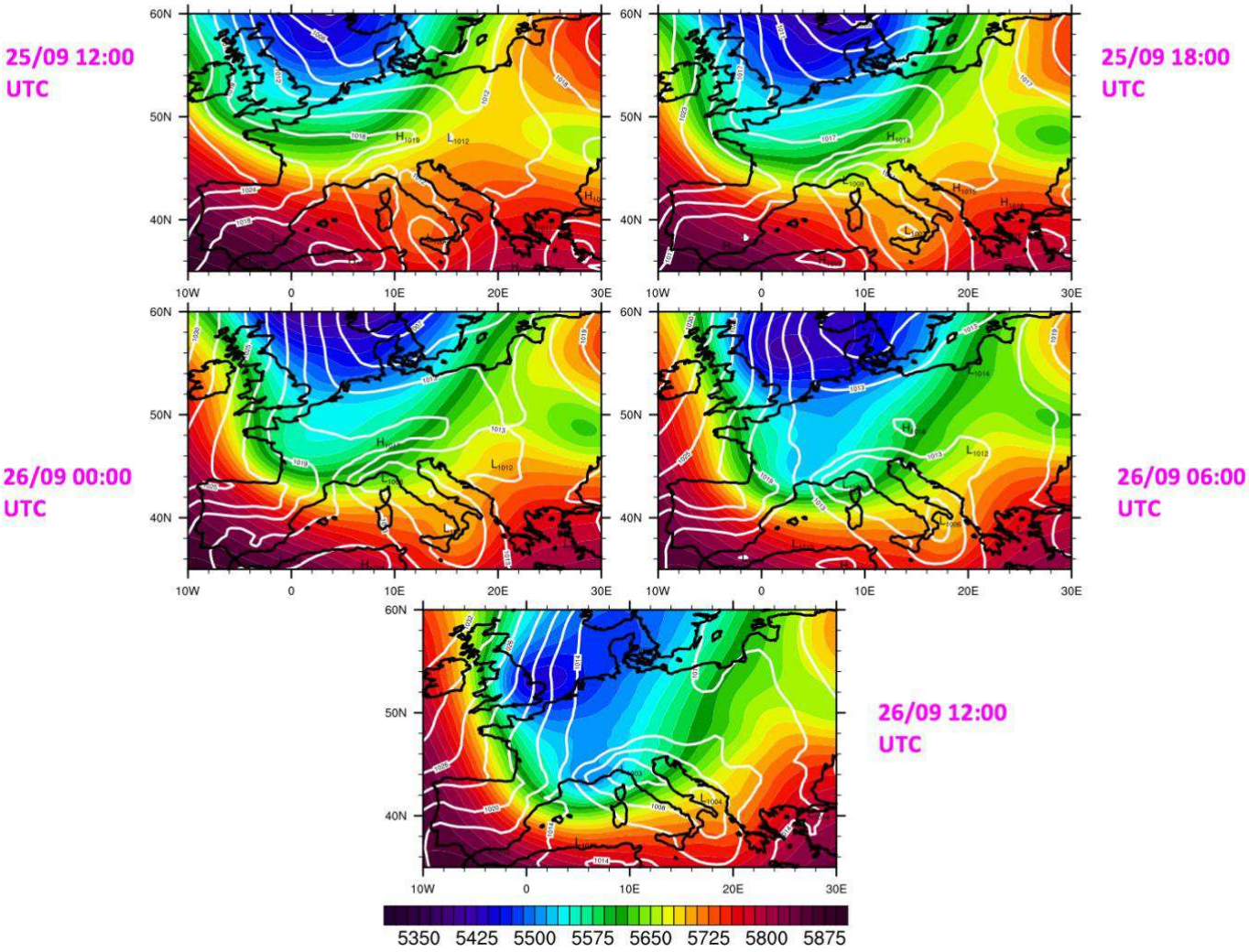

Figure 2. Synoptic analysis at 500 hpa, and sea level pressure from 25/09/2007 at 12UTC to 26/09/2007 at 12UTC

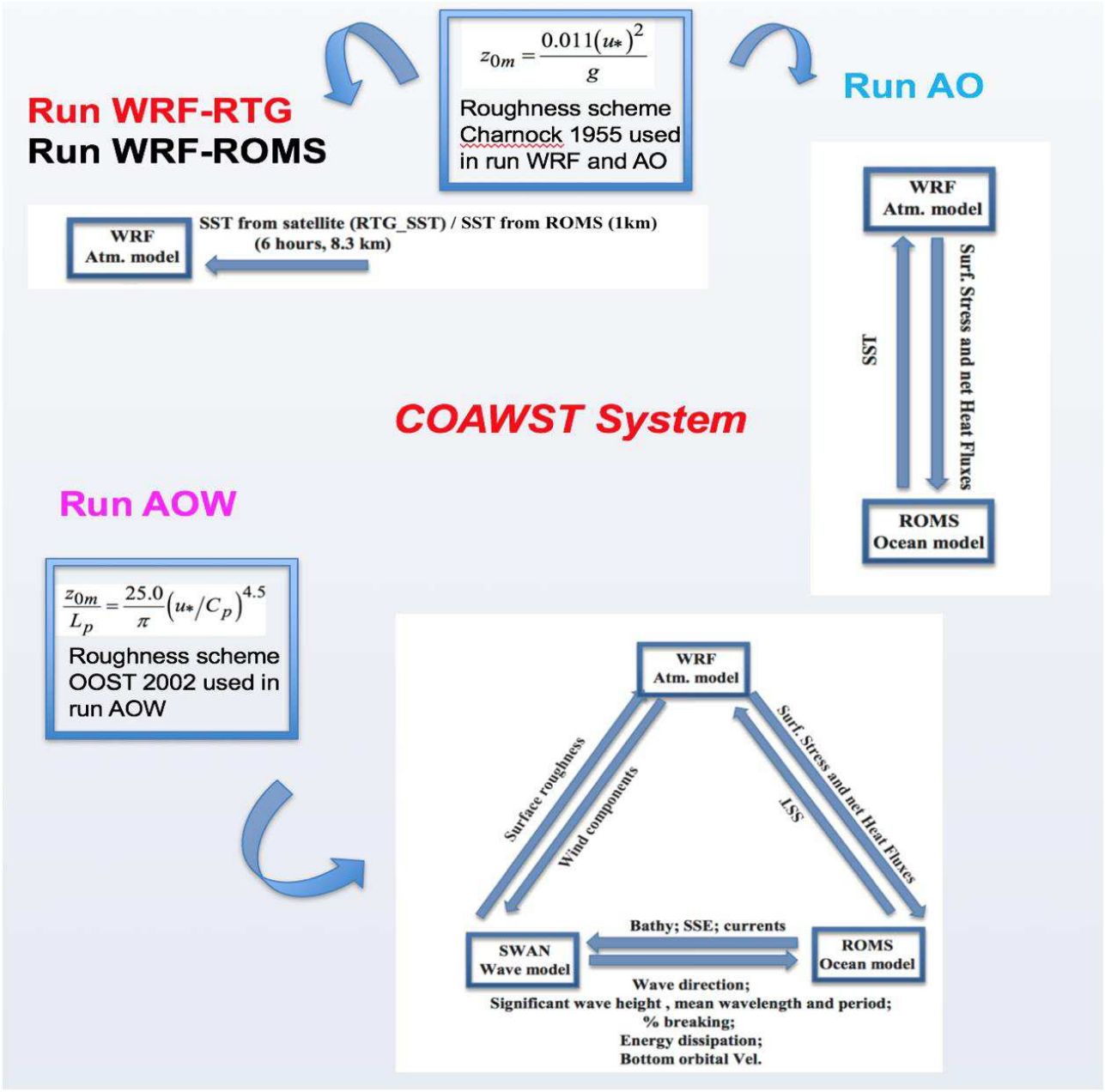

Figure 3. COAWST configuration used for the different runs.

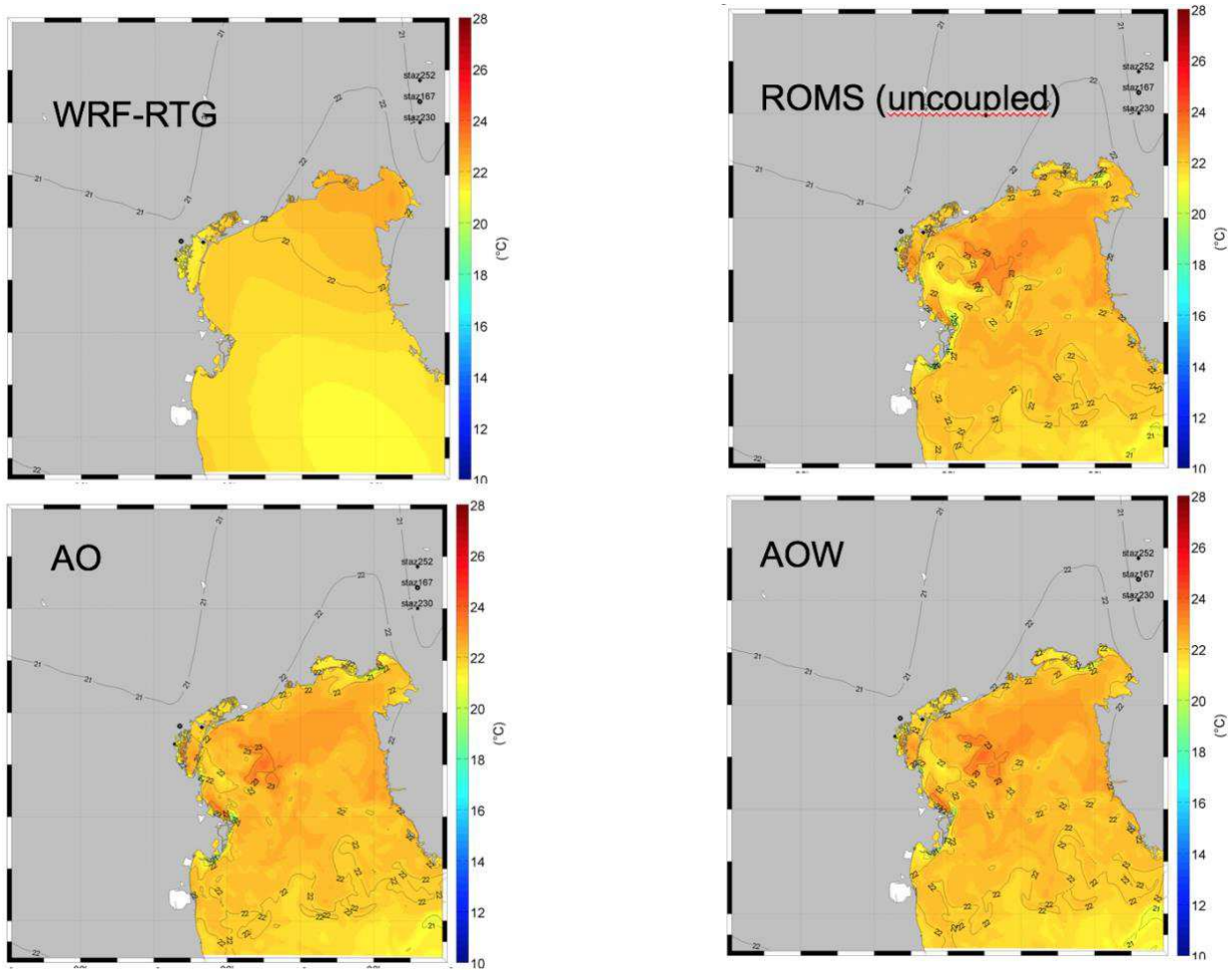

Figure 4. Sea Surface Temperature at the time of Flash-Flood formation.

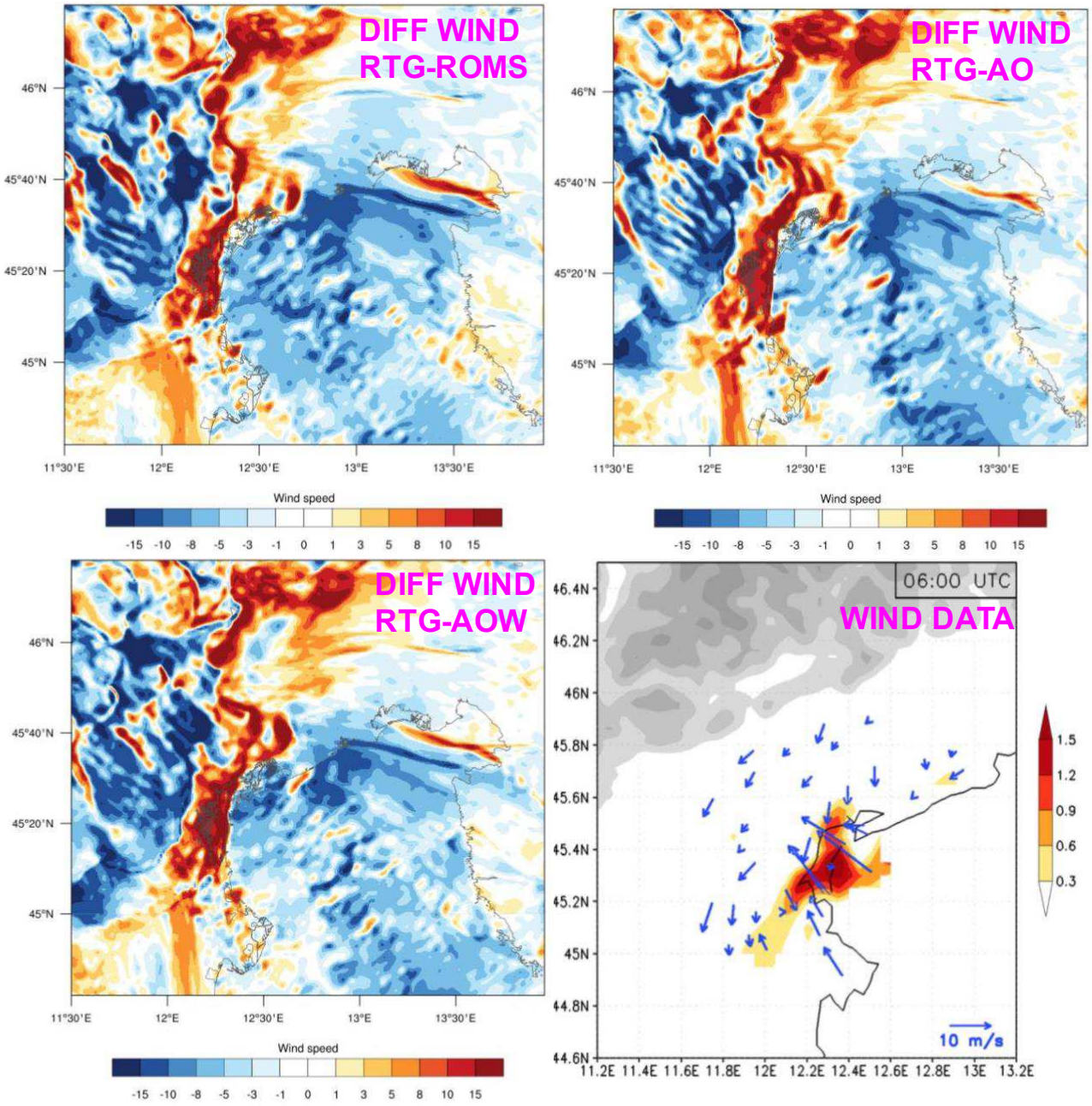

Figura 5. Wind speed difference between the four different runs (RTG minus "others") in the area near the Venice Lagoon, at the time of Flash-flood formation, and in the lower-right side, the wind data taken from ARPAV weather station network (Davolio et al 2009)

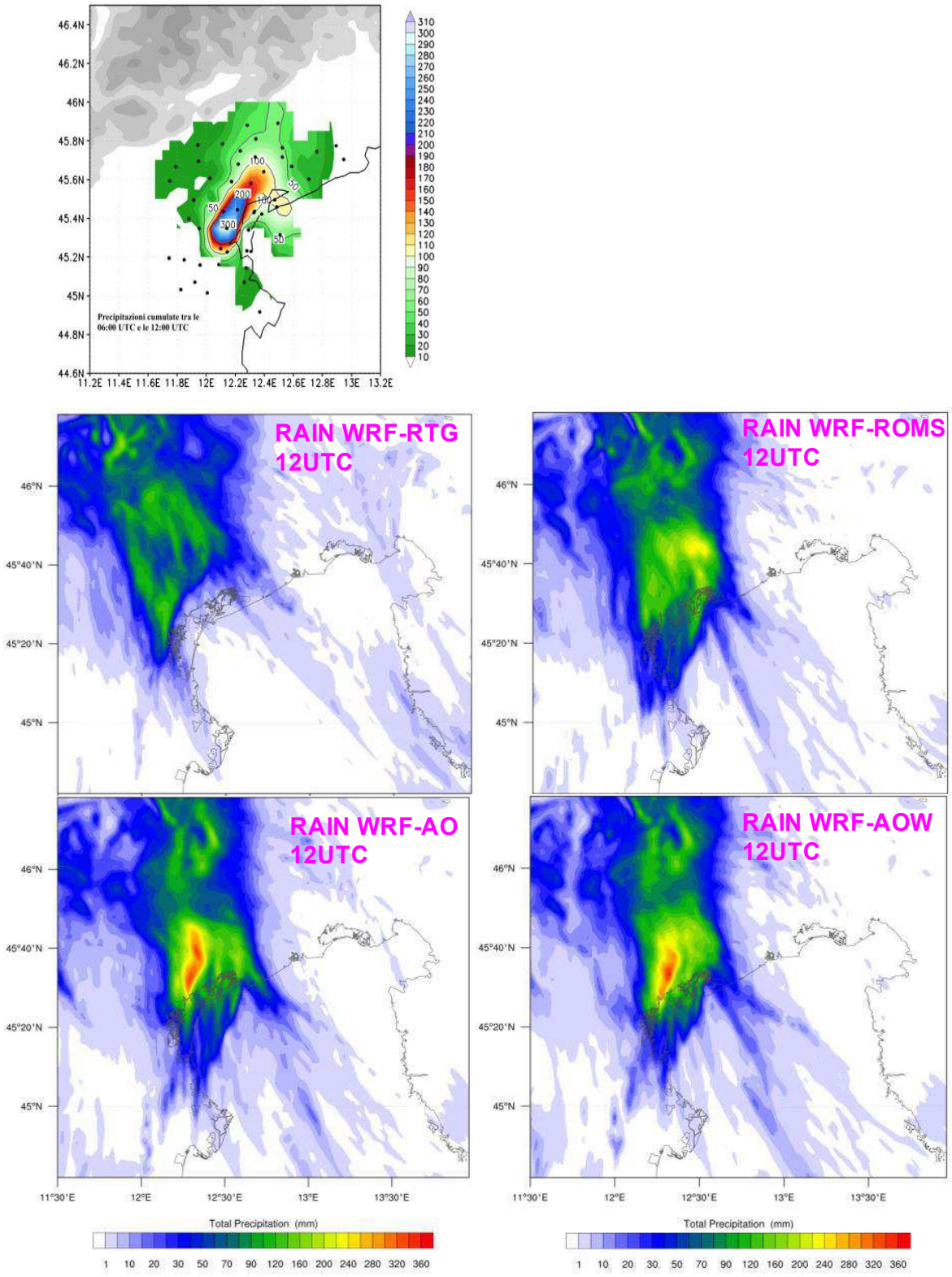

Figure 6. Rainfall accumulated in from 06UTC to 12UTC over Venice Lagoon, and in upper side panel, ARPAV rainfall data (Davolio et al 2009).

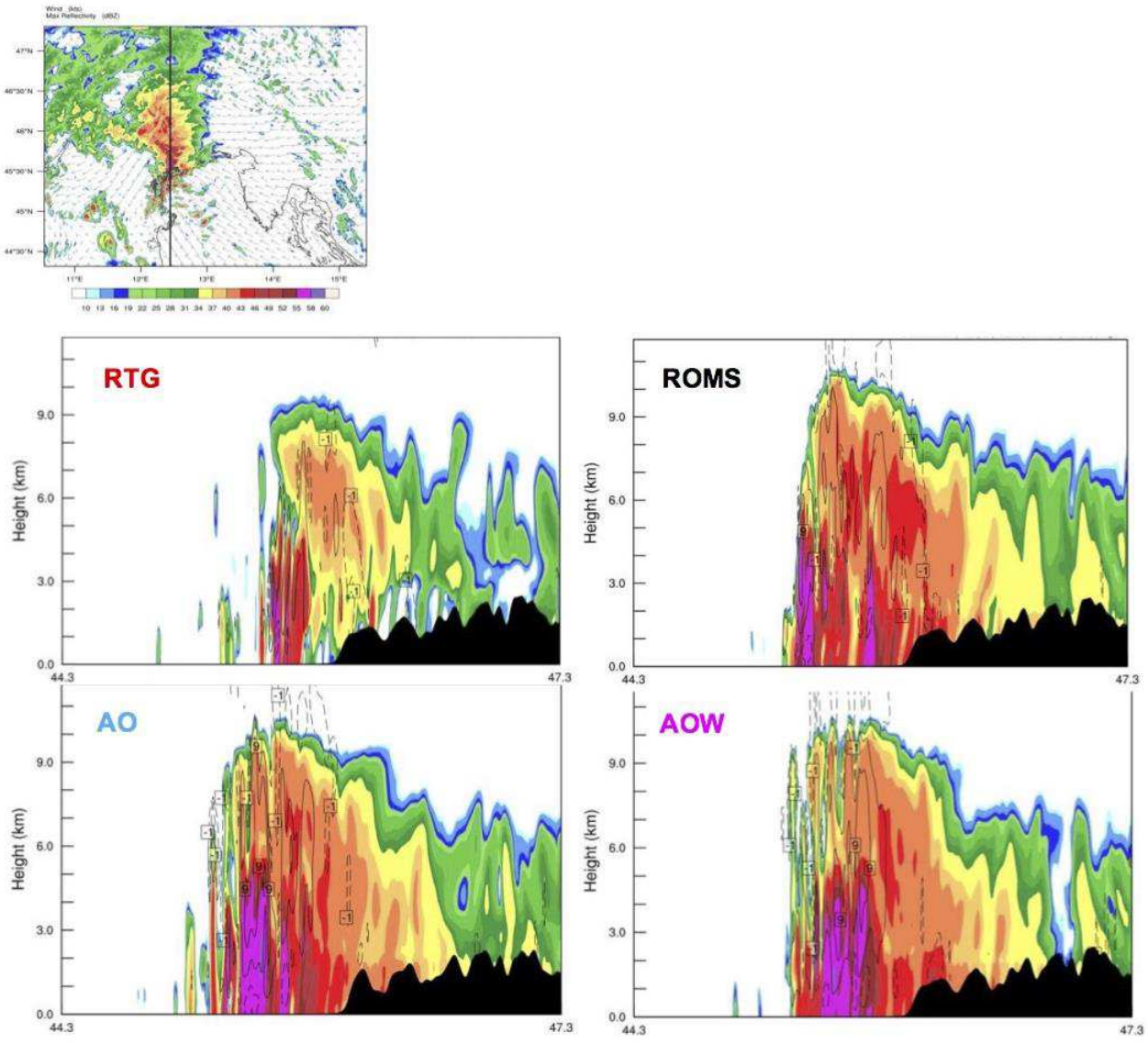

Figure 7. Cross Section of maximum Radar Reflectivity and vertical velocity (black contour)

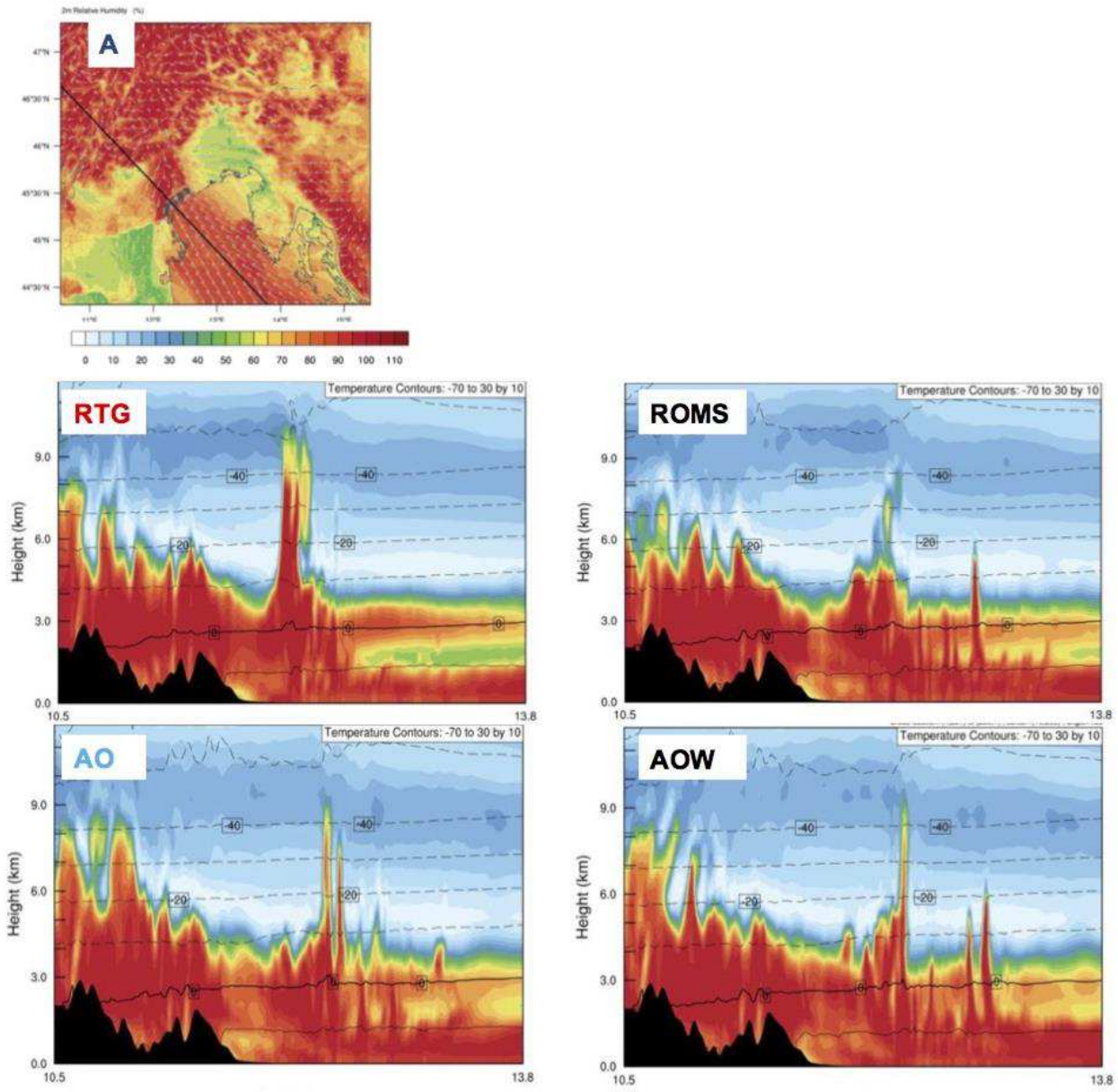

Figure 8. Cross Section of vertical humidity and temperature (black contour)

5 Final remarks

5.1. General Conclusion

In this dissertation work were proposed the results of simulations of three different extreme events on the Mediterranean basin. The events studied were selected for both their intensity and duration and the impact they had or could potentially have on the population. To better understand the effects of ocean-atmosphere interactions, the COAWST coupled numeric model has been used, which allows to perform an atmospheric model (WRF), an ocean model (ROMS), and a wave swirl model (SWAN). They are used in "Uncoupled" and "Coupled" mode with a wide range of applications and intermediate configurations. The use of the COAWST modeling system starting from the simplest implementation of the SST, using only the atmospheric model with the aid of SST fields tele-detected by satellite. This application is comparable to the use that is done in research centers and weather analysis. This configuration is often chosen for technical reasons, as the satellite SST is easier to find. This configuration is less burdensome in terms of work and calculation times. You could opt for modeling data, but these data are difficult to find, evaluate, and often do not have a spatial extension to ensure coverage of the entire computing domain of the atmospheric model. After performing the "uncoupled" simulations we ran the coupled simulation with atmosphere-ocean-wave interaction. Since the link between the ocean and the atmosphere is the air interface, and that this interface is not "flat" and “constant” (in space and time), but has a very variable distribution due to wave evolution, it is a lot of attention has been paid to the study of the sensitivity of the parametrizations that study this interface and how it moderates the energy fluxes between these two environments, through its surface roughness (the result of the wave motion). The results presented in the previous chapters will be replicated below, also raising some concerns about the use of coupled models and other technical issues.

5.2. CAO

As shown in Chapter 2 of this thesis work, the description of the SST field is crucial in CAO events on the Mediterranean basin (though focus has been on the Northern Adriatic) to understand air-sea interactions. In this work, two fundamental considerations can also be drawn for future studies and reviews.

- The use of SSTs of satellite origin is affected by considerable bias and in the order of 3-6°C in different areas of the basin. The difference between satellite data and measured data in-situ is caused by the "observation holes" that are highlighted in satellite data, particularly due to the cloudiness present during these events. The SST data are the result of the interpolation of the data acquired in the previous 7 days. This technique is used to reduce the amplitude of the "observation holes". The problem of this approach is that the SST from 7 days used for the final SST data, can change a lot, especially during such intense cooling events, and on semi-closed basins such as the Adriatic Sea basin (but also in many coastal areas in the Mediterranean). Using a SST field with relevant "bias" is difficult to improve the results of "UnCoupled" simulations, that's why the SST data are wrong. Although in the "hindcast" simulations the SST is updated every 6 hours, this simulation is affected by the quick cooling effect of previous days. Indeed, we could say that the importance and validity of the use of SST satellite data is strongly limited by the temporal variability of atmospheric dynamics. During cooling events (but also, presumably, during the heat waves), it is essential to use frequently updated data, that are not the sum of interpolation of previous days, which limits the variability of the SST. In this case it is crucial to use the SST produced by numerical models.
- The use of coupled models provides much better results than "Uncoupled" simulations in statistical terms (in the analyzed stations). The stations are predominantly on the coast and this is a determining factor for an objective analysis of the results. Satellite SST data don't solve the coastal variability in detail, due to the scattering effects produced by the high concentrations of dissolved sediments, the presence of clouds, and the rapid variation of temperature in coastal fronts, mainly because of the low resolution and interpolation used. For these reasons, coupled numerical models seem to be the much better solution, also regarding the applicability to several marine areas simultaneously, coastal as offshore. In particular, the improvements in terms of heat fluxes and wind intensity in the coupled "atmosphere-ocean-wave" runs, suggest that the presence of the wave, allow a better description of the variable, thanks to the more detailed description of the surface roughness.

- There are some open questions about running simulation. During this event, the most significant atmospheric phenomenon, in addition to record temperatures (-23°C in Turin), was the snowfall along the Adriatic coast and the Padana plain. The "Adriatic Lake Effect" is a phenomenon quite similar to the "Lake Effect", which can be seen, for example, on the "Great Lakes" of America and which causes sudden snow over the area exposed to the wind coming from the lake. The phenomenon is driven by heat fluxes. Very cold, dry air moves on mild waters, extracting a great amount of heat and water vapor, and they will become snow when the air masses reach the land. The same phenomenon occurred in the CAO in 2012, but in this work it was not possible to study the effect due to the scarcity of available snow data and the low reliability of the data few data obtained. In the future it would be interesting study this phenomenon with particular attention, having a better modeling feedback from operational forecasting models, to understand coastal dynamics as affecting the climate of the Po Valley.

3.4. Dense Water Formation

The results obtained from the three simulations based on the 2012 CAO event by analyzing DWF, with the simulation that used the ROMS model in "uncoupled" mode, atmosphere-ocean and the atmosphere-ocean-wave coupling, show substantial differences in terms of DWF and kinetic energy in the Northern Adriatic basin. The coupled run show improvements in the simulation of heat fluxes in the analyzed stations, with lower values when compared with the "uncoupled" run, which forced by an overestimated satellite SST, that produce more intense heat fluxes. This dynamic is presumably extended to the whole basin, in fact the average heat fluxes follow the same trend. Kinetic energy values follow the same trend too especially in the coupled atmosphere-ocean-wave, where mixing generated by interaction with wave motion increases energy input versus run coupled only between ocean-atmosphere (Benetazzo et al 2013, Benetazzo et al 2014). These dynamics of heat extraction and mixing are reflected in the production of dense water. If you compare the third run which other runs, you will leave a greater density and volume as result of DWF. These results suggest that :

- The coupled models simulate more realistically and consistently the fluxes at sea-air interface and this significantly affects the DWF. This suggests that a wrong SST in the atmospheric model leads to a wrong quantitative evaluation of the DW masses that form in the North Adriatic.

- The effect of mixing produced by wave action has a significant impact on mixing the water mass in the basin, and therefore in DW production, suggest the need to use the coupling with wave models.
- According to climate change, the DWF are more important for the circulation at the basin scale and for the deep ventilation of the eastern Mediterranean basin. The use of coupled models suggests a more consistent solution to reality and could suggest dynamics you can't see today about deep circulation.

3.5. Tropical-Like Cyclones

In recent years, many studies they have focused on the effect of SST on generating and maintaining TLC. Some work shows us a more realistic SST allows atmospheric models to achieve better results in terms of trajectory and intensity of cyclone. In this work we have focused further, trying to define the importance of several modeling factors such as initialization, PBL scheme, SST quality, and on the use of coupled models with different computation schemes of surface roughness. these studies have shown that :

- The correct choice of initiation is crucial, and we observed that should not be too far from the formation of the phenomenon, because this does not guarantee that you have enough data to be able to calculate the exact genesis of TLC. But initial conditions that are too close to the event can give you bad results. In this case because, even using a very realistic SST, the atmospheric model needs a spin-up time in which the atmospheric fields settle down on the grid used. In this spin-up phase (usually 12-18 hours), the model provide to dissipate the numeric noise generated by the interpolation of three-dimensional fields and the result diverge rapidly, eliminating the positive impact of high-resolution SST, since the atmosphere does not have time to settle down and become "consistent" with this new boundary condition.

- Using different calculation schemes for PBL does not produce always very different results between runs. this happens because TLC evolves very fast, and it develops almost entirely over the sea. Under these conditions, similar PBL schemes do not significantly alter the transfer of energy from the sea to atmosphere, and this is reflected in the convective phenomena that are the fuel of the TLC. Therefore, it would have an effect only in longer simulations and not for a few tens of hours.

- The coupled run seems to simulate slightly better the characteristics of the TLC. In this application the differences are not larger compared to the use of "decoupled" simulations but with high resolution SST. But in the case of coupled models we have a greater consistency between the atmospheric and oceanic fields. For a more complete view of the results, other TLC parameters, such as rainfall and vertical cyclone structure, will be analyzed in the future.

- No configuration changes the “timing” evolution of the phenomenon. So no physical parametrization or coupling, affects the timing because this field is driven more by large-scale dynamics in comparison to local scale phenomena.

- The use of different roughness schemes produce slightly different results between simulations, but none relevant better than others. However, is better use computational schemes that use "age" of the wave with respect to scheme that are based on the "steepness" of the wave, because the geometry of wave field, in these phenomena, is extremely different if we are is located near the minimum or in the surrounding areas where cyclone has already passed, due to the strong spatial variability of wave field in such intense and circumscribed.

- Significant results were obtained by studying the evolution of SST at the transit of the cyclone. The coupled runs, even in this case, provide better results in terms of the evolution of the SST (in the analyzed stations), showing how the effect of mixing caused by wave, extracts heat from the mixed Layer. It is still unclear how much heat is actually extracted in favor of the atmosphere and how it is deeply mixed, increasing the thickness of the mixed layer.

In conclusion the use of coupled models provides more consistent results than uncoupled simulations. Although they are more complex to implement, they provide information on both the atmosphere and the oceanic dynamics, making the analysis and prediction of extreme phenomena more complete, often resulting it the only solution for a realistic simulation of the phenomena mentioned above. They can also play a crucial role in the climatic field, not only for the best results obtained by simulating the extreme events of this work, but also because they are able to provide information about the amount of heat actually being transferred from the sea to the atmosphere and as it is stored in the ocean and especially in the mixed layer. Which, as we said at the beginning of this manuscript, seems to have absorbed 90% of the excess heat produced by the anthropogenic greenhouse effect from 1970 to today. Obviously it is necessary to study other numerous events. Also is essential to deepen the study of sensitivity to new calculation schemes, with the aim of implementing other schemes for surface roughness and for calculate energy fluxes at air-sea interface, that have a large range of application.

Acknowledgements

This thesis has been made possible thanks to the helpful contributions of many people. My deep gratitude goes to my supervisor prof. Aniello Russo and my cotutor and supervisor in CNR-ISMAR PhD Sandro Carniel, for having introduced me into the Numerical Environmental studies and Ocean science and supported me with his knowledge and his patient assistance throughout all the years spent together. I would also thank Phd Davide Bonaldo for the frequent and fruitful discussions provided a great improvement in the quality of my work and of my scientific growth. Other thanks go to Alvise Benetazzo, Francesco Barbariol, Mauro Sclavo and Francesco Falcieri, and Andrea Bergamasco for the continuous scientific and numerical support and for the continuous energies and passion they have shown in supporting me.

LIST OF FIGURE

INTRODUCTION

ON THE USE OF COUPLED OCEAN-ATMOSPHERE-WAVE MODEL DURING AN EXTREME COLD-AIR-OUTBREAK OVER THE ADRIATIC SEA

Fig. 6. 10 m wind speed (m s^{-1}) and direction at the peak of CAO, at 00:00 UTC, February 6. Panels represent, respectively, runs GFS (A), STA (B), OML (C), DYN (D), AO (E) and AOW (F) (see Table 1).

Fig. 7. 10 m wind speed time series at BP (two upper panels) and AA (two lower panels). Run labels are shown in Table 1.

Fig. 8. Two-meter air temperature (°C) at the peak of CAO, at 00:00 UTC, February 6. Panels represent, respectively, runs GFS (A), STA (B), OML (C), DYN (D), AO (E) and AOW (F) (see Table 1).

Fig. 9. 2 m air temperature time series at BP (upper two panels), AA (central two panels) and Ancona (lower two panels) stations. Run labels are shown in Table 1

Fig. 10. Turbulent heat fluxes (W/m^2) at the peak of CAO, at 00:00 UTC, February 6. Panels represent, respectively, runs GFS (A), STA (B), OML (C), DYN (D), AO (E) and AOW (F) (see Table 1).

Fig. 11. Turbulent heat fluxes time series at BP (upper two panels), AA (central two panels) and Ancona (lower two panels) stations. Run labels are shown in Table 1

Fig. 12. Taylor diagram relative to THF. The colors and initial letter refer to the different model simulations (see Table 1). The last two letters refer to the station (AA = Acqua Alta Platform; BP = Paloma buoy; AN = Ancona).

SCRATCHING BENEATH THE SURFACE WHILE COUPLING ATMOSPHERE, OCEAN AND WAVES : ANALYSIS OD DENSE WATER FORMATION

Table 1

Model performances compared with AA observations for different implementations in the period January 23–February 23. ATM represents ROMS forced by WRF, AO two-way coupled ROMS and WRF, AOW full two-way coupling ROMS, SWAN and WRF. Correlation coefficients (CC) are expressed in dimensionless units.

Fig. 1. Geographical setting of the study. *Left panel*: WRF (outer box) and ROMS (inner box) numerical domain and Sea Surface Temperature field (ROMS in the Adriatic Sea, radiometer in the Mediterranean) at the beginning of the event. *Right*: Adriatic Sea and Ancona-Novalja transect (reference cross section in the study, grey thick line) conventionally encompassing the "cooling" or "formation" basin. Thin (thick) grey contours represent 50 (250) m isobaths. AA and PB represent the position of Acqua Alta tower and Paloma Buoy respectively.

Fig. 2. Model results (color lines) and observations (black line) at the "Acqua Alta" tower. (For interpretation of the references to colour in this figure legend, the reader is referred to the web version of this article.)

Fig. 3. Time-averaged (January 29–February 13) sea surface temperature and current velocity in the northern Adriatic Sea for different runs. Vectors related to current speed have been omitted.

Fig. 4. Differences between time-averaged (January 29–February 14) fields of wind stress (top row) and heat fluxes (bottom row) at the sea surface for each run and the mean value from all three separate (ATM, AO, AOW) runs for the same period, identified by black contour lines.

Fig. 5. Overall mean properties evolution in the formation basin during Winter 2012 event: surface momentum stress (*top panel*), turbulent heat flux (*second panel*), water potential density (*third panel*), kinetic energy (*bottom panel*).

Fig. 6. Horizontally-averaged kinetic energy per unit volume profiles in the formation basin for the three runs.

Fig. 7. Key metrics for dense water formation, January 29–February 14. *Left*: total water mass involved in the densification process as a sum of water masses passing through the formation basin and eventually exported (red) and overall mass of the formation basin. *Middle*: Total surface heat extraction during the event. *Right*: Total surface extraction per unit mass (note that positive values for surface heat and heat density extraction mean heat directed from the ocean to

the atmosphere). (For interpretation of the references to colour in this figure legend, the reader is referred to the web version of this article.)

Fig. 8. Potential density composition of the water masses involved in the cooling event (unbiased values): initial (January 29, 2012) condition of the cooling basin (*top panel*), time-integrated inflow (*second panel*), time-integrated outflow (*third panel*), final (February 14, 2012) condition in the generation basin, including total export (*bottom panel*, thick lines representing the export depict its relative contribution to the overall mass involved in the process.

Fig. A.1. Schematic representation of the proposed COAWST experiments (ATM, AO, AOW). The arrows represent the coupling direction with in evidence the exchanged variables. SST is the Sea Surface Temperature, SSE the sea surface elevation.

SENSITIVITY OF MEDITERRANEAN TROPICAL-LIKE CYCLONE TO DIFFERENT MODEL CONFIGURATION AND COUPLING STRATEGY

Table 1. Summary of all performed runs and their numerical setup. Acronyms used: CHA = Charnock (1955) (Charnock et al 1956); OOST = Oost et al. (2002)]; TY: Taylor and Yelland et al. (2001) ; DRE: Drennan et al. (2005) [. MYI: Mellor-Yamada-Janjic' ; MYNN: Mellor Yamada.

Figure 1. Snapshots of surface pressure (white lines; c.i. = 3 hPa), and 500 hPa geopotential height (colors) on 3 November 2011, 00 UTC (panel (**a**)) and 4 November 2011, 00 UTC (panel (**b**))—during the transit of the Atlantic baroclinic wave over Spain, close to the Balearic Sea-, 5 November 2011, 00:00 UTC (panel (**c**))—during the formation of the ROLF depression over Spain-, on 6 November 2011, 00:00 UTC (panel (**d**))—during the cut-off low over the Balearic sea-, on 7 November 2011, 00:00 UTC (panel (**e**)) and 8 November 2011, 00:00 UTC (panel (**f**)). Data are from ECMWF ERA-40 (European Center for Medium range Weather Forecasting)

Figure 2. Visible channel of Meteosat Satellite images on 6 November 2011, 12:00 UTC (panel (**a**)), 7 November 2011, 12:00 UTC (panel (**b**)), 8 November 2011, 12:00 UTC (panel (**c**)) and 9 November 2011, 12:00 UTC (panel (**d**)) (source: www.sat24.com; copyright: EUMETSAT). In panel (**a**) we can see the formation of the TLC, whereas in the panel (**b**) the TLC is formed and in panel (**c**) ROLF is still well identified. In panel (**d**) the landfall of cyclone is shown.

Figure 3. SST anomaly produced by the Mediterranean Forecasting System (MFS INGV, [24]) on 8 November 2011, consisting of the difference between analysed SST from MFS and the climatology 1955–2004 supplied by the Nucleus for European Modelling of the Ocean (NEMO), with a variational data assimilation scheme (OceanVAR) for temperature and salinity vertical profiles and satellite Sea Level Anomaly along track data. The model horizontal grid resolution is 1°/16° (ca. 6–7 km) and the unevenly spaced vertical levels are 72 (Pinardi et al 2003). In this figure, we can see the positive SST anomaly in the western Mediterranean Sea, between 1–3.7 °C, in particular over the formation area of the TLC.

Figure 4. Wind speed and direction from the Advanced Scatterometer Wind data (ASCAT) shown on 8 November 10:00 UTC at 25 km of resolution. In the proximity of the pressure minimum, wind speed is approximately 25–28 ms^{-1} (50–55 knots). The area with maximum intensity is located on the northern side of TLC.

Figure 5 he three different configurations adopted in this study. Panel (a): WRF run: atmosphere standalone (WRF uses the SST data from the RTG_SST dataset, every 6 h). Panel (b): AO (Atmosphere-Ocean) run: coupling between atmosphere and ocean (WRF receives the SST from ROMS model, at 1 km resolution, every 300 s, and exchanges the turbulent heat fluxes with ROMS). Panel (c): AOW (Atmosphere-Ocean-Wave) run: full atmosphere-ocean-wave coupling (WRF and ROMS exchange SST and fluxes; WRF and SWAN exchange the wind fields and the wave parameters; ROMS and SWAN exchange currents fields and wave parameters).

Figure 6. The nested WRF domain and, delimited by the red line, the computational domain used for ROMS-SWAN which included the whole Mediterranean Sea.

Figure 7. Trajectory and intensity of the cyclone for all simulations. In purple the trajectory estimated using observations from geo-referenced satellite image, which starts at 00:00 UTC, 6 November 2011, and ends at 12:00 UTC, 9 November 2011. The trajectory identifies the minimum pressure of ROLF every 3 h. Values of pressure minimum are highlighted by the color of the dots. The black arrows show the direction of propagation of the Medicane. In the different panels we can observe the trajectories resulting from the various runs, compared with the trajectory obtained from the satellite, and the trajectory proposed by the NOAA. Panels (a-g): runs WRF1-7 (atmosphere standalone). Panel (h): runs WRF5 and WRF8 (MYJ and MYNN PBL). Panel (i): runs WRF5 (with MYJ) and WRF9 (WRF with SST decreased by 3 °C). Panel (l): runs WRF5, WRF10 (with high resolution SST from MFS-system), AO1 and AOW1 (AO and AOW with MYJ PBL scheme). Panel (m): runs WRF8, AO2 and AOW2, using MYNN PBL scheme. Panel (n): runs AOW1, AOW3, AOW4 using the different surface roughness schemes (OOST, TY, DRE)

Figure 8. Time evolution of the pressure minimum (in hPa) and the maximum wind speed (m/s) around the eye, as resulting from different experiments. Black dots represent estimated NOAA data for the pressure minimum of the cyclone and wind speed around the minimum. Panels (a) and (b): comparison between the evolutions of the various WRF1-7 runs for the pressure minimum and wind intensity. Panels (c) and (d): comparison between WRF5 and WRF8 (using, respectively, MYJ and MYNN PBL schemes). Panels (e) and (f): results from WRF5 and WRF9 (SST spectrum radiometer and SST +3 ° C). Panels (g) and (h): comparison among runs WRF8, AO2, AOW2, with MYNN PBL scheme. Panels (i) and (l): results for runs WRF5, WRF10, AO1, AOW1.

Figure 9. Panel (a): time evolution of the pressure minimum (hPa). Panel (b): maximum wind intensity (m/s) around the eye, for runs AOW1, AOW3 and AOW4. The black dots refer to the real-time estimation given by NOAA.

Figure 10. urface roughness values (log10) in different runs. Panels (a-c): values for runs WRF5, AO1 (using Charnock 1955 scheme) and AOW1 (using the OOST scheme), on 7 November 2011, 12:00 UTC (36 hours after the start of simulation). Panels (d-f): values for runs AOW1 (OOST scheme), AOW3 (TYscheme) and AOW4 (DRE scheme), on 7 November 2011, 12:00 UTC. Panels (g-i): values for runs AOW1, AOW3 and AOW4, on 9 November 2011, 00:00 UTC.

Figure 11. SST fields for the day 9 November 2011 at 12 UTC, for run WRF5 (**a**), AO1 (**b**), AOW1 (**c**). In panel (**a**) the position of the buoy #61002 (Meteo France) is shown. From the time series (panel (**d**)), we can notice that the three modeling approaches provide to the atmospheric model a very different SST field and only the coupled runs reproduce the variation of SST correctly, in particular the run AOW1, due to the additional effect of wave mixing [54]. It is colder than 1 °C, compared to the value from which the models are initialized (reanalysis). This is because the buoy is located in a sea zone characterized by the thermal front, composed of cold water masses, produced in the Gulf of Lions, and warmer water masses typical of the Balearic Sea.

Figure 12. Average geometric distance between simulated and observed trajectories (km).

PRELIMINARY RESULT OBOUT : DESCRIBING A FLASH-FLOOD EVENT OVER THE NORTH-EAST ITALY USING A VERY-HIGH RESOLUTION ATMOSPHERE-OCEAN-WAVE COUPLED MODEL

Figure 1. Satellite image that show the V-shape of thunderstorm developed over Venice Lagoon.

Figure 2. Synoptic analysis at 500 hpa, and sea level pressure from 25/09/2007 at 12UTC to 26/09/2007 at 12UTC

Figure 3. COAWST configuration used for the different runs.

Figure 4. Sea Surface Temperature at the time of Flash-Flood formation.

Figura 5. Wind speed and wind direction in the area near the Venice Lagoon, at the time of Flash-flood formation, and in the right side, the wind data taken from ARPAV weather station network (Davolio et al 2009)

Figure 6. Rainfall accumulated in from 06UTC to 12UTC over Venice Lagoon, and in upper side panel, ARPAV rainfall data (Davolio et al 2009).

Figure 7. Cross Section of maximum Radar Reflectivity and vertical velocity (black contour)

Figure 8. Cross Section of vertical humidity and temperature (black contour)